Reviews of Geophysics

Mathematical and physical ideas for climate science

Valerio Lucarini[1,2,3], Richard Blender[1], Corentin Herbert[4], Francesco Ragone[1,5], Salvatore Pascale[1], and Jeroen Wouters[1,6]

[1]Klimacampus, Meteorologisches Institut, University of Hamburg, Hamburg, Germany, [2]Department of Mathematics and Statistics, University of Reading, Reading, UK, [3]Walker Institute for Climate System Research, University of Reading, Reading, UK, [4]National Center for Atmospheric Research, Boulder, Colorado, USA, [5]Klimacampus, Institut für Meereskunde, University of Hamburg, Hamburg, Germany, [6]Laboratoire de Physique, École Normale Supérieure de Lyon, Lyon, France

Abstract The climate is a forced and dissipative nonlinear system featuring nontrivial dynamics on a vast range of spatial and temporal scales. The understanding of the climate's structural and multiscale properties is crucial for the provision of a unifying picture of its dynamics and for the implementation of accurate and efficient numerical models. We present some recent developments at the intersection between climate science, mathematics, and physics, which may prove fruitful in the direction of constructing a more comprehensive account of climate dynamics. We describe the Nambu formulation of fluid dynamics and the potential of such a theory for constructing sophisticated numerical models of geophysical fluids. Then, we focus on the statistical mechanics of quasi-equilibrium flows in a rotating environment, which seems crucial for constructing a robust theory of geophysical turbulence. We then discuss ideas and methods suited for approaching directly the nonequilibrium nature of the climate system. First, we describe some recent findings on the thermodynamics of climate, characterize its energy and entropy budgets, and discuss related methods for intercomparing climate models and for studying tipping points. These ideas can also create a common ground between geophysics and astrophysics by suggesting general tools for studying exoplanetary atmospheres. We conclude by focusing on nonequilibrium statistical mechanics, which allows for a unified framing of problems as different as the climate response to forcings, the effect of altering the boundary conditions or the coupling between geophysical flows, and the derivation of parametrizations for numerical models.

1. Introduction

The Earth's climate provides an outstanding example of a high-dimensional forced and dissipative complex system. The dynamics of such system is chaotic, so that there is only a limited time horizon for skillful prediction, and is nontrivial on a vast range of spatial and temporal scales, as a result of the different physical and chemical properties of the various components of the climate system and of their coupling mechanisms [*Peixoto and Oort*, 1992].

Thus, it is extremely challenging to construct satisfactory theories of climate dynamics and is virtually impossible to develop numerical models able to describe accurately climatic processes over all scales. Typically, different classes of models and different phenomenological theories have been and are still being developed by focusing on specific scales of motion [*Holton*, 2004; *Vallis*, 2006], and simplified parametrizations are developed for taking into account at least approximately what cannot be directly represented [*Palmer and Williams*, 2009; *Franzke et al.*, 2014].

As a result of our limited understanding of and ability to represent the dynamics of the climate system, it is hard to predict accurately its response to perturbations, such as changes in the opacity of the atmosphere, in the solar irradiance, in the position of continents, and in the orbital parameters, which have been present for our planet during all epochs [*Saltzman*, 2001]. The full understanding of slow- and fast-onset climatic extremes, such as drought and flood events, respectively, and the assessment of the processes behind tipping points responsible for the multistability of the climate system are also far from being accomplished [*Lenton et al.*, 2008].

Such limitations are extremely relevant for problems of paleoclimatological relevance such as the onset and decay of ice ages or of snowball conditions, for contingent issues like anthropogenic global warming, and for the perspective of developing a comprehensive knowledge on the dynamics and thermodynamics of

general planetary atmospheres, which seems to be a major scientific challenge of the coming years, given the extraordinary development of our abilities to observe exoplanets [*Dvorak*, 2008].

Climate science *at large* has always been extremely active in taking advantage of advances in basic mathematical and physical sciences and, in turn, in providing stimulations for addressing new fundamental problems. The most prominent cases of such interaction are related to the development of stochastic and chaotic dynamical systems, time series analysis, extreme value theory, radiative transfer, and fluid dynamics, among others. At this regard, one must note that the year 2013 has seen a multitude of initiatives all around the world dedicated to the theme *Mathematics of Planet Earth* (see http://mpe2013.org), and in this context, climate-related activities have been of great relevance.

In this review we wish to present some interdisciplinary research lines at the intersection between climate science, physics, and mathematics, which are extremely promising for advancing, on the one hand, our ability to understand and model climate dynamics, and represent correctly climate variability and climate response to forcings. On the other hand, the topics presented here provide examples of how problems of climatic relevance may pave the way for new, wide-ranging investigations of more general nature.

The literature related to the scientific interface mentioned above is enormous, and the selection of the material we present here is partial and nonexhaustive. We leave almost entirely out of this review very important topics such as extreme value theory [*Ghil et al.*, 2011], multiscale techniques [*Klein*, 2010], adjoint methods and data assimilation [*Wunsch*, 2012], partial different equations [*Cullen*, 2006], linear and nonlinear stability analysis [*Vallis*, 2006], general circulation of the atmosphere [*Schneider*, 2006], macroturbulence [*Lovejoy and Schertzer*, 2013], network theory [*Donges et al.*, 2009], and many relevant applications of dynamical systems theory to geophysical fluid dynamical problems [*Kalnay*, 2003; *Dijkstra*, 2013].

Let us now mention what we are going to cover in this review and give a motivation to the specific perspective we have chosen. We are motivated by the desire of bridging the gap between some extremely relevant results in mathematical physics, statistical mechanics, and theoretical physics, and open problems and issues of climate science, hoping to stimulate further investigations and interdisciplinary activities. Our selection of topics will focus on the concepts of energy, entropy, symmetry, coupling, fluctuations, and response.

We will first concentrate on the properties of inviscid and unforced flows relevant for geophysical fluid dynamics (GFD). In section 2, we provide an overview of a very powerful formulation of hydrodynamics based on the formalism introduced by *Nambu* [1973] and present its applications in a geophysical context, suggesting how these ideas help clarifying somewhat *hidden* properties of fluid flows, and how the Nambu formulation of GFD could lead to a new generation of numerical models, to be used in a variety of weather and climate applications. In section 3, starting from the classical investigation by *Onsager* [1949] of the dynamics of point vortices, we will show how to develop an equilibrium statistical mechanical theory of turbulence for GFD flows and will discuss its relevance for interpreting observed climatic phenomena.

Equilibrium methods allow investigating many properties of GFD flows. Nonetheless, at this point we cannot ignore anymore the *elephant in the room*, *i.e.*, the fact that the dynamics of the climate system cannot be assimilated to an inviscid and unforced GFD flow, because forcing and dissipative processes are of extreme relevance. Thus, we move toward the paradigm of nonequilibrium systems. In section 4, taking inspiration from the points of view of *Prigogine* [1961] and of *Lorenz* [1967], we explore how through classical nonequilibrium thermodynamics one can construct tools for assessing the energy budget and transport of the climate system, define and estimate the efficiency of the *climate machine*, and study the irreversible processes by evaluating the climatic material entropy production. This allows for characterizing the large-scale properties of climate, for developing tools for auditing climate models, for gathering information on tipping points, and for exploring the properties of general planetary atmospheres. In section 5, we address the nonequilibrium statistical mechanics formulation of climate dynamics and explore how the formalism of response theory allows for addressing in a rigorous framework the climatic response to perturbations, taking inspiration from the work of *Ruelle* [1997]. We will show how it is possible to construct operators useful for the prediction—in an ensemble sense—of climate change. A last aspect of GFD we want to discuss in a statistical mechanical setting is the derivation of parametrizations providing a surrogate description of the effect of fast, small-scale variables, which are hard to represent explicitly in numerical models, on the larger scale, slow variables of more direct climatic relevance. Thus, in section 6, we present averaging and homogenization techniques, describe how projector operator methods due to *Mori* [1965] and *Zwanzig*

[1961] provide powerful tools for deriving parametrizations and firm ground to the inclusion of stochastic terms and memory effects, and discuss how response theory can be used to derive similar results. Finally, in section 7, we draw our conclusions and present some perspectives of future research.

2. Beyond the Hamiltonian Paradigm: Nambu Representation of Geophysical Fluid Dynamics

Hamiltonian formalism constitutes the backbone of most physical theories. In the case of a discrete autonomous system, the basic idea is to provide a full description of the degrees of freedom by defining a set of canonical variables q and of the related momenta p ($q, p \in R^N$, i.e., they are N-dimensional vectors) and by identifying the time evolution to a flow in phase space such that the canonical Hamiltonian function $\mathcal{H}$ acts as a stream function, $\dot{q} = \nabla_p \mathcal{H}, \dot{p} = -\nabla_q \mathcal{H}$, where $\mathcal{H}(q, p)$ corresponds to the energy of the system, whose value is constant in time. The flow is inherently divergence-free (*solenoidal*), so that the phase space does not contract nor expands, as implied by the Liouville theorem [*Landau and Lifshits*, 1996]. The time evolution of any function $X(q, p)$ can be expressed as follows:

$$\frac{\mathrm{d}}{\mathrm{d}t}X = \dot{X} = \{X, \mathcal{H}\}_P = \nabla_q X \cdot \nabla_p \mathcal{H} - \nabla_p X \cdot \nabla_q \mathcal{H}, \tag{1}$$

where $\{,\}_P$ are the so-called Poisson brackets and · indicates the usual scalar product. As suggested by Noether's theorem, the presence of symmetries in the system implies the existence of so-called physically conserved quantities X_i, such that $\dot{X}_i = 0 = \{X_i, \mathcal{H}\}_P$. An autonomous system possesses time invariance and its energy is constant, while in a system possessing translational invariance, the total momentum M is also constant. A system can possess many constants of motions, called *Casimirs*, apart from energy, but the Hamiltonian plays a special role as it is the only function of phase space appearing *explicitly* in the definition of the evolution of the system [*Landau and Lifshits*, 1996].

Nambu [1973] presented a generalization of canonical Hamiltonian theory for discrete systems. The dynamical equations are constructed in order to satisfy Liouville's theorem and are written in terms of two or more conserved quantities. The Nambu approach has been extremely influential in various fields of mathematics and physics and is viable to extension to the case of continuum, so that it can be translated into a field theory. The construction of a Nambu field theory for geophysical fluid dynamics went through two decisive steps. The first was the discovery of a Nambu representation of 2-D and 3-D incompressible hydrodynamics [*Névir and Blender*, 1993]. The second important step was the finding that the Nambu representation can be used to design conservative numerical algorithms in geophysical models and that classical heuristic methods devised by Arakawa for constructing accurate numerical models actually reflected deep symmetries coming from the Nambu structure of the underlying dynamics of the flow [*Salmon*, 2005].

The physical basis for the relevance of the Nambu theory for describing and simulating conservative geophysical fluid dynamics comes from the existence of relevant conserved quantities apart from energy when forcing and dissipative terms are disregarded from the evolution equations. Such a property is found in several models relevant for studying geophysical flows, is valid for 2-D and 3-D hydrodynamics, Rayleigh-Bénard convection, quasi-geostrophy, and shallow water model, and extends to the fully baroclinic 3-D atmosphere. In other terms, the Nambu representation provides the natural description of geophysical fluid dynamics and is superior to the more traditional approaches based essentially on Euler equations, just like the action-angle representation of the dynamics of a spring is superior to the simple description provided by the second Newton's law of motion.

2.1. Hydrodynamics in 2-D and 3-D
In incompressible hydrodynamics enstrophy (in 2-D) and helicity (3-D) are known as integral conserved quantities besides energy [*Kuroda*, 1991]. *Névir and Blender* [1993] adapted Nambu's formalism to incompressible nonviscous hydrodynamics by using enstrophy and helicity in the dynamical equations.
2.1.1. Two-Dimensional Hydrodynamics
The evolution of two-dimensional incompressible inviscid and unforced flows described by the velocity field $\boldsymbol{u}$ is governed by the vorticity equation

$$\frac{\partial \omega}{\partial t} = \partial_t \omega = -\boldsymbol{u} \cdot \nabla \omega, \tag{2}$$

where customary symbols are used for indicating partial derivatives, the vorticity ω can be expressed, in Cartesian coordinates (x, y), as $\omega = v_x - u_y$, and incompressibility is described by $\nabla \cdot \boldsymbol{u} = 0$, where $\nabla \cdot \boldsymbol{u} = \partial_x u_x + \partial_y u_y$ is the divergence of the vector field $\boldsymbol{U}$. As a result, we can write $\boldsymbol{u} = S\boldsymbol{\nabla}\psi = (-\partial_y\psi, \partial_x\psi)$, where S is the symplectic matrix $[0, -1; 1, 0]$, ψ is the stream function, and $\nabla\phi = (\partial_x\phi, \partial_y\phi)$ is the gradient of the function ϕ. Note that $\omega = \nabla^2\psi$. In this section, we consider a compact domain (e.g., a square of side L) with periodic boundary conditions.

The Hamiltonian $\mathcal{H}$ is the kinetic energy is a functional of the velocity

$$\mathcal{H} = \frac{1}{2}\int \boldsymbol{u}^2 \, \mathrm{d}A = \frac{1}{2}\int \nabla\psi \cdot \nabla\psi \, \mathrm{d}A = -\frac{1}{2}\int \omega\psi \, \mathrm{d}A \tag{3}$$

where we have used integration by parts. In general, a functional $\mathcal{F}[\phi]$ maps a function ϕ of the phase space into a number. The functional derivative $\delta\mathcal{F}/\delta\phi$ the change of the functional $\mathcal{F}$ with respect to a change in the function ϕ. The functional derivative can be defined by considering the first term in the expansion

$$\mathcal{F}[\phi + \delta\phi] - \mathcal{F}[\phi] = \delta\mathcal{F}[\phi] = \int \frac{\delta\mathcal{F}}{\delta\phi(x)}\delta\phi(x)\mathrm{d}x + \dots \tag{4}$$

The functional derivative $\delta\mathcal{H}/\delta\omega$ for (3) is explicitly calculated by

$$\delta\mathcal{H} = \int \nabla\psi \cdot \delta\nabla\psi \, \mathrm{d}A = \int \nabla \cdot (\psi\delta\nabla\psi) \, \mathrm{d}A - \int \psi\delta\omega \, \mathrm{d}A.$$

Since the first integral vanishes due to the boundary conditions, and since $\omega = \nabla^2\psi$, we obtain $\delta\mathcal{H}/\delta\omega = -\psi$.

Equation (2) says that vorticity is transported across the domain by a nondivergent flow. One can prove easily that any functional of the vorticity is conserved

$$C = \int s(\omega) \, \mathrm{d}A, \tag{5}$$

where the integration is performed over the whole domain of the system. The most familiar of such functional is the total enstrophy of the flow:

$$\mathcal{E} = \frac{1}{2}\int \omega^2 \, \mathrm{d}A. \tag{6}$$

The functional derivative of the enstrophy is simply $\delta\mathcal{E}/\delta\omega = \omega$.

Since $\boldsymbol{u} = S\boldsymbol{\nabla}\psi = (-\partial_y\psi, \partial_x\psi)$, the 2-D vorticity equation can be expressed as

$$\frac{\partial\omega}{\partial t} = -\mathcal{J}(\psi, \omega) = \mathcal{J}(\omega, \psi) = -\mathcal{J}\left(\frac{\delta\mathcal{E}}{\delta\omega}, \frac{\delta\mathcal{H}}{\delta\omega}\right), \tag{7}$$

with the antisymmetric Jacobi operator

$$\mathcal{J}(a, b) = \partial_x a \, \partial_y b - \partial_y a \, \partial_x b = -\mathcal{J}(b, a). \tag{8}$$

Relating ψ and ω to the functional derivatives of two conserved quantities amounts to expressing the evolution equation in a Nambu form using the enstrophy $\mathcal{E}$.

The time evolution of an arbitrary functional of vorticity $\mathcal{F} = \mathcal{F}[\omega]$ is determined by

$$\frac{\mathrm{d}\mathcal{F}}{\mathrm{d}t} = -\int \frac{\delta\mathcal{F}}{\delta\omega}\mathcal{J}\left(\frac{\delta\mathcal{E}}{\delta\omega}, \frac{\delta\mathcal{H}}{\delta\omega}\right)\mathrm{d}A = \{\mathcal{F}, \mathcal{E}, \mathcal{H}\}, \tag{9}$$

which defines a Nambu bracket for the three functionals involved. The bracket is antisymmetric in all arguments, $\{\mathcal{E}, \mathcal{H}, \mathcal{F}\} = -\{\mathcal{H}, \mathcal{E}, \mathcal{F}\}$, etc. Using rearrangements of these functionals and partial integration it can be shown that the Nambu bracket is cyclic

$$\{\mathcal{F}, \mathcal{E}, \mathcal{H}\} = \{\mathcal{E}, \mathcal{H}, \mathcal{F}\} = \{\mathcal{H}, \mathcal{F}, \mathcal{E}\}. \tag{10}$$

The cyclicity of this bracket is a main ingredient in Salmon's application of Nambu mechanics [*Salmon*, 2005] to construct conservative numerical codes (see section 2.2.2).

In the following the relationship between Nambu mechanics and Hamiltonian theory of two-dimensional flows is briefly summarized. As mentioned above, a Hamiltonian description of the dynamics is obtained when we can write

$$\frac{\mathrm{d}\mathcal{F}}{\mathrm{d}t} = \{\mathcal{F}, \mathcal{H}\}_P \tag{11}$$

with an antisymmetric Poisson bracket, to be seen in general as an antisymmetric map in the space of functionals, such that $\{\mathcal{A}, \mathcal{B}\}_P = -\{\mathcal{B}, \mathcal{A}\}_P$. Deriving such a bracket amounts to defining the dynamics of the system.

The Poisson bracket for 2-D hydrodynamics [*Salmon*, 1988; *Shepherd*, 1990] is easily obtained from the Nambu bracket if the dependency $\delta\mathcal{E}/\delta\omega = \omega$ is evaluated

$$\{\mathcal{F}, \mathcal{H}\}_P = \{\mathcal{F}, \mathcal{E}, \mathcal{H}\} = \int \omega \mathcal{J}\left(\mathcal{F}_\omega, \mathcal{H}_\omega\right) \mathrm{d}A, \tag{12}$$

where we indicate $\mathcal{H}_\omega = \delta H/\delta\omega$; here cyclicity is used (see equation (10)).

The Poisson bracket used in Eulerian hydrodynamics is degenerate because of the presence of an infinite number of so-called Casimirs, i.e., the functionals defined in equation (5), which are automatically conserved so that $\{\mathcal{C}, H\}_P = 0$. In this case, we talk about noncanonical Hamiltonian mechanics.

The relationship (12) demonstrates that noncanonical Hamiltonian mechanics is embedded in Nambu mechanics. The main extension is that in Nambu mechanics two functionals acting as an Hamiltonian, the enstrophy, and the energy are used (7) and that the Nambu bracket (9) is nondegenerate and void of Casimir functionals.

2.1.2. Three-Dimensional Incompressible Hydrodynamics

The dynamics of incompressible unforced and inviscid fluid flows in three dimensions is determined by the vorticity $\boldsymbol{\omega} = \nabla \times \boldsymbol{u}$ evolution equation:

$$\frac{\partial \boldsymbol{\omega}}{\partial t} = \boldsymbol{\omega} \cdot \nabla \boldsymbol{u} - \boldsymbol{u} \cdot \nabla \boldsymbol{\omega}, \tag{13}$$

where $\boldsymbol{u}$ is the velocity field and $\nabla \cdot \boldsymbol{u} = 0$. Note that in Cartesian coordinates we have that the curl of $\boldsymbol{u}$ ($\nabla \times \boldsymbol{u}$) can be expressed as $(\nabla \times u)_i = \epsilon_{ijk}\partial_j u_k$, where ϵ_{ijk} is the standard totally antisymmetric Levi-Civita symbol and $\nabla \cdot \boldsymbol{u} = \partial_x u_x + \partial_y u_y + \partial_z u_z$ is the divergence in three dimensions. Similarly to the two-dimensional case, the total energy

$$\mathcal{H} = \frac{1}{2}\int \boldsymbol{u}^2 \,\mathrm{d}V = -\frac{1}{2}\int \boldsymbol{\omega} \cdot \boldsymbol{A} \,\mathrm{d}V \tag{14}$$

is conserved, where we have introduced $\boldsymbol{A}$ as the vector potential such that $\boldsymbol{u} = -\nabla \times \boldsymbol{A}$. Note that in deriving the second identity we use integration by parts and consider periodic boundary conditions. It is important to note that the total helicity

$$h = \frac{1}{2}\int \boldsymbol{\omega} \cdot \boldsymbol{u} \,\mathrm{d}V \tag{15}$$

is also conserved, while, e.g., the enstrophy is not. Following the procedure detailed in equation (4), we derive that the functional derivative of the energy with respect to the vorticity is given by $\delta\mathcal{H}/\delta\boldsymbol{\omega} = -\boldsymbol{A}$ and for helicity $\delta h/\delta\boldsymbol{\omega} = \boldsymbol{u}$ (compare the 2-D version (5)).

The Nambu form of the vorticity equation is

$$\frac{\partial \boldsymbol{\omega}}{\partial t} = K\left(\frac{\delta h}{\delta\boldsymbol{\omega}}, \frac{\delta\mathcal{H}}{\delta\boldsymbol{\omega}}\right) = -K(\boldsymbol{u}, \boldsymbol{A}) \tag{16}$$

with

$$K(\boldsymbol{u}, \boldsymbol{v}) = -\nabla \times [(\nabla \times \boldsymbol{u}) \times (\nabla \times \boldsymbol{v})]. \tag{17}$$

Considering that $\boldsymbol{\omega} = \nabla \times \boldsymbol{u}$ and using some standard vector calculus identities, we obtain that equation (16) agrees with equation (13). We can derive the evolution equations for functional $\mathcal{F} = \mathcal{F}[\omega]$ as follows:

$$\frac{\mathrm{d}\mathcal{F}}{\mathrm{d}t} = -\int \left(\nabla \times \frac{\delta\mathcal{F}}{\delta\boldsymbol{\omega}}\right) \times \left(\nabla \times \frac{\delta h}{\delta\boldsymbol{\omega}}\right) \cdot \left(\nabla \times \frac{\delta\mathcal{H}}{\delta\boldsymbol{\omega}}\right) \mathrm{d}V$$
$$= \{\mathcal{F}, h, \mathcal{H}\}, \tag{18}$$

where the last equation defines the Nambu bracket for 3-D incompressible hydrodynamics based on the vorticity equation. Helicity is no longer a hidden conserved quantity but enters the dynamics on the same level as the Hamiltonian. Therefore, the Nambu mechanics is able to account explicitly for conservation laws of the system and correspondingly to its symmetries.

2.2. Geophysical Fluid Dynamics

A Nambu representation can be constructed also for some of the most important mathematical models relevant for geophysical fluid dynamics on large scales: the quasi-geostrophic potential vorticity equation [*Névir and Sommer*, 2009], the shallow water model [*Salmon*, 2005; *Sommer and Névir*, 2009], and the baroclinic stratified atmosphere [*Névir and Sommer*, 2009]. Other models of geophysical relevance can also be treated in this way, as, most notably, the Rayleigh-Bénard equations for two-dimensional convection, which have been studied in detail in *Bihlo* [2008] and *Salazar and Kurgansky* [2010]. We will not treat this latter case in this review.

2.2.1. Quasi-Geostrophic Approximation

Quasi-geostrophic (QG) theory is one of the most important and most studied pieces of geophysical fluid dynamics and is of crucial relevance for studying the large-scale dynamics of the Earth's atmosphere and ocean, and, more recently, of planetary atmospheres [*Holton*, 2004; *Pedlosky*, 1987; *Klein*, 2010]. QG dynamics is relevant when, within a good approximation, the fluid motions are (1) hydrostatic and (2) the Coriolis acceleration balances the horizontal pressure gradients. This is typically realized, e.g., in the atmospheric midlatitudes. In the absence of dissipative processes and of forcings, QG dynamics is described by the material conservation of the QG potential vorticity. We consider customary Cartesian coordinates plus time (x, y, z, t), where x indicates the zonal direction, y the meridional direction, and z the vertical direction as defined by gravity as in *Holton* [2004]. The evolution equation reads as follows:

$$\frac{\partial Q}{\partial t} + \frac{1}{f_0} \mathcal{J}(\Phi, Q) = 0,$$ (19)

where $\mathcal{J}$ is the Jacobian (8). Q is the QG approximation of Ertel's potential vorticity

$$Q = \omega_g + \frac{f_0}{N^2} \frac{\partial^2 \Phi}{\partial z^2} + f$$ (20)

with the geostrophic vorticity $\omega_g = 1/f_0 \nabla_h^2 \Phi$, geopotential Φ, ∇_h^2 is the Laplacian operator limited to the x and y directions, Brunt-Väisälä frequency N, and Coriolis parameter $f = f_0 + \bar{\beta} y$, where the effect of latitude-dependent planetary vorticity (beta effect) is included taking the beta-plane approximation. The geostrophic velocity $\boldsymbol{u_g}$ has nonzero components only along the x and y directions, so that we can write $\boldsymbol{u_g} = \left(\boldsymbol{u_g^h}, 0 \right)$, where $\boldsymbol{u_g^h} = 1/f_0 S \nabla_h \Phi = 1/f_0 (-\partial_y \Phi, \partial_x \Phi)$, where ∇_h is the gradient operator limited to the x and y directions.

The first conserved integral is the total energy of the system

$$\mathcal{H} = \frac{1}{2} \int \left[\left(\frac{\nabla_h \Phi}{f_0} \right)^2 + \left(\frac{1}{N} \frac{\partial \Phi}{\partial z} \right)^2 \right] dV,$$ (21)

where the first term is the density of kinetic energy and the second term is the density of potential energy. At each level z the geopotential acts as a stream function in defining the geostrophic velocity field, while the vertical derivative of the geopotential is proportional to the temperature fluctuations of the system [*Holton*, 2004]. The second conserved integral is the potential enstrophy

$$\mathcal{E} = \frac{1}{2} \int Q^2 dV,$$ (22)

which is defined similarly to the enstrophy in equation (6). One can prove that QG dynamics can be written in a Nambu form as follows:

$$\frac{\partial Q}{\partial t} = -\mathcal{J} \left(\frac{\delta \mathcal{E}}{\delta Q}, \frac{\delta \mathcal{H}}{\delta Q} \right),$$ (23)

Thus, the mathematical structure is analogous to the two-dimensional vorticity equation (9). Moreover, we can construct the evolution of any functional $\mathcal{F}[Q]$ by defining the Nambu bracket as follows:

$$\frac{d\mathcal{F}}{dt} = -\int \frac{\delta \mathcal{F}}{\delta Q} J \left(\frac{\delta \mathcal{E}}{\delta Q}, \frac{\delta \mathcal{H}}{\delta Q} \right) dV = \{\mathcal{F}, \mathcal{E}, \mathcal{H}\}$$ (24)

with $\delta \mathcal{E}/\delta Q = Q$ and $\delta \mathcal{H}/\delta Q = -\Phi/f_0$.

2.2.2. Shallow Water Model

Roughly speaking, shallow water equations are useful two-dimensional approximations of Navier-Stokes equations often used for describing some fluid motions where the horizontal scale of motion is much larger than its vertical extent, such as in the case of tidal waves or tsunami in the ocean, or Rossby and Kelvin waves in the atmosphere. Here the single-layer model is summarized [*Sommer and Névir*, 2009]. The dynamics is given by the evolution of the vorticity ω and the divergence $\mu = \nabla \cdot \boldsymbol{u}$ of the horizontal velocity $\boldsymbol{u}$

$$\partial_t \omega = -\nabla \cdot (\omega_a \boldsymbol{u}) \tag{25}$$

$$\partial_t \mu = k \cdot \nabla \times (\omega_a \boldsymbol{u}) - \nabla^2(\boldsymbol{u}^2/2 + g h_T) \tag{26}$$

$$\partial_t h_T = -\nabla \cdot (h_T \boldsymbol{u}), \tag{27}$$

where ρ is the density and h_T is the total height of the fluid and $\omega_a = \omega + f$ is the absolute vorticity. The shallow water model possesses two conserved integrals, the total energy, given by the sum of kinetic and potential energy

$$\mathcal{H} = \frac{1}{2} \int \rho \left(h_T \boldsymbol{u}^2 + g h_T^2 \right) \mathrm{d}A \tag{28}$$

and potential enstrophy

$$\mathcal{E} = \frac{1}{2} \int \rho q^2 h_T \mathrm{d}A \tag{29}$$

with the absolute potential vorticity $q = \omega_a / h_T$. The functional derivatives of the conserved integrals are $\delta\mathcal{H}/\delta\omega = -\rho\psi$, $\delta\mathcal{H}/\delta\mu = -\rho\gamma$, $\delta\mathcal{H}/\delta h_T = \rho\Psi$, $\delta\mathcal{E}/\delta\omega = \rho q$, $\delta\mathcal{E}/\delta\mu = 0$, and $\delta\mathcal{E}/\delta h_T = -(1/2)\rho q^2$, where ψ is the stream function, γ is the velocity potential for $h\boldsymbol{u} = S\nabla\psi + \nabla\gamma$, and $\Psi = (1/2)\boldsymbol{u}^2 + g h_T$ is the specific energy.

The Nambu representation of the shallow water model was derived by *Salmon* [2005] and is a bit more cumbersome than in, e.g., QG case. *Sommer and Névir* [2009] present a numerical simulation of these equations on a spherical grid, and *Névir and Sommer* [2009] published the multilayer shallow water equations. In the case of a single-layer shallow water equations, the dynamics of any functional $\mathcal{F}$ is determined by the sum of three Nambu brackets

$$\frac{\mathrm{d}}{\mathrm{d}t}\mathcal{F} = \{\mathcal{F}, \mathcal{H}, \mathcal{E}\}_{\omega,\omega,\omega} + \{\mathcal{F}, \mathcal{H}, \mathcal{E}\}_{\mu,\mu,\omega} + \{\mathcal{F}, \mathcal{H}, \mathcal{E}\}_{\omega,\mu,h_T} \tag{30}$$

The first bracket is

$$\{\mathcal{F}, ,\mathcal{H}, \mathcal{E}\}_{\omega,\omega,\omega} = \int J(F_\omega, ,\mathcal{H}_\omega)\mathcal{E}_\omega \mathrm{d}A \tag{31}$$

where $\mathcal{X}_\omega = \delta\mathcal{X}/\delta\omega$. Such first bracket is analogous to the 2-D Nambu bracket (9) (apart from the sign). For the other brackets we refer to *Salmon* [2005] and *Sommer and Névir* [2009]. *Salmon* [2007] calculated the Nambu brackets based on the velocities instead of vorticity.

2.2.3. Baroclinic Atmosphere

Névir and Sommer [2009] published the equations determining the dynamics of a baroclinic dry atmosphere in Nambu form (denoted as energy-vorticity theory of ideal fluid mechanics). The Nambu representation encompasses the Eulerian equation of motion in a rotating frame, the continuity equation, and the first law of thermodynamics. The Nambu dynamics uses three brackets for energy, helicity, energy-mass, and energy-entropy. Due to its special role in all three brackets, the integral of Ertel's potential enstrophy is coined as a super-Casimir.

The Nambu form shows an elegant structure where fundamental processes are combined by additive terms. Incompressible, barotropic, or baroclinic atmospheres are associated to additive contributions. Thus, approximations are simply attained by the neglect of terms.

In the absence of forcings and of dissipative processes, the momentum equation, the continuity equation, and the first law of thermodynamics equation are [*Peixoto and Oort*, 1992]

$$\partial_t \boldsymbol{u} = -\boldsymbol{u} \cdot \nabla \boldsymbol{u} - 2\boldsymbol{\Omega} \times \boldsymbol{u} - \frac{1}{\rho}\nabla p - \nabla \Phi \tag{32}$$

$$\partial_t \rho = -\nabla \cdot (\rho \boldsymbol{u}) \tag{33}$$

$$\partial_t s = -\boldsymbol{u} \cdot \nabla s, \tag{34}$$

where $\boldsymbol{u}$ is velocity, $\boldsymbol{\Omega}$ is the angular velocity of the Earth, Φ is the sum of the gravitational and centrifugal potential of the Earth, ρ is density, and s is the specific entropy per unit mass, determined by the equation of state of the gas.

These equations possess four conservation laws. The first is the total energy

$$\mathcal{H} = \int \rho e \, dV; \quad e = \frac{1}{2}\boldsymbol{u}^2 + i + \Phi, \tag{35}$$

where e is the specific total energy and i is its internal energy component. The absolute helicity is

$$h_a = \int \boldsymbol{u}_a \cdot \boldsymbol{\omega}_a \, dV, \tag{36}$$

where the absolute velocity is $\boldsymbol{u}_a = \boldsymbol{u} + \boldsymbol{\Omega} \times \boldsymbol{r}$ and $\boldsymbol{\omega}_a = \nabla \times \boldsymbol{u} + 2\boldsymbol{\Omega}$, with the angular velocity of the Earth $\boldsymbol{\Omega}$, and $\boldsymbol{r}$ is the position vector. The total mass and entropy are given by

$$\mathcal{M} = \int \rho \, dV, \quad \mathcal{S} = \int \rho s \, dV, \tag{37}$$

and the total potential enstrophy is defined starting from Ertel's potential vorticity Π

$$\mathcal{E}_\rho = \int \rho \Pi^2 \, dV, \quad \Pi = \frac{\boldsymbol{\omega}_a \cdot \nabla s}{\rho}, \tag{38}$$

analogously to the definition in the QG context given in equation (22). The functional derivatives of the conservation laws are $\delta\mathcal{H}/\delta\boldsymbol{u} = \rho\boldsymbol{u}$, $\delta\mathcal{H}/\delta\rho = (1/2)\boldsymbol{u}^2 + i + p/\rho - Ts + \phi$, $\delta\mathcal{H}/\delta\sigma = T$, $\delta\mathcal{M}/\delta\boldsymbol{u} = 0$, $\delta\mathcal{M}/\delta\rho = 1$, $\delta\mathcal{M}/\delta\sigma = 0$, $\delta\mathcal{S}/\delta\boldsymbol{u} = 0$, $\delta\mathcal{S}/\delta\rho = s$, $\delta\mathcal{S}/\delta\sigma = 1$, $\delta h_a/\delta\boldsymbol{u} = \boldsymbol{\omega}_a$, $\delta h_a/\delta\rho = 0$, and $\delta h_a/\delta\sigma = 0$, where T is temperature and $\sigma = \rho s$.

An arbitrary functional $\mathcal{F}$ of $\boldsymbol{u}$, ρ, and σ evolves according to the sum of three brackets which are defined below

$$\frac{d}{dt}\mathcal{F} = \{\mathcal{F}, h_a, \mathcal{H}\}_h + \{\mathcal{F}, M, \mathcal{H}\}_m + \{\mathcal{F}, S, \mathcal{H}\}_s. \tag{39}$$

The three brackets are defined below. The first one is the so-called helicity bracket,

$$\{\mathcal{F}, h_a, \mathcal{H}\}_h = -\int \left[\frac{1}{\rho}\frac{\delta\mathcal{F}}{\delta\boldsymbol{u}} \cdot \left(\frac{\delta h_a}{\delta\boldsymbol{u}} \times \frac{\delta\mathcal{H}}{\delta\boldsymbol{u}} \right) \right] dV; \tag{40}$$

the second is the so-called mass bracket,

$$\{\mathcal{F}, \mathcal{M}, \mathcal{H}\}_m = -\int \left[\frac{\delta\mathcal{M}}{\delta\rho}\frac{\delta\mathcal{F}}{\delta\boldsymbol{u}} \cdot \nabla\frac{\delta\mathcal{H}}{\delta\rho} + \frac{\delta\mathcal{F}}{\delta\rho}\nabla \cdot \left(\frac{\delta\mathcal{M}}{\delta\rho}\frac{\delta\mathcal{H}}{\delta\boldsymbol{u}} \right) \right] dV + cyc(\mathcal{F}, \mathcal{M}, \mathcal{H}); \tag{41}$$

where cyc indicates permutations in cyclic order of the arguments. The third one is the so-called entropy bracket,

$$\{\mathcal{F}, \mathcal{S}, \mathcal{H}\}_s = -\int \left[\frac{\delta\mathcal{S}}{\delta\rho}\frac{\delta\mathcal{F}}{\delta\boldsymbol{u}} \cdot \nabla\frac{\delta\mathcal{H}}{\delta\sigma} + \frac{\delta\mathcal{F}}{\delta\sigma}\nabla \cdot \left(\frac{\delta\mathcal{S}}{\delta\rho}\frac{\delta\mathcal{H}}{\delta\boldsymbol{u}} \right) \right] dV + cyc(\mathcal{F}, \mathcal{S}, \mathcal{H}). \tag{42}$$

For a barotropic flow the first law of thermodynamics is physically not relevant and the entropy bracket is discarded in (39) because the functional derivatives with respect to σ vanish. The continuity equation remains unapproximated, and the pressure gradient term is replaced by the gradient of enthalpy. Note the different brackets for helicity (40) and vorticity (18) in 3-D hydrodynamics.

LUCARINI ET AL.   8

2.3. Conservative Algorithms and Numerical Models

Salmon [2005, 2007] recognized that the existence of a Nambu bracket with two conserved integrals allows the design of high-precision numerical algorithms for studying geophysical flows. The idea is in fact simple: just like in the usual case we aim at writing numerical codes able to conserve energy when dissipation and forcing are neglected; Nambu mechanism provides encouragement and conceptual support for expanding this point of view by encompassing other important physical quantities. The approach is useful in GFD turbulence simulations because these flows are characterized by the existence of conservation laws besides total energy. In particular, the conservation of enstrophy inhibits spurious accumulation of energy at small scales.

For the numerical design of conservative codes based on a Nambu structure, the following remarks are noted:

1. A Nambu form of the continuous physical system is required.
2. The quantities used in the Nambu bracket are conserved.
3. The discrete form of the Jacobian needs to preserve its antisymmetry.
4. The approach is applicable to any kind of discretization, e.g., for finite differences, finite volumes, or spectral models.
5. Arbitrary approximations of the conservation laws are possible; these approximations are conserved exactly.
6. For the barotropic vorticity equation the classic Arakawa Jacobian could be retrieved by equally weighting the cyclic permutations of the Nambu bracket. In other terms, Arakawa found heuristically a discrete Nambu representation of barotropic dynamics [*Dubinkina and Frank*, 2007].

In recent years, various authors have provided promising examples of actual implementations of GFD codes which take into explicit consideration the underlying Nambu dynamics of the unforced and inviscid case. *Salmon* [2007] presents the first numerical simulation of a shallow water model derived from the Nambu brackets formalism. The simulation is on a square rectangular grid, and the design on an unstructured triangular mesh is outlined.

Sommer and Névir [2009] report the first simulation of a shallow water atmosphere using Nambu brackets. The authors use an isosahedric grid (as in the Icosahedric Nonhydrostatic (ICON) model of the German Weather Service and the Max Planck Institute for Meteorology, Hamburg). The construction of the algorithm is as follows [*Sommer and Névir*, 2009]:

1. First, the continuous versions of the Nambu brackets and conservation laws need to be obtained.
2. On the grid, the following expressions need to be calculated: functional derivatives, discrete operators (div and curl), and discretization of the Jacobian and the Nambu brackets.
3. Finally, the prognostic equations are obtained by inserting the variables in the brackets. Various options are available for the time stepping is arbitrary; *Sommer and Névir* [2009] use a leapfrog with Robert-Asselin filter.

The authors find quasi-constant enstrophy and energy compared to a standard numerical design (Figure 1).

Along these lines, *Gassmann and Herzog* [2008] suggest a radically new concept for a global numerical simulation of the nonhydrostatic atmosphere using the Nambu representation for the energy-helicity bracket $\{\mathcal{F}, h_a, \mathcal{H}\}$ given in equation (40) [*Névir*, 1998]. Their suggestion incorporates a careful description of Reynolds averaged subscale processes and budgets. *Gassmann* [2013] describes a global nonhydrostatic dynamical core based on an icosahedral nonhydrostatic model on a hexagonal C-grid. The model conserves mass and energy in a noncanonical Hamiltonian framework, even if some still unsolved numerical problems occur when the non-hydrostatic compressible equations are in a Nambu bracket form. The use of dynamical cores constructed according to the sophisticated version of fluid dynamics discussed here might provide crucial for improving the ability of atmospheric models in representing correctly the global budgets of physically relevant quantities also in the case when forcing and dissipative processes are taken into account. As discussed by *Lucarini and Ragone* [2011] for the case of energy, this is far from being a trivial task.

2.4. Perspectives

Like Hamiltonian mechanics, the Nambu approach is a versatile tool for the analysis and simulation of dynamical systems. Here some possible research directions are outlined.
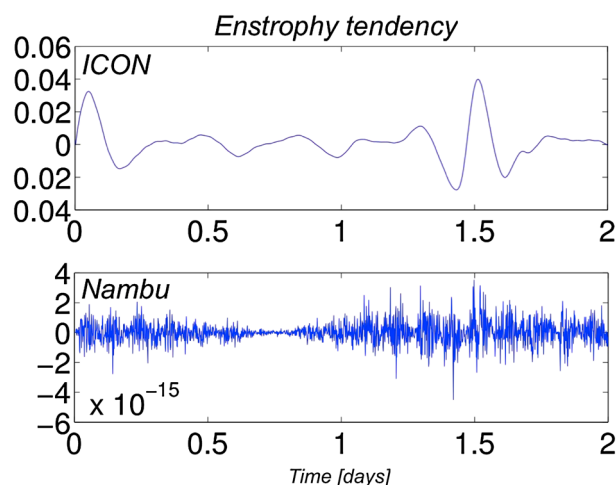
Figure 1. Enstrophy tendencies in the enstrophy conserving ICON shallow water model and the Nambu model of *Sommer and Névir* [2009] (courtesy of Matthias Sommer, Ludwig-Maximilians-Universität München). Note that the tendency in the Nambu model is of the order of the numerical accuracy.

Modular Modeling and Approximations. In several applications a Nambu representation can be found by adding brackets which conserve a particular Casimir; this is already mentioned by *Nambu* [1973]; see the baroclinic atmosphere [*Névir and Sommer*, 2009] and the classification by *Salazar and Kurgansky* [2010]. The dynamics is determined by these "constitutive" Casimirs (a notion coined in *Névir and Sommer* [2009]) which are not conserved in the complete system. Decomposition leads to subsystems where the constitutive Casimirs are conserved. An example is helicity which is constitutive in the baroclinic atmosphere and only conserved in the 3-D incompressible flow. The decomposition is directly associated with approximations [*Névir and Sommer*, 2009]. Composition allows a process-oriented model design.

Statistical Mechanics. The statistical mechanics of fluids is characterized by the existence of conservation laws besides total energy [*Bouchet and Venaille*, 2012] (see also section 3 in this review). Thus, these conservation laws have a twofold impact: They determine the dynamics in a Nambu bracket and the canonical probability distribution in equilibrium.

Dynamics of Casimirs. Casimir functions of a conservative system are ideal observables to characterize the dynamics in the presence of forcing and dissipation. This might prove especially interesting when studying the response of a system to perturbations in the context of the Response theory proposed by *Ruelle* [1997, 1998a, 1998b, 2009] and recently used in a geophysical context by various authors with promising results [*Eyink et al.*, 2004; *Abramov and Majda*, 2008; *Lucarini*, 2009; *Lucarini and Sarno*, 2011] (see also section 5 in this review).

As illuminating example, we mention the recent work of *Pelino and Maimone* [2007] and *Gianfelice et al.* [2012], who have used recurrence maps of extremes of energy and a Casimir in a Lorenz-like map to assess predictability of the system and study the properties of the invariant measure.

3. Equilibrium Statistical Mechanics for Geophysical Flows

We have seen in the previous section that different models of geophysical flows have a specific mathematical structure: they are Hamiltonian systems and have an infinite number of conserved quantities—the Casimirs. The previous section has shown how one could take advantage of these features and construct theoretically rich representation of the dynamics and provide proposals for constructing new numerical codes of GFD flows. This section goes in the direction of constructing a probabilistic description of GFD flows, basically taking the point of view that due to the large amount of degrees of freedom involved, one can consider the state of the atmosphere and the ocean as random variables. Here we shall review the progress that has been made by using the simplest class of possible probability distributions: the equilibrium distributions depending only on the conserved quantities. However, most of the standard applications of equilibrium statistical mechanics deal with dynamics on a finite dimensional phase space (e.g., a gas with a finite number of molecules), with a finite number of dynamical invariants (often just the energy). The equations describing the dynamics of geophysical flows violate both these constraints. Several solutions have thus been proposed: they are reviewed briefly in the next sections, going from the main fundamental ideas to selected geophysical applications.

3.1. Finite-Dimensional Models: Point Vortices
3.1.1. Negative Temperature States and Clustering of Vortices
Onsager [1949] was the first to understand that the coherent structures and persistent circulations that appear ubiquitously in planetary atmospheres and in the Earth's oceans could be explained on statistical
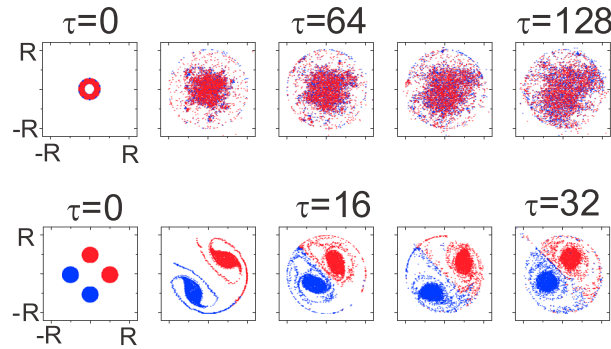
Figure 2. Time evolution for a numerical simulation of two-sign point vortices (shown in red and blue), for (top row) positive temperatures and (bottom row) negative temperatures. For negative temperatures, we observe the clustering of same-sign vortices, while for positive temperatures, positive and negative vortices are distributed homogeneously in the domain. Reprinted with permission from *Yatsuyanagi et al.* [2005]. Copyright (2005) by the American Physical Society.

grounds. His work focused on 2-D incompressible, inviscid fluids given in equation (2). To make the system tractable, he introduced an approximation of the vorticity field in terms of N point vortices with *circulation* γ_i and position $\mathbf{r}_i(t)$: $\omega(\mathbf{r}, t) = \sum_{i=1}^{N} \gamma_i \delta(\mathbf{r}_i(t) - \mathbf{r})$, where $\delta(x)$ is the usual Dirac's delta distribution. Introducing the Hamiltonian $\mathcal{H} = -\sum_{i<j} \gamma_i \gamma_j G(\mathbf{r}_i, \mathbf{r}_j)$, where G is the Green function of the Laplacian (the response to an impulse source: $\Delta G(\mathbf{r}_i, \mathbf{r}_j) = \delta(\mathbf{r}_i - \mathbf{r}_j)$), the dynamics reads simply

$$\gamma_i \frac{dx_i}{dt} = \frac{\partial \mathcal{H}}{\partial y_i}, \quad \gamma_i \frac{dy_i}{dt} = -\frac{\partial \mathcal{H}}{\partial x_i}. \quad (43)$$

This is a canonical Hamiltonian system with a finite number of degrees of freedom, for which the standard methods of statistical mechanics apply directly. In particular, the *microcanonical* probability measure, acting as invariant—i.e., unaltered by the dynamics—measure of the system, assigning a uniform probability to all the configurations with a given energy, is given by

$$\rho(\{\mathbf{r}_i\}_{1 \leq i \leq N}) = \frac{\delta(\mathcal{H}(\{\mathbf{r}_i\}_{1 \leq i \leq N}) - E)}{\Omega(E)}, \quad (44)$$

where $\Omega(E)$ is the *structure function*, which measures the volume in phase space occupied by configurations with energy E. It is easily proved that, for a bounded domain, and hence a finite volume phase space, this function reaches a maximum for a given value of the energy. Hence, the thermodynamic entropy $S(E) = k_B \ln \Omega(E)$ decreases for a range of energies, and the statistical temperature $1/T = \partial S/\partial E$ becomes negative. Negative temperatures, although counterintuitive, have since been commonly encountered in the study of other systems with long-range interactions [*Dauxois et al.*, 2002] and correspond to self-organized states. Here the energy increases when two same-sign vortices move closer, while it decreases for opposite signs. When the temperature is negative, configurations with maximum energy are favored. Hence, negative temperature equilibrium states exhibiting clusters of same-sign vortices are expected. This behavior has been confirmed by numerical simulations with up to $N = 6724$ point vortices (see Figure 2).

3.1.2. Mean-Field Equation

The above argument is qualitative; to characterize the coherent structures which are expected to emerge from the clustering of same-sign vortices, we introduce the probability density $\rho_i(\mathbf{r}, t)$ for a vortex with strength γ_i to be found at point $\mathbf{r}$ at time t. It satisfies the normalization $\int \rho_i(\mathbf{r}, t)d\mathbf{r} = 1$. We define a *coarse-grained* vorticity field $\overline{\omega}(\mathbf{r}, t) = \sum_i \gamma_i \rho_i(\mathbf{r}, t)$. This probability density is expected to converge toward its statistical equilibrium: the equilibrium distribution maximizes the statistical entropy $\mathcal{S} = -\sum_i \int \rho_i(\mathbf{r}) \ln \rho_i(\mathbf{r}) d\mathbf{r}$. The solution of this variational problem is given by $\rho_i(\mathbf{r}) = e^{\beta(\gamma_i \overline{\psi}(\mathbf{r}) + \mu_i)}/\mathcal{Z}$, where β (inverse temperature) and $\beta \mu_i$ are the Lagrange parameters associated with conservation of global energy and normalization of each ρ_i, respectively, and $\overline{\psi} = \Delta^{-1}\overline{\omega}$ is the coarse-grained stream function, while the normalization factor $\mathcal{Z}$ is called the *partition function*. Averaging over this equilibrium distribution gives the coarse-grained vorticity field, which satisfies the *mean-field equation*:

$$\overline{\omega}(\mathbf{r}) = \frac{1}{\mathcal{Z}} \sum_i \gamma_i e^{\beta(\gamma_i \overline{\psi}(\mathbf{r}) + \mu_i)}. \quad (45)$$

This is an equation of the form $\omega = F(\psi)$, characteristic of the steady states of the 2-D Euler equations. A well-known particular case is that of N vortices with circulation $1/N$ and N vortices with circulation $-1/N$. In that case, the mean-field equation can be recast as $\omega = A \sinh(\beta \Psi)$, with $\Psi = \psi - (\mu_+ - \mu_-)/2$ [*Montgomery and Joyce*, 1974].

The theory can be generalized in a straightforward manner to quasi-geostrophic (QG) flows [*Miyazaki et al.*, 2011]. *DiBattista and Majda* [2001] have given solutions of the mean-field equation for a two-layer

model—i.e., a QG model where the stream function is defined only at two discrete values of the vertical coordinate and the temperature is defined at the interface between such level [*Holton*, 2004]—where the point vortices stand for *hetons*, introduced by *Hogg and Stommel* [1985] as a model of individual convective towers in the ocean. They have shown that a background barotropic current (the *barotropic governor*) confines potential vorticity and temperature anomalies, thereby suppressing the baroclinic instability, in agreement with numerical simulations [*Legg and Marshall*, 1993].

The point vortex model suffers from a number of limitations inherent to the approach. First of all, when we let the number of vortices tend to infinity (the *thermodynamic limit*), we have to introduce an ad hoc scaling of the Lagrange parameters to retain the organized, negative temperature states. Besides, there is no unique way to approximate a vortex patch by a finite number of vortices. A consequence is also that the area of vorticity patches cannot be conserved in this singular formulation. We shall see in section 3.3 that dealing directly with the vorticity field will solve these issues while predicting a relation between vorticity and stream function very similar to the one obtained above.

3.2. Finite-Dimensional Models: Truncated Fourier Modes
3.2.1. Two-Dimensional Turbulence

Rather than a discretization in physical space, one may consider a finite number of modes in Fourier space, as proposed by *Lee* [1952] and *Kraichnan* [1967] in the context of the Euler equations. For 2-D flows—for simplicity, we consider here a rectangular geometry with periodic boundary conditions; the case of a spherical geometry can be found in *Frederiksen and Sawford* [1980]—writing the vorticity field as a truncated Fourier series $\omega(\mathbf{x}) = \sum_{\mathbf{k}} \hat{\omega}(\mathbf{k}) e^{i\mathbf{k}\cdot\mathbf{x}}$, the evolution in time of the Fourier coefficients follows an equation of the form $\partial_t \hat{\omega}(\mathbf{k}) = \sum_{\mathbf{p},\mathbf{q}} A_{\mathbf{kpq}} \hat{\omega}(\mathbf{p})\hat{\omega}(\mathbf{q})$, where the summation is restricted to a finite set of wave vectors $\mathcal{B} = \{\mathbf{k} \in 2\pi/L\ \mathbb{Z}^3, k_{\min} \leq k \leq k_{\max}\}$ and $A_{\mathbf{kpq}}$ takes care of the quadratic nonlinearity terms. This dynamics preserves two quadratic quantities: the energy $E = \sum_{\mathbf{k}} |\hat{\omega}(\mathbf{k})|^2/(2k^2)$ and the enstrophy $\Gamma_2 = \sum_{\mathbf{k}} |\hat{\omega}(\mathbf{k})|^2$. *Kraichnan* [1967] suggested to consider the canonical probability distribution:

$$\rho(\{\hat{\omega}(\mathbf{k})\}_{\mathbf{k}\in\mathcal{B}}) = \frac{e^{-\beta E - \alpha \Gamma_2}}{\mathcal{Z}}. \tag{46}$$

In particular, the average energy at *absolute equilibrium* is given by

$$\langle E \rangle = -\frac{\partial \ln \mathcal{Z}}{\partial \beta} = \frac{1}{2} \sum_{\mathbf{k}\in\mathcal{B}} \frac{1}{\beta + 2\alpha k^2}, \tag{47}$$

which corresponds to an equipartition spectrum for the general invariant $\beta E + \alpha \Gamma_2$: $E(k) = \pi k/(\beta + 2\alpha k^2)$, where $E(k)$ is the energy of all the modes with wavenumber k. Inviscid numerical runs indeed relax to this spectrum [*Fox and Orszag*, 1973; *Basdevant and Sadourny*, 1975]. Note that the Lagrange parameters α and β cannot take arbitrary values; they are constrained by the *realizability* condition—for the Gaussian integral defining $\mathcal{Z}$ to converge. Here this condition reads $\beta + 2\alpha k_{\min}^2 > 0$ and $\beta + 2\alpha k_{\max}^2 > 0$. In particular, when $\alpha > 0$, negative temperatures can be attained. In this regime, which corresponds to $\langle \Gamma_2 \rangle/(2\langle E \rangle)$ small enough [*Kraichnan and Montgomery*, 1980], the energy spectrum is a decreasing function of k. When $\beta \rightarrow -2\alpha k_{\min}^2$, a singularity appears at $k \rightarrow k_{\min}$, which means that the energy is expected to concentrate in the largest scales. Hence, statistical mechanics for the truncated system predicts that when the enstrophy is small enough compared to the energy, we expect the energy to be transferred to the large scales. *Kraichnan* [1967] gives other arguments to support and refine this view; in particular he shows the existence of two inertial ranges, with a constant flux of energy and enstrophy, respectively, with the energy spectrum scaling as $E(k) \sim C\varepsilon^{2/3}k^{-5/3}$ and $E(k) \sim C'\eta^{2/3}k^{-3}$, respectively, where ε and η are the energy and enstrophy fluxes. In particular, the equilibrium energy spectrum at large scales is shallower than the energy inertial range spectrum. Assuming a tendency for the system to relax to equilibrium—although the equilibrium is never attained in the presence of forcing and dissipation—we thus expect the flux of energy to be towards the large scales; a process referred to as the *inverse cascade* of 2-D turbulence. Similarly, the transfer of enstrophy in the corresponding inertial range should be towards the small scales. The dual cascade scenario has been confirmed both by numerical simulations [*Boffetta*, 2007] and laboratory experiments [*Paret and Tabeling*, 1997].

3.2.2. Quasi-Geostrophic Turbulence

The dynamical equations of QG flow are very similar to the Euler equations, replacing vorticity by potential vorticity (see section 2.2.1). In particular, they conserve similar quadratic invariants, and the theory can
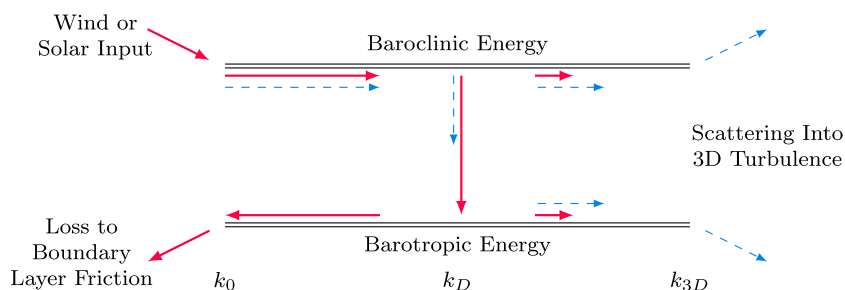
Figure 3. Energy (solid arrows) and potential enstrophy (dashed arrows) flux diagram for two-layer quasi-geostrophic turbulence, taking inspiration from *Salmon* [1978]. The energy injected in the baroclinic mode at large scales is cascaded downscale until the deformation scale is reached, then it is transferred to the barotropic mode and cascaded upscale like in 2-D turbulence, in agreement with the predictions of equilibrium statistical mechanics.

be extended in a straightforward manner [*Holloway*, 1986; *Salmon*, 1998]. We will discuss in this section the effect of stratification and beta effect, resulting from the fact that the planetary vorticty depends on the latitude.

Perhaps the simplest framework to consider the role of stratification is the two-layer QG case. As in section 3.2.1, a canonical probability distribution can be constructed, taking into account the three invariants: the total energy E and the potential enstrophies of each layer, Z_1 and Z_2. The corresponding partition function can be computed, and the spectrum studied in the various regimes, with similar results. In particular, negative temperature states are accessible, which correspond to condensation of the energy on the largest horizontal scales and the *Fofonoff* [1954] solutions mentioned below. Maybe more interestingly, although the various forms of energy (kinetic energy K_1, K_2 in each layer and potential energy P) are not individually conserved, we can compute their average value at equilibrium, as *Salmon et al.* [1976] did. Alternatively, the standard decomposition in terms of the barotropic and baroclinic modes (constructed by taking the average and the difference of the stream functions in the two layers), with their kinetic energies K_T and K_B, can be used. As *Salmon et al.* [1976] highlighted, the Rossby deformation scale $k_D = 2\pi/R_D$ plays an important role. $R_D = NH/f_0$, where H is the vertical extent of the domain and f_0 is the reference Coriolis parameter, defines the typical horizontal scale of perturbations of vertical extent equal to H, with $N/f_0 \gg 1$ defining the typical geometric aspect ratio. At scales smaller than the deformation scale ($k \gg k_D$), the two layers behave essentially as two independent copies of 2-D turbulence; the energy spectrum in each layer is the same as in the 2-D case, the correlation at statistical equilibrium is low, and there is about as much energy in the barotropic mode and the baroclinic mode: $\langle K_T(k)\rangle/\langle K_B(k)\rangle \sim 1$. Besides, the potential energy is small compared to the kinetic energy: $\langle P(k)\rangle/\langle K_T(k)\rangle = O(k_D/k)$. At scales larger than the deformation radius ($k \ll k_D$), the system rather behaves as a unique barotropic layer: the amount of energy in the two layers is about the same, but the energy is essentially in the barotropic mode, with negligible energy in the baroclinic mode, and a statistical correlation between the two layers of order 1. This theoretical analysis goes in strong support of the standard picture of two-layer QG turbulence, developed on phenomenological grounds [*Salmon*, 1978; *Rhines*, 1979, see also *Vallis*, 2006, chapter 9] and is in agreement with numerical simulations [*Rhines*, 1976]. See also Figure 3. These results have been extended to an arbitrary number of layers and to continuously stratified flows by *Merryfield* [1998]. Although the equilibrium mean, vertically integrated stream function remains similar to the two-layer case, the distribution of the statistics on the vertical differs as higher-order moments are considered. The ratio of potential to kinetic energy, for instance, can become significantly underestimated, especially in the limit of strong stratification ($k_D \rightarrow 0$) where the two-layer model does not capture well the possibility that an important fraction of the energy may be trapped near the bottom.

The second dominant effect in geophysical flows, in addition to stratification, is rotation. The Coriolis force introduces a linear term in the equations, which does not affect directly the previous analysis of the nonlinear energy transfers: the conserved quantities remain the same and the statistical theory is easily extended by replacing relative vorticity with absolute vorticity. However, the variation of the Coriolis force with latitude is responsible for the appearance of Rossby waves, which modify the physical interpretation of the predicted cascade of energy. As anticipated by *Rhines* [1975] and verified numerically [e.g., *Vallis and Maltrud*, 1993], the Rossby waves deflect the inverse energy cascade: they dominate over nonlinear effects

in a part of Fourier space and prevent access to low wave numbers along one direction in Fourier space. This leads to the preferential formation of zonal flows.

3.2.3. Beyond Balanced Motion

Although the large-scale motions of the atmosphere and oceans of the Earth are very close to geostrophic and hydrostatic balance, these relations break up when moving down to the mesoscale, and the transfers of energy due to turbulence, or the nonlinear interaction of inertia-gravity waves, might not follow the inverse cascade scenario described in sections 3.2.1 and 3.2.2. As a matter of fact, a downscale transfer of energy is needed in the ocean to feed enhanced vertical mixing [e.g., *Ledwell et al.*, 2000] or small-scale dissipation in the ocean interior [*Nikurashin et al.*, 2013]. Such processes are necessary to close the energy budget of the ocean [*Wunsch and Ferrari*, 2004]. It is therefore natural to ask how equilibrium statistical mechanics can help understanding how energy is exchanged by nonlinear interactions between the slow, balanced motions and the fast, wave motions.

Errico [1984] first observed a tendency for unforced inviscid flows described by hydrostatic primitive equations to reach an energy equipartition state, in which the energy in the fast wave modes is comparable to that in the slow balanced modes. The study by *Warn* [1986], in the context of the shallow water equations, essentially confirms that QG flows are not equilibrium states and that a substantial part of the energy may end up in the fast (surface) wave modes at statistical equilibrium, implying a direct cascade of energy to the small scales. *Bartello* [1995] has obtained analytically the equilibrium energy spectrum for the Boussinesq equations (neglecting the nonlinear part of potential vorticity), in the presence of rotation, confirming the direct cascade of energy. In particular, there is no negative temperature states in this case, due to the presence of the inertia-gravity waves. In fact, numerical simulations [*Pouquet and Marino*, 2013] indicate that turbulence with rotation and stratification might have at the same time an inverse and a direct cascade of energy. A natural interpretation would be that vortical modes are responsible for the inverse cascade while waves cascade energy downscale simultaneously. *Bartello* [1995] had discussed the possibility of a wave-vortical mode decoupling on the basis of resonant triadic interactions. Without any assumptions on the dynamics, another interpretation in the statistical mechanics framework uses an analogy with metastable states: restricting the equilibrium probability distribution to the slow manifold yields an inverse cascade, while taking into account the whole phase space including the waves results in a direct cascade [*Herbert et al.*, 2014].

3.3. The Mean-Field Theory for the Continuous Vorticity Field
3.3.1. Mean-Field Theory

Above, we have considered finite-dimensional models conserving at most two quadratic quantities, the energy and the enstrophy. In fact, the majority of the flows considered above—and in particular 2-D and QG flows—conserve an infinite family of invariants, called Casimir invariants: for any function s, $\int s(\omega)d\mathbf{r}$ is conserved (see equation (5)). The specific case $s_n(x) = x^n$ corresponds to the moments of the vorticity distribution. Instead, the conservation of $s_\sigma(x) = \delta(x - \sigma)$ implies that the area $\gamma(\sigma)$ where the vorticity takes value σ is conserved. This is due to the absence of a vortex stretching term, in contrast with full 3-D flows; here the vorticity (or potential vorticity, in the QG case) patches are stirred in such a way that their area remains conserved. The theory developed by *Miller* [1990] and *Robert and Sommeria* [1991] (see also *Bouchet and Venaille* [2012] for a review) introduces a coarse-grained vorticity field $\overline{\omega}$, which corresponds to the macroscopic state of the flow. This coarse-grained vorticity field can be predicted based on the invariants using statistical mechanics. To do so, we introduce $\rho(\sigma, \mathbf{r})$, the probability density for the vorticity field to take value σ at point $\mathbf{r}$. The coarse-grained vorticity field is given by $\overline{\omega}(\mathbf{r}) = \int_{-\infty}^{\infty} \sigma \rho(\sigma, \mathbf{r})d\sigma$. The invariants of the system are the energy

$$\mathscr{E}[\rho] = \int_{D^2} d\mathbf{r}d\mathbf{r}' \int_{\mathbb{R}^2} d\sigma d\sigma' \sigma\sigma' G(\mathbf{r}, \mathbf{r}')\rho(\sigma, \mathbf{r})\rho(\sigma', \mathbf{r}'), \qquad (48)$$

with G the Green function of the Laplacian, and the Casimir invariants

$$\mathscr{G}_n[\rho] = \int_D d\mathbf{r} \int_{\mathbb{R}} d\sigma \sigma^n \rho(\sigma, \mathbf{r}), \qquad (49)$$

or equivalently, the vorticity levels

$$\mathscr{D}_\sigma[\rho] = \int_D d\mathbf{r}\rho(\sigma, \mathbf{r}). \qquad (50)$$

The idea of the theory is to select the probability distribution ρ which maximizes a *mixing entropy* $\mathscr{S}[\rho] = -\int_D \int_{\mathbb{R}} \mathrm{d}\mathbf{r}\mathrm{d}\sigma\rho(\sigma,\mathbf{r})\ln\rho(\sigma,\mathbf{r})$, under the constraints of conservation of the invariants, and pointwise normalization $\mathscr{N}[\rho](\mathbf{r}) = \int_{\mathbb{R}} \mathrm{d}\sigma\rho(\sigma,\mathbf{r}) = 1$. Hence, we are interested in the variational problem:

$$S(E, \{\Gamma_n\}_n) = \max_{\rho,\mathscr{N}[\rho](\mathbf{r})=1}\{\mathscr{S}[\rho] \mid \mathscr{E}[\rho] = E, \forall n \in \mathbb{N}, \mathscr{G}_n[\rho] = \Gamma_n\}, \tag{51}$$

or equivalently,

$$S(E, \gamma) = \max_{\rho,\mathscr{N}[\rho](\mathbf{r})=1}\{\mathscr{S}[\rho] \mid \mathscr{E}[\rho] = E, \forall \sigma \in \mathbb{R}, \mathscr{D}_\sigma[\rho] = \gamma(\sigma)\}. \tag{52}$$

The solutions of this variational problem correspond to the most probable states for a given set of conserved quantities.

The critical points of the variational problem (52) are simply given by $\delta\mathscr{S} - \int \mathrm{d}\mathbf{r}\zeta(\mathbf{r})\delta\mathscr{N}(\mathbf{r}) - \beta\delta\mathscr{E} - \int \mathrm{d}\sigma\alpha(\sigma)\delta\mathscr{D}_\sigma = 0$, where β and $\alpha(\sigma)$ are the Lagrange multiplier associated with the conservation constraints. One obtains the solution

$$\rho(\sigma,\mathbf{r}) = \frac{1}{\mathcal{Z}}e^{\beta\sigma\overline{\psi}(\mathbf{r})-\alpha(\sigma)}, \tag{53}$$

so that the coarse-grained vorticity is given by

$$\overline{\omega} = F(\overline{\psi}), \quad \text{with } F(\overline{\psi}) = \frac{1}{\beta}\frac{\delta\ln\mathcal{Z}}{\delta\overline{\psi}}, \tag{54}$$

and $\mathcal{Z}(\overline{\psi}) = \int_{\mathbb{R}} \mathrm{d}\sigma e^{\beta\sigma\overline{\psi}-\alpha(\sigma)}$. To compute the equilibrium states of the system, one should solve the partial differential equation (54), referred to as the mean-field equation, and check afterward that the obtained critical points are indeed maxima of the constrained variational problem by considering the second derivatives. This will automatically ensure that the equilibrium states are nonlinearly stable steady states [*Chavanis*, 2009].

3.3.2. Equilibrium States for 2-D and Barotropic Flows

The mean-field equation (54) is in general difficult to solve; one issue is that the $\overline{\omega} - \overline{\psi}$ relation is in general nonlinear. Most of the analytical solutions have been obtained in the linear case, by decomposing the fields on a basis of eigenfunctions of the Laplacian on the domain $\mathcal{D}$. This technique was first introduced in a rectangular domain by *Chavanis and Sommeria* [1996], who showed that the statistical equilibrium is either a monopole or a dipole, depending on the aspect ratio (Figure 4). The same method was extended to the case of barotropic flows, replacing vorticity by potential vorticity. Taking into account the beta effect, *Fofonoff* [1954] flows are obtained as statistical equilibria in a rectangular basin [*Naso et al.*, 2011; *Venaille and Bouchet*, 2011]. Such solutions correspond to flows with two gyres (anticyclonic in the northern basin, cyclonic in the southern basin) in a rectangular basin (see Figure 5). The relative vorticity is confined to a boundary layer, whose width decreases with the total energy or when the beta effect (i.e., the relative strength of the gradient of the planetary vorticity) increases. The flow is westward in the interior of the basin, with an eastward compensating flow near the boundaries.

Different geometries can be studied: in a rotating sphere, the equilibria, in the linear limit, can be either solid-body rotations, dipole flows [*Herbert et al.*, 2012], or quadrupoles, taking into account conservation of angular momentum [*Herbert*, 2013]. In the latter case, a perturbative treatment of the nonlinearity in the $\overline{\omega}$-$\overline{\psi}$ relationship leads to the same flow topology, but sharper vortex cores [*Qi and Marston*, 2014]. *Bouchet and Simonnet* [2009] have also considered the role of a small nonlinearity in the $\overline{\omega}$-$\overline{\psi}$ relationship for a rectangular domain of aspect ratio close to 1, with periodic boundary conditions, thereby obtaining two topologies for the equilibrium states: dipole and unidirectional flows. Adding a small stochastic forcing generates transitions from one to the other equilibrium.

3.3.3. Stratified Flows

In addition to the 2-D and quasi-2-D cases mentioned above, the theory has also been applied to stratified fluids (essentially in the quasi-geostrophic regime). *Herbert* [2014] has obtained and classified the statistical equilibria of the two-layer QG model in the framework of the Robert-Miller-Sommeria theory, and updated the discussion of the vertical distribution of energy at statistical equilibrium (see section 3.2.2): in particular, it is shown that even at statistical equilibrium, there will remain some residual energy in the baroclinic mode, unless the initial vertical profile of fine-grained enstrophy is uniform. In the context of continuously
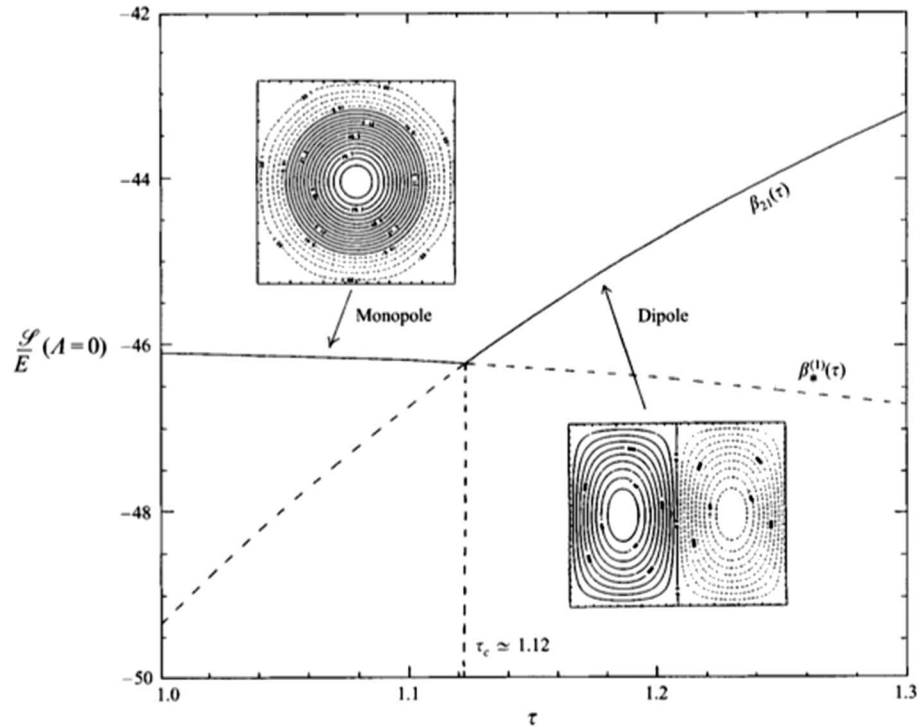
Figure 4. Maximum entropy states as a function of the aspect ratio for a rectangular domain, in the linear (*strong mixing*) ω-ψ limit. For $\tau < \tau_c$, the equilibrium is a monopole, while for $\tau > \tau_c$, it is a dipole. Reprinted from *Chavanis and Sommeria* [1996] with the permission of Cambridge University Press.

stratified flows, *Venaille* [2012] has taken up the thread initiated by *Merryfield* [1998] (see section 3.2.2) and shown that bottom-trapped currents are indeed statistical equilibria of the Robert-Miller-Sommeria theory. Still in the continuous case, *Venaille et al.* [2012] have also studied the vertical distribution of energy at statistical equilibrium, focusing on the tendency to reach barotropic equilibrium states; as also observed in the two-layer model, the constraint of conservation of fine-grained enstrophy prevents complete elimination of energy in the baroclinic mode. As the beta effect increases, barotropization is facilitated, until we enter a regime dominated by waves. It is well known that baroclinic dynamics is hindered by strong rotation [*Holton*, 2004].
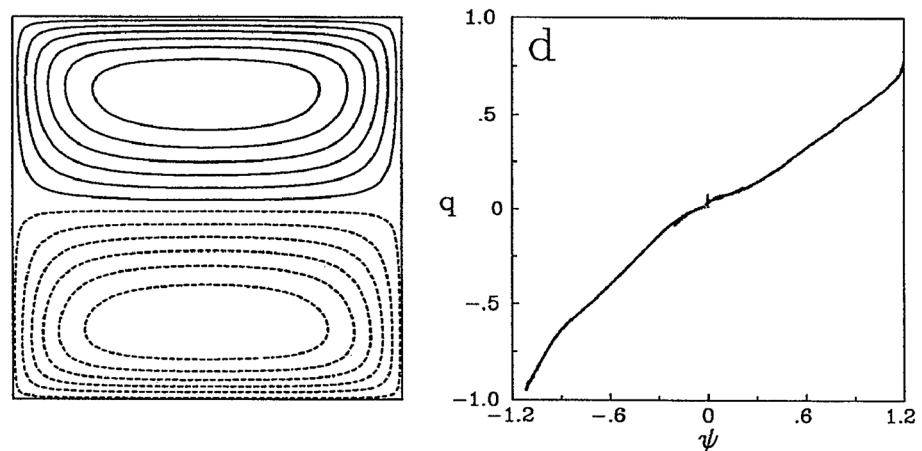
Figure 5. Convergence toward the statistical equilibrium in inviscid truncated barotropic flow on a beta-plane. (left) Stream function. (right) Scatterplot of the q-ψ relation. Reprinted with permission from *Wang and Vallis* [1994].

3.4. Subgrid-Scale Parameterization

Results from equilibrium statistical mechanics have found practical applications in the development of parameterization methods. *Holloway* [1992] suggested to replace the usual subgrid-scale parameterizations in ocean models, where, e.g., viscous forces are represented with terms of the form $v_*\Delta(\mathbf{u})$, where v_* is the eddy viscosity. He proposed to replace such formula with $v_*\Delta(\mathbf{u} - \mathbf{u}^*)$, so that viscosity relaxes the system toward the statistical equilibrium state $\mathbf{u}^*$. Such a parameterization has been implemented, tested, and commented in a number of studies [e.g., *Cummins and Holloway*, 1994]. For more perspective on this type of subgrid-scale parameterizations, the reader is referred to *Holloway* [2004] and *Frederiksen and O'Kane* [2008].

Along similar lines, *Kazantsev et al.* [1998] have proposed more generally to treat the subgrid scales so as to maximize the entropy production, inspired by the relaxation equations formulated in the Robert-Miller-Sommeria theory as an algorithm to construct equilibrium states [*Chavanis and Sommeria*, 1997]. Note also that it has been shown in direct numerical simulations of ideal 3-D turbulence that the small scales thermalize progressively and act as a sort of effective viscosity in the ideal system, leading to the appearance of transient Kolmogorov scaling laws [*Cichowlas et al.*, 2005]. This seems to be consistent with the above suggestions for subgrid-scale parameterizations.

4. Climate as a Forced-Dissipative Thermodynamic System

In the previous sections the focus has been on identifying symmetry properties and conservation laws of GFD flows and relate these to dynamical features and statistical mechanical properties. Neglecting forcing and dissipation has led us to study reversible equations whose statistical properties can be described using equilibrium statistical mechanics.

Indeed, this provides the backbone of the properties of GFD flows and are of great relevance for studying more realistic physical conditions. Nonetheless, at this stage, a reality check is necessary. The atmosphere and the oceans are out-of-equilibrium systems, which exchange irreversibly matter and energy from their surrounding environment and export it in a more degraded form at higher entropy. For example, Earth absorbs short-wave radiation (low-entropy solar photons emitted at a temperature of ≈ 6000 K), which is then reemitted to space as infrared radiation (high-entropy thermal photons emitted at a temperature of ≈ 255 K). In addition to that, spatial gradients in chemical concentrations and temperature as well as their associated internal matter and energy fluxes can be established and maintained for a long time within nonequilibrium systems (e.g., the temperature contrast between the polar and equatorial regions and the associated large-scale, atmospheric and oceanic circulation). In this and in the next sections we will take such a point of view.

The basis of the physical theory of climate was established in a seminal paper by *Lorenz* [1955], who elucidated how the mechanisms of energy forcing, conversion, and dissipation are related to the general circulation of the atmosphere. Oceanic and atmospheric large-scale flows results from the conversion of available potential energy—coming from the differential heating due to the inhomogeneity of the absorption of solar radiation—into kinetic energy through different mechanisms of instability due to the presence of large temperature gradients [*Charney*, 1947; *Eady*, 1949]. Such instabilities create a negative feedback, as they tend to reduce the temperature gradients they feed upon by favoring the mixing between masses of fluids at different temperatures. Furthermore, in a forced and dissipative system like the Earth's climate, entropy is continuously produced by irreversible processes [*Prigogine*, 1961; *de Groot and Mazur*, 1984]. Contributions to the total *material entropy production*, which is related to the nonradiative irreversible processes [*Goody*, 2000; *Kleidon*, 2009], come from the following: dissipation of kinetic energy due to viscous processes, turbulent diffusion of heat and chemical species, irreversible phase transitions associated to various processes relevant for the hydrological cycle, and chemical reactions relevant for the biogeochemistry of the planet.

It is important to note that the study of the climate *entropics* has been revitalized after *Paltridge* [1975, 1978] proposed a principle of maximum entropy production (MEPP) as a constraint on the climate system. While the scientific community disagrees on the validity of such a point of view—see, e.g., *Goody* [2007]—the discussion revolving around MEPP has led the scientific community to refocus on the importance of a thermodynamical approach—as complementary to the dynamical one—in providing physical insights for studying the climate system. In this paper we will not discuss MEPP and other nonequilibrium variational principles (for an updated review, see *Dewar et al.* [2013]).

4.1. Climatic Energy Budget and Energy Flows
4.1.1. Energy Budget

We first focus on developing equations describing the energy budget of the climate system. The total specific (per unit mass) energy of a geophysical fluid is given by the sum of internal, potential, kinetic, and latent energy. This can be expressed as $e = \mathbf{u}^2/2 + i + \phi + Lq$ for the atmosphere, where $\mathbf{u}$ is the velocity vector, $i = c_v T$ is the internal energy, with c_v the specific heat at constant volume for the gaseous atmospheric mixture and T is its temperature, Φ is the gravitational (plus centrifugal) potential, L is the latent heat of evaporation, and q is the specific humidity. In this formula, we neglect the heat content of the liquid and solid water and the heat associated to the phase transition between solid and liquid water. The approximate expression for the specific energy of the ocean reads $e = \mathbf{u}^2/2 + i + \Phi$, where $i = c_W T$ is the specific heat at constant volume of water (we neglect the effects of salinity and of pressure), while we can consider $e = c_S T + \phi$ as the specific energy for solid earth or ice. The conservation of energy and the conservation of mass imply that [*Peixoto and Oort*, 1992]:

$$\frac{\partial \rho e}{\partial t} = -\nabla \cdot (\mathbf{J_h} + \mathbf{F_R} + \mathbf{F_S} + \mathbf{F_L}) - \nabla(\tau \cdot \mathbf{u}), \tag{55}$$

where ρ is the density; p is the pressure; $\mathbf{J_h} = (\rho e + p)\mathbf{u}$ is the total enthalpy transport; $\mathbf{F_R}, \mathbf{F_S},$ and $\mathbf{F_L}$ are the vectors of the radiative, turbulent sensible, and turbulent latent heat fluxes, respectively; and τ is the stress tensor. By expressing equation (55) in spherical coordinates (r, λ, φ), and assuming the usual thin shell approximation $r = R + z, z/R \ll 1$, where R is the Earth's radius and z is the vertical coordinate of the fluid, we have [*Peixoto and Oort*, 1992]

$$[\dot{E}] = -\frac{1}{R\cos\varphi}\frac{\partial T_T}{\partial \varphi} + \left[F_R^{\text{TOA}}\right], \tag{56}$$

where $[X](\varphi, t) \equiv \int X(\lambda, \varphi, t)\mathrm{d}\lambda$, F_R^{TOA} is the net radiation at the top of the atmosphere (with the convention that the value is positive when there is an excess of incoming over outgoing radiation) and the meridional enthalpy transport has been defined as

$$T_T(\varphi, t) \equiv \iint J_{h\varphi}(\varphi, \lambda, z, t)R\cos\varphi\mathrm{d}z\mathrm{d}\lambda. \tag{57}$$

Equation (56) relates the rate of change of the vertically and zonally integrated total energy to the divergence of the meridional transport by the atmosphere and oceans and the zonally integrated radiative budget at the top of the atmosphere. Integrating along φ ($\{X\} = \int X\mathrm{d}\varphi$), the expression for the time derivative of the net global energy balance is straightforwardly derived:

$$\left\{\left[F_R^{\text{TOA}}\right]\right\} = \left\{\left[\dot{E}\right]\right\}. \tag{58}$$

Similar relationships can be written for the atmosphere, ocean, and land provided that energy fluxes of sensible, latent heat as well as radiative fluxes are taken into account at the surface [*Peixoto and Oort*, 1992]. A schematic view of the surface and TOA energy fluxes for present-day Earth [*Trenberth and Fasullo*, 2012] can be seen in Figure 6. Under steady state conditions, the long-term average energy budget is zero: $\{[\dot{E}]\} = 0$. Therefore, from equation (58), the stationarity condition implies that

$$\overline{\{[F_R]_{\text{toa}}\}} = 0. \tag{59}$$

Equation (59) describes the basic fact that the climate system, at steady state, does not on the average receive nor emit energy.

These constraints can be used for auditing climate models. At observational level nonzero energy balances are found at TOA and at the surface [*Trenberth and Fasullo*, 2012; *Wild et al.*, 2013], due to the fact that the actual Earth is not at a stationary state, most notably because of the ongoing greenhouse gas forcing (see Figure 6). However, a physically consistent climate model should feature a vanishing net energy balance when its parameters are held fixed and statistical stationarity is eventually obtained. *Lucarini and Ragone* [2011] analyzed the behavior of more than 20 atmosphere-ocean coupled climate models (Program For Climate Model Diagnosis and Intercomparison (PCMDI)/Coupled Model Intercomparison Project Phase 3 (CMIP3), http://www-pcmdi.llnl.gov/) under steady state conditions (preindustrial scenario) and found that the various models feature average global balances ranging between -0.2 and $2\,\text{W m}^{-2}$, with a few ones
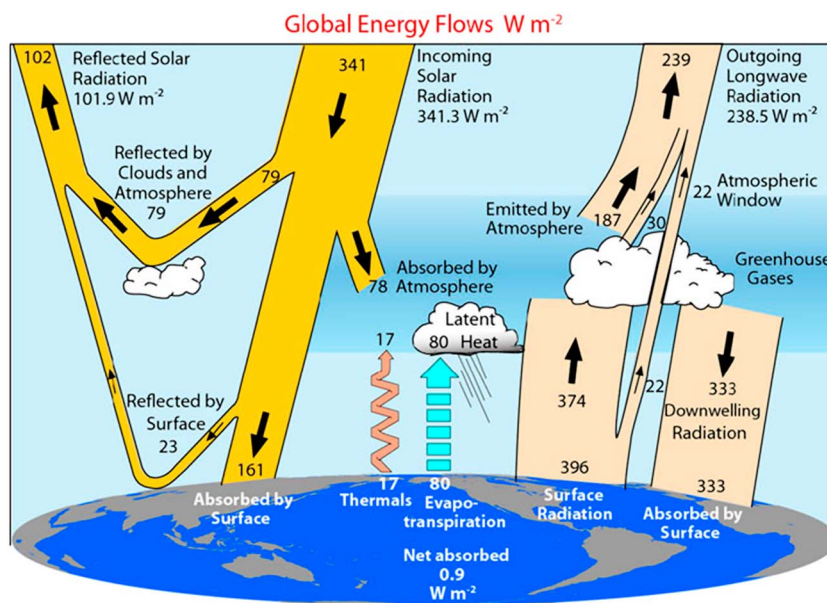
Figure 6. Global annual mean Earth's energy budget for 2000–2005 (W m^{-2}). Reprinted with permission from *Trenberth and Fasullo* [2012].

featuring imbalances larger than 3 W m^{-2}. The analysis of similar budgets for the last generation of climate models (Coupled Model Intercomparison Project Phase 5 (CMIP5) [*Taylor et al.*, 2012]) does not show a significant improvement (Figure 7). Spurious energy biases may be associated with nonconservation of water in the atmospheric branch of the hydrological cycle [*Liepert and Previdi*, 2012; *Liepert and Lo*, 2013] and in the water surface fluxes [*Lucarini et al.*, 2008; *Hasson et al.*, 2013], with the fact that dissipated kinetic energy is not reinjected in the system as thermal energy [*Becker*, 2003; *Lucarini and Fraedrich*, 2009], as well as with nonconservative numerical schemes [*Gassmann*, 2013].

4.1.2. Meridional Enthalpy Transport

The next step in constructing the energetics of the climate system is the study of the large-scale transport of various forms of energy. The meridional distribution of the radiative fields at the top of the atmosphere poses a strong constraint on the meridional general circulation [*Stone*, 1978]. As clear from equation (56), the stationarity condition (59) leads to the following indirect relationship for T_T:

$$\overline{T}_T(\varphi) = -2\pi \int_{\varphi}^{\pi/2} R^2 \cos \varphi' \overline{(F_R)_{\text{toa}}(\varphi')}. \tag{60}$$

In other terms, the flux T_T transports enthalpy from the low latitudes, which feature a positive imbalance between the net input of solar radiation—determined by planetary albedo, determined mostly by clouds [*Donohoe and Battisti*, 2012] and by surface properties—and the output of long-wave radiation, to the high latitudes, where a corresponding negative imbalance is present. Atmospheric and oceanic circulations act as responses needed to equilibrate such an imbalance [*Peixoto and Oort*, 1992].

The climatic meridional enthalpy transport $T_T(\varphi)$ reduces the temperature difference between the low- and high-latitude regions with respect to what imposed by the radiative-convective equilibrium picture. *Stone* [1978] showed that T_T depends essentially on the mean planetary albedo and on the equator-to-pole contrast of the incoming solar forcing, while being mostly independent from dynamical details of atmospheric and oceanic circulations. As emphasized by *Enderton and Marshall* [2009], if one assumes drastic changes in the meridional distributions of planetary albedo differences emerge with respect to Stone's theory. A comprehensive thermodynamic theory of the climate system that is able to predict the peak location and strength of the meridional transport, the partition between atmosphere and ocean [*Rose and Ferreira*, 2013], and to accommodate the variety of processes contributing to it is still missing.

Besides theoretical difficulties, observational estimations of T_T, T_A, and T_O also poses nontrivial challenges. For simplicity, we here refer to T_T. There is still not an accurate estimate of such a fundamental quantity for testing the output of climate models, despite the efforts of several authors [*Trenberth and Caron*, 2001;
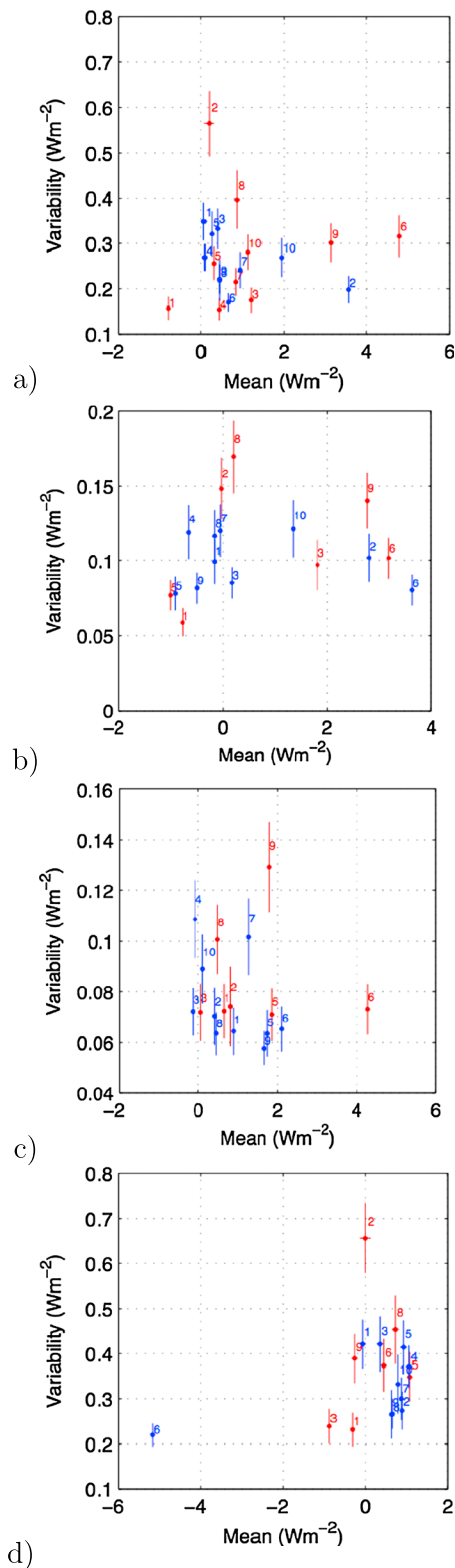
Figure 7. Mean and standard deviation of (a) globally averaged top-of-the-atmosphere radiative budget, (b) atmosphere energy budget, (c) ocean, and (d) land energy budget for intercomparable CMIP3 (red) and CMIP5 (blue) climate models control simulations (updated from *Lucarini and Ragone* [2011]). See the model codes in Table 1.

Wunsch, 2005; *Fasullo and Trenberth*, 2008; *Trenberth and Fasullo*, 2010; *Mayer and Haimberger*, 2012]. The precision of the estimates relies on the knowledge of the *boundary* fluxes F_R, F_S, and F_L and on the reanalysis data sets. *Wunsch* [2005], by using measurements of the radiative fluxes at the top of the atmosphere and previous estimates of the oceanic enthalpy transport, gave a range of values of 3.0–5.2 PW (1 PW = 10^{15} W) for the maximum of the total poleward transport in the Northern Hemisphere (NH) and 4.0–6.7 PW for the maximum of the total poleward transport in the Southern Hemisphere (SH). *Trenberth and Fasullo* [2010], by combining measurements of top-of-the-atmosphere radiative fields with different reanalyses and ocean data sets, found the range to be 4.7–5.1 PW for the SH peak transport and 4.6–5.6 PW for NH peak transport. *Mayer and Haimberger* [2012], using two reanalysis data sets (ERA-40 and the more recent European Centre for Medium-Range Weather Forecasts (ECMWF) reanalysis ERA-Interim), constrained the two peaks in narrower confidence intervals: 5.1–5.6 PW in the SH (4.4–4.9 PW in the NH) for the ERA-40 data and 5.1–5.6 PW in the SH (4.4–4.9 PW in the NH) for the ERA-Interim data. Unfortunately reanalysis data sets are affected by mass and energy conservation (e.g., +1.2 W m^{-2} at the top of the atmosphere and +6.8 W m^{-2} over oceans in ERA-Interim [*Mayer and Haimberger*, 2012]) problems that may potentially bias the transport estimates. Furthermore, these estimates are dependent on the analysis method and the model used; *Trenberth and Caron* [2001], using other reanalysis data set (National Centers for Environmental Prediction), found a value of the maxima 0.6 PW larger in the NH than those found with the ECMWF reanalysis. Estimates from *Trenberth and Caron* [2001] are shown in Figure 8.

The use of numerical climate model does not necessarily help reducing such uncertainties. *Lucarini and Ragone* [2011] analyzed a large data set of coupled climate models (PCMDI/CMIP3, http://www-pcmdi.llnl.gov/) and found a large spread in the meridional enthalpy transports peaks with discrepancies of the order of 15–20 % around a typical value of about 5.5 PW. State-of-the-art climate models (CMIP5 see http://cmip-pcmdi.llnl.gov/cmip5/index.html, [*Taylor et al.*, 2012]) show little improvement in terms of mutual agreement (Figure 9). *Donohoe and Battisti* [2012] attributed such a large spread in T_T to intermodel differences in the meridional contrast of absorbed solar radiation, which, in turn, is mainly due to the intermodel difference in the short-wave optical properties of the atmosphere. For an intercomparison of the

Table 1. Numerical Codes of the GCMs Considered in Figures 7 and 9[a]

CMIP3	CMIP5
1. CGCM3.1(T47)	CanESM2
2. CNRM-CM3	CNRM-CM5
3. CSIRO-Mk3.0	CSIRO-Mk6.0
4. GISS-EH	GISS-E2H
5. UKMO-HadGEM1	HadGEM1-AO
6. INM-CM3.0	INM-CM4
7. MIROC3.2(medres)	MIROC5
8. ECHAM5/MPI-OM	MPI-ESM-MR
9. MRI-CGCM2.3.2	MRI-CGCM3
10.	CCSM4

[a]We have used the official names of models given in the PCMDI/CMIP3 and CMIP5 websites. See text.

cloud distribution in different climate models, see *Probst et al.* [2012]. Figure 9 also shows that while the disagreement among models for the peak of the atmospheric transport is comparable to that for the peak of the total transport, enormous differences emerge when comparing oceanic transports.

Interesting information emerge when looking at the position of the peaks of the transport. *Stone* [1978] predicted that the position of the maximum of T_T is well constrained by the geometry of the system and weakly dependent of longitudinal homogeneities, and accordingly in Figure 9, both CMIP3 and CMIP5 models feature small spread in the position of the peak of T_T, with minute differences between the two hemispheres, except one outlier. Similarly, the spread among models is small with respect to the position of the peak of T_A in both hemispheres and of T_O in the Northern Hemispheres, while a larger uncertainty exists in the position of the peak of T_O in the Southern Hemisphere.

4.2. The Maintenance of Thermodynamical Disequilibrium

The basic understanding of the maintenance of the atmospheric general circulation was achieved nearly 60 years ago by *Lorenz* [1955, 1967] through the concepts of available potential energy and atmospheric energy cycle. The concept of available potential energy, first introduced by *Margules* [1905] to study storms, is defined as $A = \int c_p(T - T_r)dV$, where T_r is the temperature field of the reference state, obtained by an isentropic redistribution of the atmospheric mass so that the isentropic surfaces become horizontal and the mass between the two isentropes remains the same. By its own definition, this state minimizes the total potential energy at constant entropy. Such a definition is somewhat arbitrary, and different definitions lead to different formulations of atmospheric energetics [*Tailleux*, 2013]. For example, the choice of a reference state maximizing entropy at constant energy [*Dutton*, 1973] leads in a natural way to the concept of exergy. Exergy is the part of the internal energy measuring the departure of the system from its thermodynamic and mechanical equilibrium, i.e., a state of maximum entropy at constant energy, and is a commonly used concept in heat engines theory [*Rant*, 1956].

Lorenz [1967] proposed the following picture of the transformation of energy in the atmosphere. We define $E = P + K$, where $K = (1/2) \int dV\rho\mathbf{u}^2$ represents the total kinetic energy and $P = \int dV\rho(c_v T + \Phi)$ represents the dry static energy, and we integrate over the atmospheric domain V. Under hydrostatic approximation one can show that $\int dz\rho(c_v T + gz) = \int dz\rho(c_v T + RT) = \int dz\rho c_p T$ [see, e.g., *Lorenz*, 1967]. In the Lorenz framework one considers the hydrological cycle as a forcing to the atmospheric circulation. This amounts to separating the budget of the moist static energy and of the part related to the phase changes of water [see *Peixoto and Oort*, 1992, chapter 13]. We obtain the following:

$$\dot{P} = -W(P, K) + \dot{\Psi} + D, \qquad (61)$$

$$\dot{K} = -D + W(P, K), \qquad (62)$$

where $D = \int dV\rho\epsilon^2 > 0$ is the dissipation of kinetic energy due to turbulent cascades to small scales and to the wind shear associated to falling hydrometeors, $W(P, K) = -\int dV\rho\mathbf{u} \cdot \nabla p$
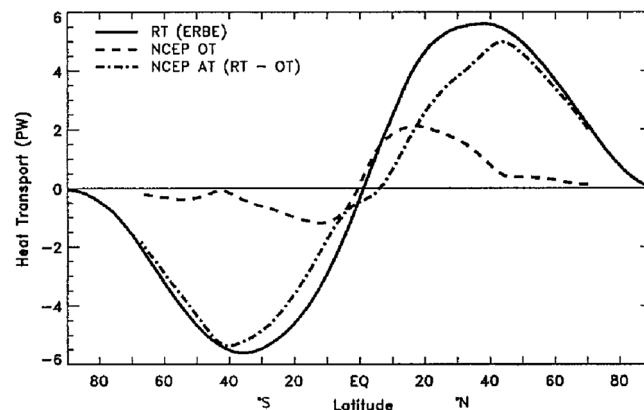
Figure 8. Annual meridional enthalpy transports of ocean (dashed), atmosphere (dash-dotted), and total (solid) estimated from satellite and reanalysis data (PW). Reprinted with permission from *Trenberth and Caron* [2001]. Copyright ©American Meteorological Society.
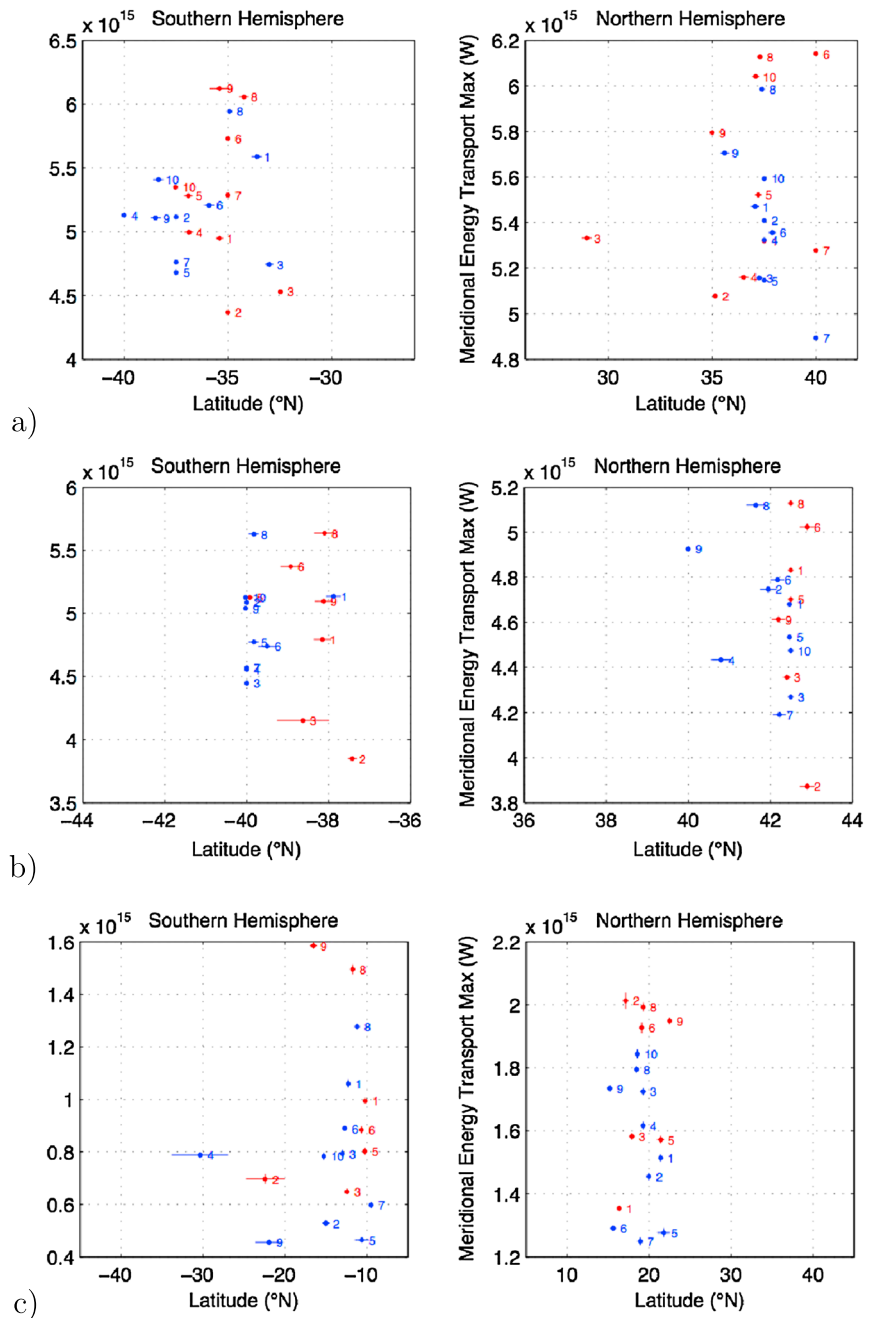
Figure 9. Value and position of the peak of the poleward meridional enthalpy transport in the preindustrial scenario for (a) the whole climate, (b) atmosphere, and (c) ocean for the some of the CMIP3 (red) and CMIP5 (blue) general circulation models (updated from *Lucarini and Ragone* [2011]). See the model codes in Table 1.

is the potential-to-kinetic energy conversion rate, and $\Psi = \int dV \rho \dot{q}_{nf}$ is the nonfrictional diabatic heating due to the convergence of turbulent sensible heat fluxes, condensation/evaporation inside the atmosphere, and convergence of radiative fluxes. The conversion term W can be interpreted as the instantaneous work performed by the system. In this respect, equation (61) represents the statement of the first law of thermodynamics for the atmosphere. Equations (61) and (62) imply that $\dot{E} = \dot{P} + \dot{K} = \Psi$, and therefore, the frictional heating D does not increase the total energy since it is just an internal conversion between kinetic and potential energy. Stationarity implies that $\overline{\dot{P}} = \overline{\dot{K}} = 0$, and therefore, $\overline{D} = \overline{W}$, which is referred to as the intensity of the Lorenz energy cycle. One has to note that the latter can be expressed as the average rate of

generation of available potential energy, $\overline{G} = \int dV \overline{\rho \dot{q}_{nf}(1 - T/T_r)}$, where T_r is the temperature field of the reference state [*Lorenz*, 1967].

The strength of the Lorenz energy cycle is a fundamental nonequilibrium property of the atmosphere, which, just as the meridional enthalpy transport (section 4.1.2), is known with a certain degree of uncertainty for the present climate. Reanalysis data sets (with all associated problems, see section 4.1.2) constrain $\overline{D}$ in the range 1.5–2.9 W m^{-2} [*Li et al.*, 2008]. On the other hand, general circulation models feature values of $\overline{D}$ ranging from 2 to 3.5 W m^{-2} [*Marques et al.*, 2011]. Numerical simulations show that a CO_2 doubling causes a decrease of $\overline{G}$ of nearly 10% [*Lucarini et al.*, 2010a]. Warming patterns can alter G either by affecting the gross static stability (stronger stability implies a weaker energy cycle, as clear from the theory of baroclinic instability) or the meridional temperature/diabatic heating distribution. *Hernandez-Deckers and von Storch* [2012] show that the decrease in G is mostly associated with changes in the gross static stability changes rather than with meridional temperature gradient changes.

Another aspect to be considered is that the intensity of the Lorenz energy cycle is formulated assuming hydrostatic conditions. Therefore, the Lorenz energy cycle in itself neglects any systematic transfer of potential into kinetic energy occurring through nonhydrostatic, small-scale motions [*Steinheimer et al.*, 2008]. Along these lines, *Pauluis and Dias* [2012] suggest that small-scale processes such as precipitation may significantly contribute to $\overline{D}$, which might therefore be considerably underestimated when computed for models that do not treat explicitly convection.

In the case of the ocean, available potential energy is generated through thermohaline forcings due to the correlation of density inhomogeneities and density forcings (e.g., through heat and freshwater fluxes) at surface. In addition to that, mechanical energy enters the ocean through direct transfer of kinetic energy by surface winds (and though tidal effects). Kinetic energy is dissipated through a variety of frictional processes, occurring mostly at the bottom of the ocean, and, similarly, available potential energy is lost through diffusion mostly due to small-scale eddies [*Wunsch and Ferrari*, 2004]. The understanding of the details of the oceanic Lorenz energy cycle is still at a relatively early stage. Estimates of dissipation and generation terms range within $(1-2) \times 10^{-2}$ W m^{-2} [*Oort et al.*, 1994; *Storch et al.*, 2012; *Tailleux*, 2013].

4.2.1. Atmospheric Heat Engine and Efficiency

Johnson [2000] proposed an interesting construction for further elucidating the idea that the climate can be seen as a heat engine. We define the total diabatic heating $\dot{q} = \dot{q}_{nf} + \rho\epsilon^2$ and splitting the atmospheric domain V into the subdomain V^+ in which $\dot{q} = \dot{q}^+ > 0$, and V^-, where $\dot{q} = \dot{q}^- < 0$. From equation (61) we derive

$$\overline{W} = \overline{\int_{V+} \overline{\dot{q}^+ \rho} dV} + \overline{\int_{-} \overline{\dot{q}^- \rho} dV} \equiv \overline{\Phi^+} + \overline{\Phi^-}, \tag{63}$$

where $\overline{\Phi^+} > 0$ and $\overline{\Phi^-} < 0$ by definition. We underline that the domains V^+ and V^- change with time. Therefore, the atmosphere can be interpreted as a heat engine, in which $\overline{\Phi^+}$ and $\overline{\Phi^-}$ are the net average heat gain and loss and $\overline{W}$ is the average mechanical work. The efficiency of the atmospheric heat engine, i.e., the capability of generating mechanical work given a certain heat input, can therefore be defined as

$$\eta = \frac{(\overline{\Phi^+} + \overline{\Phi^-})}{(\overline{\Phi^+})} = \frac{\overline{W}}{\overline{\Phi^+}}. \tag{64}$$

The analogy between the atmosphere and a (Carnot) heat engine can be pushed further if we introduce the total rate of entropy change of the system, $\dot{S} = \int dV \rho\dot{q}/T = \dot{S}^+ + \dot{S}^-$. In a steady state the following expression holds

$$\overline{\dot{S}} = \frac{\overline{\Phi^+}}{T^+} + \frac{\overline{\Phi^-}}{T^-} = 0, \tag{65}$$

where $T^{\pm} \equiv \overline{\Phi^{\pm}} / \int_{V\pm} dV \overline{\rho\dot{q}^{\pm}/T}$ from which it follows that $\eta = 1 - T^-/T^+$. Johnson's approach provides a self-consistent treatment of the heat engine of a geophysical fluid and extends closely related thermodynamical theories of hurricane dynamics [*Emanuel*, 1991].

In Emanuel's theory a mature hurricane is depicted as an ideal Carnot engine driven by the thermal disequilibrium between the sea surface temperature T_s and the cooling temperature T_0 with an efficiency

$1 - T_0/T_s \approx 1/3$. A similar approach was extended also to moist convection [*Emanuel and Bister*, 1996; *Rennò and Ingersoll*, 1996] for determining that the wind speed reached by the convective system for a certain rate of heat input F_{in} from the sea, $W = F_{in}(1 - T_0/T_s)$. Such an approach has been used to study large-scale, open systems like the Hadley cell [*Adams and Rennò*, 2005] and the monsoonal circulation [*Johnson*, 1989].

4.2.2. Entropy Production in the Climate System

We wish now to emphasize a different aspect of the climate's thermodynamics, namely its irreversibility by the investigation of its material entropy production, i.e., the entropy produced by the geophysical fluids neglecting the change in the properties of the radiative fields [*Goody*, 2000; *Ozawa et al.*, 2003]. The entropy budget of the fluid can be rewritten as

$$\dot{S} = -\int dV \frac{\nabla \cdot \mathbf{F_R}}{T} + \dot{S}_{mat}, \tag{66}$$

so that we separate the contribution coming from the absorption of the radiation from other effects related to the other irreversible processes occurring in the fluid. Note that, in the previous formula, we refer to the entropy budget of the whole climate, not of the atmosphere, as done, instead, in the previous section.

The material entropy production rate $\dot{S}_{mat}$ can be expressed as $\dot{S}_{diff} + \dot{S}_{fric} + \dot{S}_{hyd}$, i.e., the sum of contributions associated with heat diffusion, frictional heating and the hydrological cycle (due to diffusion of water and phase changes), respectively. Detailed estimates of the entropy budget of the climate system and of the average material entropy production rate ($\overline{\dot{S}_{mat}} \approx 50 \text{ mW m}^{-2} \text{ K}^{-1}$) can be found in *Goody* [2000] and *Pascale et al.* [2011]. The oceanic entropy production due to small-scale mixing in the interior gives a small contribution ($\approx 1 \text{ mW m}^{-2} \text{ K}^{-1}$) to $\dot{S}_{mat}$ [*Pascale et al.*, 2011]. Therefore, we will limit the discussion to processes occurring in the interior and at the boundaries of the atmosphere.

The average entropy production rate due to heat diffusion $\overline{\dot{S}_{diff}} = -\int dV \overline{\nabla \cdot \mathbf{J_S}/T}$ is generally small ($\approx 2 \text{ mW m}^{-2} \text{ K}^{-1}$ [*Kleidon*, 2009]) and associated mostly with dry atmospheric convection occurring nearby the surface and with vertical mixing in the mixed layer of the ocean. The average entropy production rate due to frictional heating — $\overline{\dot{S}_{fric}} = \int dV \overline{\rho \epsilon^2/T} \approx 10 \text{ mW m}^{-2} \text{ K}^{-1}$ [*Fraedrich and Lunkeit*, 2008; *Pascale et al.*, 2011] — is associated with turbulent energy cascades bringing kinetic energy from large scales down to scales (millimeters or less for geophysical flows) where viscosity can efficiently operate. Finally, $\dot{S}_{hyd}$ is related to irreversible processes associated with the hydrological cycle—evaporation of liquid water in unsaturated air, condensation of water vapor in supersaturated air, and molecular diffusion of water vapor [*Pauluis and Held*, 2002a, 2002b]—and requires the knowledge of relative humidity H and the molecular fluxes of water vapor $\mathbf{J}_v = \mathbf{F_L}/L$:

$$\dot{S}_{hyd} = \int dV(C - E)R(\ln H + \mathbf{J}_v \cdot \nabla p_w) - \int_{z=surf} dA J_{v,z} R \ln H, \tag{67}$$

where C and E indicate condensation and evaporation, respectively, and p_w is the partial pressure of the water vapor. The importance of $\dot{S}_{diff}$ and $\dot{S}_{hyd}$ in the context of thermodynamic theories of moist convection is extensively discussed in *Pauluis and Held* [2002b] and *Pauluis* [2010]. The impact of water vapor on the production of kinetic energy in deep convection can be described as a steam engine, and it is to lower the maximum possible amount of work which can produced by an equivalent Carnot cycle [*Emanuel and Bister*, 1996; *Rennò and Ingersoll*, 1996] acting between the same temperature reservoirs. An indirect estimate of (67) can be obtained from the entropy budget for water

$$\dot{S}_W = \int_{V_W} dV \rho_W \dot{s}^w = \int_{V_W} dV \rho_W \frac{\dot{q}_W}{T} + \dot{S}_{hyd}$$

as discussed in *Pauluis and Held* [2002b], where $\dot{S}_W$ is the rate of change of entropy of water and $\dot{q}_W$ is the neat heating amount of heat per time that the water substance receives from its environment (i.e., through evaporation and condensation). At steady state $\overline{\dot{S}_W} = 0$ and so $\overline{\dot{S}_{hyd}} = \int_{V_W} dV \overline{\rho_W \dot{q}_W/T} \approx 37 \text{ mW m}^{-2} \text{ K}^{-1}$ [*Pascale et al.*, 2011]. Therefore, it is possible to compute the material entropy production by considering exclusively the heat exchanges and the temperature at which such exchanges take place, thus bypassing the need for looking into the complicated details of phase separation processes.

Furthermore, in climate models physical entropy sources due to diffusive/dispersive numerical advection schemes and parameterizations are also present [*Johnson*, 1997; *Egger*, 1999]. In particular, *Woollings and*

Thuburn [2006] showed that dispersive dynamical cores can lead to negative numerical entropy production. More generally, it has been argued that parameterizations of subgrid turbulent fluxes of heat, water vapor and momentum should conform to the second law of thermodynamics and therefore should lead to locally positive definite entropy production, this being generally not the case [*Gassmann*, 2013].

4.3. Applications and Future Perspectives
4.3.1. Auditing Climate Models
At steady state, we have that $\overline{\dot{S}} = 0$. Hence, from equation (66) we derive

$$\overline{\dot{S}_{\text{mat}}} = \int -dV \overline{\frac{\nabla \cdot \mathbf{F_R}}{T}}. \tag{68}$$

Usually, this is referred to as *indirect formula* for computing the material entropy production [*Goody*, 2000], because it provides an alternative way for estimating the material entropy production of the geophysical fluid by only looking at the correlation between radiative heating rates and temperature fields. Therefore, this formula allows for computing the material entropy production due to fluid motions bypassing all the complex fluid dynamical behavior of the system (see *Lucarini and Pascale* [2014] for an in-depth discussion of different ways for computing the material entropy production and of the effect of coarse graining the thermodynamic fields). Starting from equation (68), it is possible to derive for Earth conditions an approximate formula for the long-term average of the material entropy production, and to disentangle the contributions due to horizontal and vertical processes [*Lucarini et al.*, 2011] as $\overline{\dot{S}_{\text{mat}}} \approx \overline{\dot{S}_{\text{mat}}^{v}} + \overline{\dot{S}_{\text{mat}}^{h}}$, where

$$\overline{\dot{S}_{\text{mat}}^{h}} = -\int_A dA \frac{\boldsymbol{\nabla}_h \cdot \overline{\boldsymbol{\Upsilon}}}{T_E} = -\int_A dA \frac{\overline{F_R^{\text{TOA}}}}{T_E} \tag{69}$$

where $\boldsymbol{\Upsilon} = \int dz \rho \mathbf{J_h}$ is the vertically integrated atmospheric enthalpy flux introduced in equation (55), $F_R^{\text{TOA}} = \overline{F_R^{\text{TOA,SW}}} - \overline{F_R^{\text{TOA,LW}}}$, where SW and LW refer to the short- and long-wave contributions, respectively, and $T_E = \left(\overline{F_R^{\text{TOA,LW}}}/\sigma\right)^{1/4}$ is the emission temperature at a given location. The contribution to the material entropy production coming from vertical processes can instead be written as

$$\overline{\dot{S}_{\text{mat}}^{v}} = \int_A dA \left(\overline{F_R^{\text{surf}}}\right) \left(\frac{1}{T_s} - \frac{1}{T_E}\right) \tag{70}$$

where $\overline{F_R^{\text{surf}}} = \overline{F_R^{\text{surf,SW}}} + \overline{F_R^{\text{surf,LW}}}$ is the net radiation at surface (defined as positive when the there is a net incoming radiation into the atmosphere), SW and LW refer to the short- and long-wave components, and T_s is the surface skin temperature defined as $T_s = \left(\overline{F_R^{\text{surf,LW}}}/\sigma\right)^{1/4} \sim T_{\text{surf}}$ [*Lucarini et al.*, 2011]. Equations (69) and (70) allow one to compute the material entropy production due to internal irreversible processes making use only of 2-D radiative fields at the boundaries of the relevant planetary fluid envelope (surface and top of the atmosphere). This makes equations (69) and (70) suitable for the postprocessing of data hosted in publicly available archives of GCMs output, intercomparison studies, and studies of observational data sets of the Earth and other planets (where radiative data are the only available source of information). Instead, direct computations of $\overline{\dot{S}_{\text{mat}}}$ require the knowledge of the full 3-D time-dependent heating and temperature fields, making their applicability nontrivial for numerical models and unfeasible for observations.

Figure 10 shows a scatterplot of the globally averaged annual mean values of the vertical and horizontal components of the material entropy production computed from the outputs of several general circulation models (GCMs) from the CMIP3 data set in preindustrial and postindustrial conditions (updated from *Lucarini et al.* [2011], limiting to the models for which the data availability made possible the comparison). The postindustrial case corresponds to the first 100 years after the stabilization of the CO_2 in the A1B climate change scenario. Issues related to the effective nonstationarity of the system have been treated as in *Lucarini and Ragone* [2011].

Comparing with the direct computation [*Pascale et al.*, 2011] of $\overline{\dot{S}_{\text{mat}}}$ for the case of Had-CM3 (model 13) in the preindustrial case shows that the relative error on the estimate is less than 5% [*Lucarini et al.*, 2011]. The typical values of the annual material entropy production in preindustrial conditions range for most models between 47 and 53 mW m^{-2} K^{-1}, matching well the approximate estimate by *Ambaum* [2010]. The contribution due to vertical processes is dominant by about 1 order of magnitude with respect to the contribution
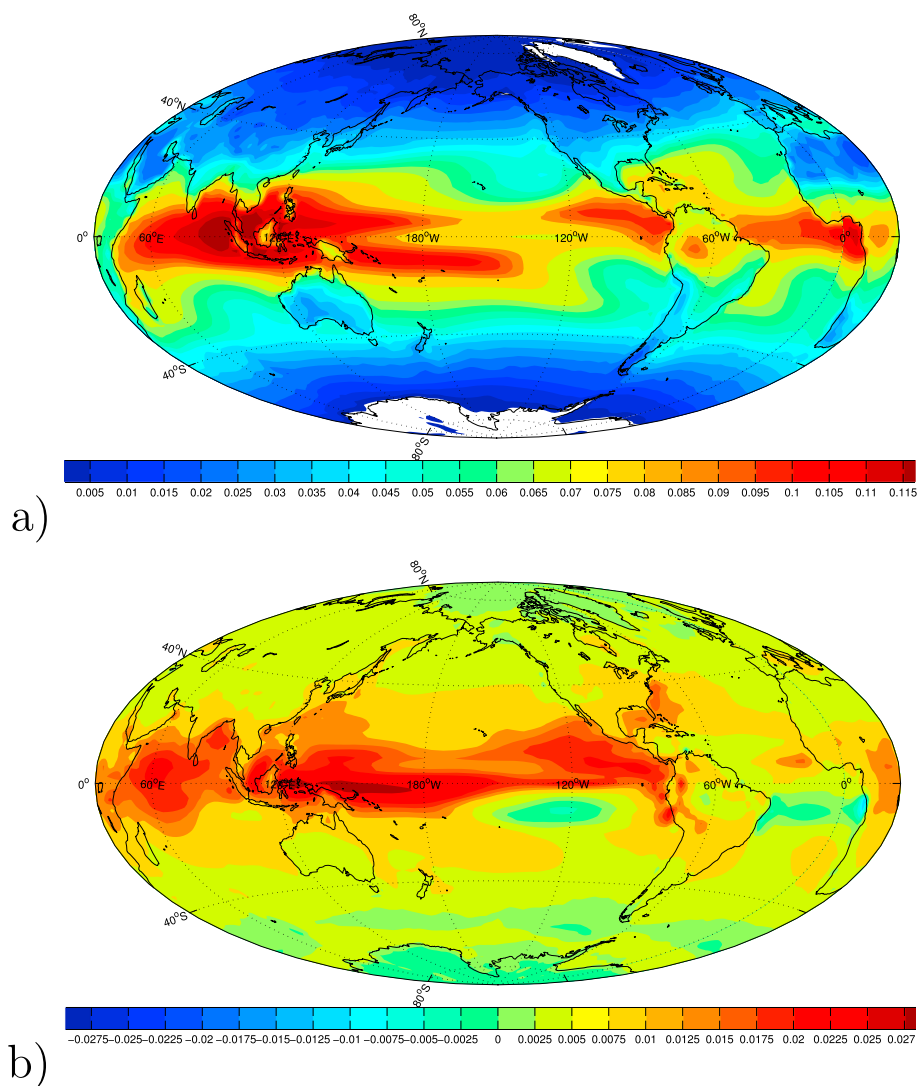
a)

b)
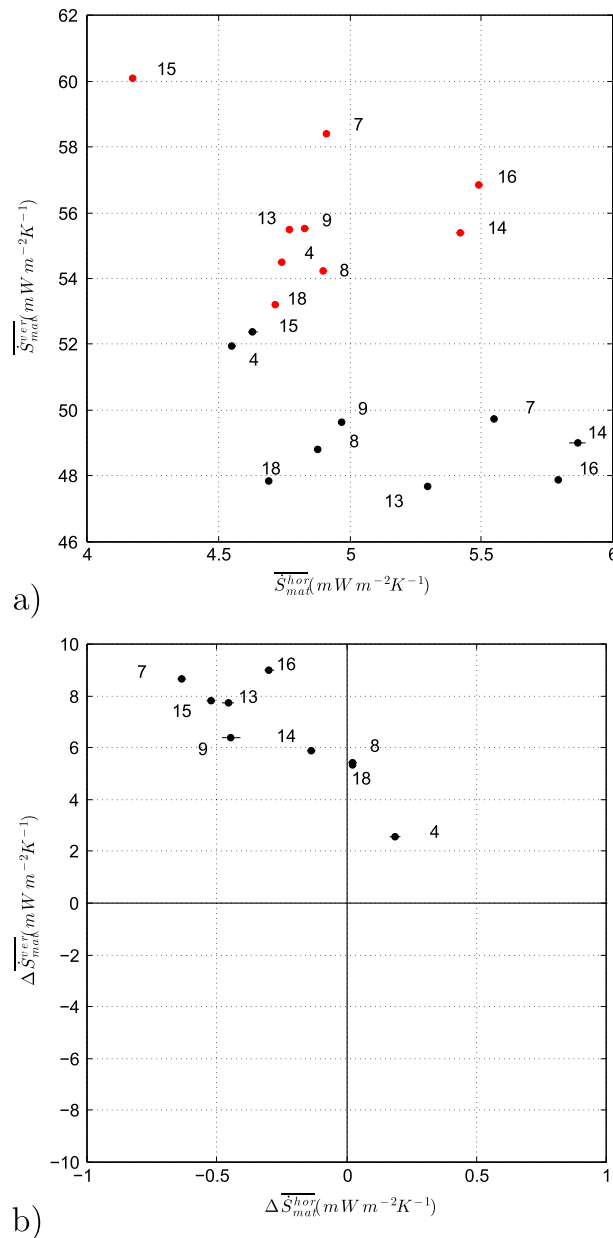
Figure 10. (a) Scatterplot of contributions to the rate of material entropy production due to horizontal (*x* axis) and vertical (*y* axis) processes. Each point corresponds to a GCM from the CMIP3 data set in preindustrial (black) and postindustrial (red) scenarios (updated from *Lucarini et al.* [2011]). (b) Difference between the SRESA1B scenario run (average of the last 30 years of the 23rd century and the preindustrial climatology). Model codes as in the reference.

due to horizontal processes. This suggests that from the point of view of the entropy production, the climate system approximately behaves as a collection of weakly coupled vertical columns where mixing takes place [*Lucarini and Pascale*, 2014].

In increased CO_2 concentration conditions, the rate of material entropy production increases for all the models between 10% and 20%. Such a change is dominated by the increase in the vertical component, while the horizontal component sees in most cases a reduction of up to 10%, despite the fact that large-scale horizontal enthalpy transports increase for all models [*Lucarini and Ragone*, 2011]. This implies—see equation (69)—a projected strong reduction in the large-scale gradients of emission temperature, thus suggesting that in warmer conditions the climate system becomes more homogeneous in terms of meridional and zonal temperature differences. This fits well with what reported in *Lucarini et al.* [2010a, 2010b] in terms of climate response to global warming-like conditions and hints to a dominant role of the latent heat release due to convective processes in the response to the climate change [*Lucarini and Ragone*, 2011].

Figure 11a shows the spatial distribution of the integrand of equation (70) for the Had-CM3 model in preindustrial conditions [*Lucarini et al.*, 2011], i.e., the local contribution to the vertical component of material entropy production. First, the integrand in equation (70) is positive everywhere, indicating that vertical exchange processes lead to irreversible mixing of the fluid properties. Small deviations can be found over Antarctica and Greenland, where

the approximations leading to equation (70) are not necessarily valid (see the discussion in *Lucarini et al.* [2011]). Overall, the local material entropy production due to vertical processes seems to be a good indicator of the geographical distribution of convective activity: the highest values are observed in the warm pool of the western Pacific and Indian Ocean and in land areas characterized by warm and moist climates, while relatively low values are instead observed in the cold tongue of the eastern Pacific, near western boundary currents, and in the temperate and cold oceans, as well as on deserts and middle and high latitudes of terrestrial areas. Note that also in this case the role of latent heat releases is fundamental in determining the characteristics of the system, showing how the hydrological cycle is a crucial aspect of thermodynamics of the climate system.

Figure 11. (a) Spatial distribution of the contribution to the rate of material entropy production due to vertical processes in preindustrial scenario for Had-CM3 (model 13 in Figure 10). (b) Anomalies in the postindustrial scenario with respect to the preindustrial case for the same model (updated from *Lucarini et al.* [2011]).

Figure 11b shows the difference between the postindustrial and preindustrial cases. The local vertical component of material entropy production increases almost everywhere, with negative anomalies confined to polar regions and to limited areas of the Southern Hemisphere, with very small values. The positive anomalies are extremely high in the tropical regions, particularly in the eastern and western Pacific Ocean. Note that the pattern of increase does not strictly follow the pattern of the absolute value in the preindustrial case. In particular, the maximum of the increase is located eastward to the maximum of the entropy production in the preindustrial case, a signature of a shifting of the warm pool and a modification of the Walker circulation [*Bayr et al.*, 2014; *DiNezio et al.*, 2013; *Intergovernmental Panel on Climate Change* (*IPCC*), 2013]. High values are also found in the Indian Ocean, suggesting an increase of the convective activity connected with the monsoon [*Turner and Annamalai*, 2012; *IPCC*, 2013]. Significant local maxima are also observed in the Gulf of Mexico and along the Gulf Stream, and in the Mediterranean Sea.

The local entropy production due to vertical processes behaves as a robust indicator of the impact of the climate change on large-scale features connected to convective activity. The pattern of increase is correlated to the pattern of variation of the surface temperature only to a minor extent. The reason is that this indicator contains in a synthetic way the information of the change in the surface temperature, in the vertical stability of the atmosphere, and in the intensity of the energy fluxes connected to the vertical processes. Therefore,
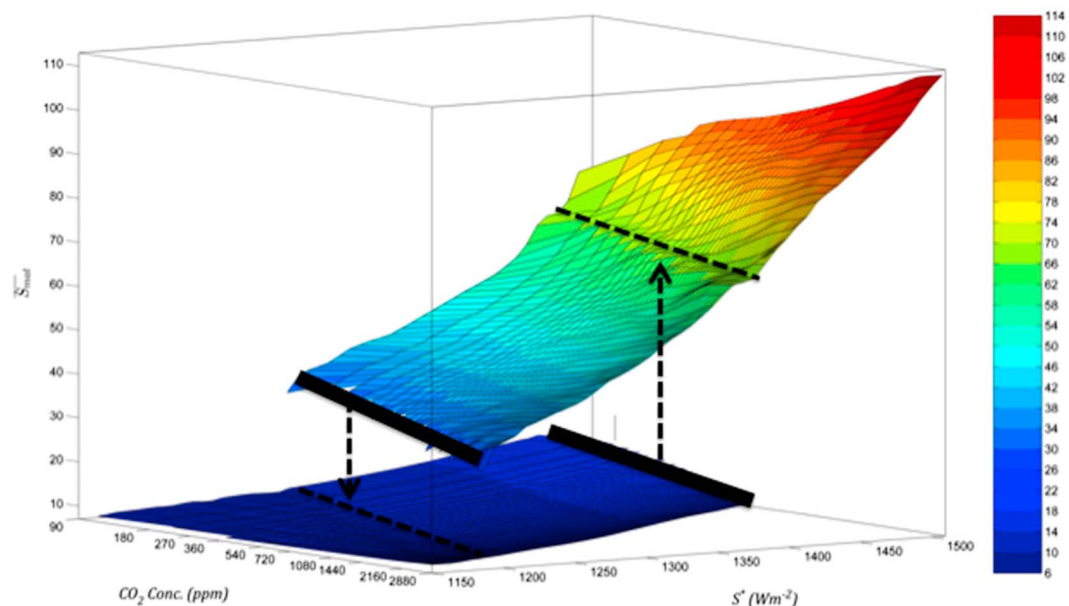
Figure 12. Material entropy production (mW m^{-2} K^{-1}) as a function of solar constant S^* and the CO_2 concentration. The transition SB→W and W→SB are marked with dashed arrows starting from the tipping point regions (courtesy of Robert Boschi, Universität Hamburg).

it could be used in order to define robust indexes for large-scale processes for which strong convection is an important component. Moreover, the range of variation due to climate change of the local vertical entropy production is rather high if compared to the range of variation of standard fields like surface temperature or pressure. Therefore, one could expect a better signal-to-noise ratio and a more distinctive signature of climate change from indicators based on this quantity compared with what obtained with indicators based on simpler observables, similarly to what is discussed by *Lucarini et al.* [2010a, 2010b] and by *Boschi et al.* [2013] in the context of the identification of multistable regimes of the climate system.

4.3.2. Bistabiliy and Tipping Points

Based on the evidence supported by *Hoffman and Schrag* [2002] and from numerical models [*Budyko*, 1969; *Sellers*, 1969; *Ghil*, 1976], it is expected that the Earth is potentially capable of supporting multiple steady states for the same values of some parameters such as, for example, the solar constant. Such states are the presently observed *warm* state (W), and the entirely ice-covered *Snowball Earth* state (SB). This is due to the presence of two disjoint strange (chaotic) attractors. The W→SB and SB→W transitions are due, mathematically, to the catastrophic disappearance of one of the two strange attractors [*Arnold*, 1992] and, physically, to the positive ice-albedo feedback. The SB condition, which might be a common feature also of Earth-like planets, hardly allows for the presence of life, so this issue is of extreme relevance for defining habitability condition in extraterrestrial planets.

The Planet Simulator (PLASIM), a GCM of intermediate complexity [*Fraedrich et al.*, 2005], was used by *Boschi et al.* [2013] and by *Lucarini et al.* [2013] to reconstruct an extensive portion of the region of multistability in the plane described by the parameters $(S^*, [CO_2])$. The surface temperature $T_s(S^*, [CO_2])$ is shown in Figure 12. The boundary of the domain in the parametric space where two states are admissible corresponds to the tipping points of the system.

The thermodynamical and dynamical properties of the W and SB states are largely different. In the W states, surface temperature is 40–60 K higher than in the corresponding SB state and the hydrological cycle dominates the dynamics. This leads to a material entropy production (Figure 12) larger by a factor of 4—order of $(40–60) \times 10^{-3}$ W m^{-2} K^{-1} versus $(10–15) \times 10^{-3}$ W m^{-2} K^{-1}—with respect to the corresponding SB states [*Boschi et al.*, 2013]. The SB state is eminently a dry climate, with entropy production mostly due to sensible heat fluxes and dissipation of kinetic energy.

The response to increasing temperatures of the two states is rather different: the W states feature a decrease of the efficiency of the climate machine, as enhanced latent heat transports reduces energy availability by

a)

b)
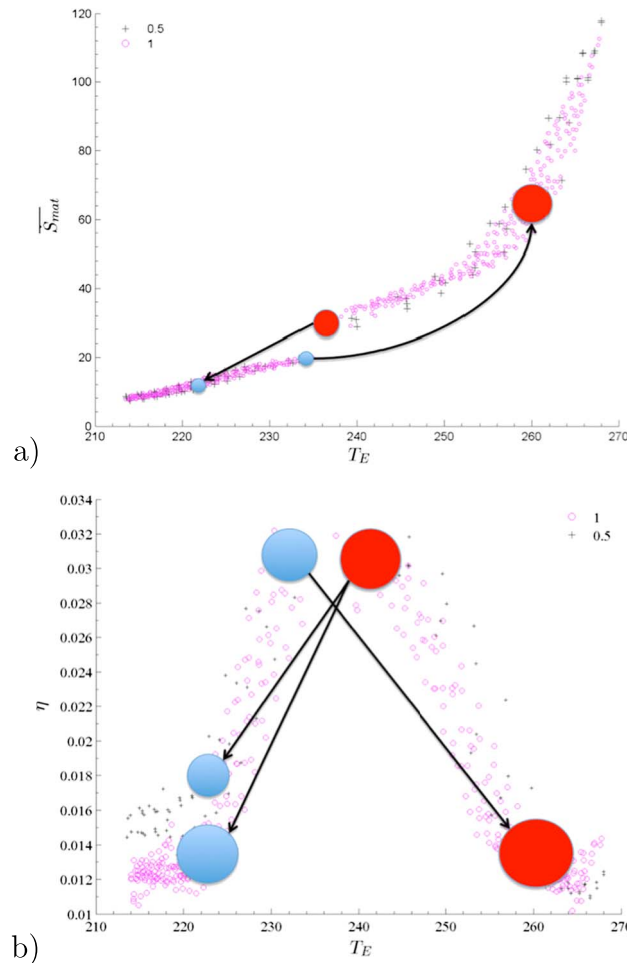
Figure 13. (a) Average rate of material entropy production (10^{-3} W m^{-2} K^{-1}) versus emission temperature $T_E(K)$ for $\Omega = 0.5\Omega_{earth}$ (black) and for $\Omega = \Omega_E$ (purple). (b) As in Figure 13a but for efficiency (courtesy of Robert Boschi, Universität Hamburg).

dampening temperature gradients, while in the SB states the efficiency is increased, because warmer states are associated to lower static stability, which favors large-scale atmospheric motions (Figure 12). The entropy production increases for both states, but for different reasons: the system becomes more irreversible and less efficient in the case of W states, while stronger atmospheric motions lead to stronger dissipation and stronger energy transports in the case of SB states. In both regimes, the efficiency η increases for steady states getting closer to tipping points and dramatically drops at the transition to the new state belonging to the other attractor (Figure 12). In a rather general thermodynamical context, this can be framed as follows: the efficiency gives a measure of how far from equilibrium the system is, because it is related - see equation (65) - to the presence of temperature differences inside the fluid. The negative feedbacks tend to counteract the differential heating due to the stellar insolation pattern, thus leading the system closer to equilibrium. At the bifurcation point, the negative feedbacks are overcome by the positive feedbacks, so that the system makes a global transition to a new state, where, in turn, the negative feedbacks are more efficient in stabilizing the system [*Boschi et al.*, 2013].

It is interesting to study the possibility of constructing empirical relations between different thermodynamical quantities for a variety of parametric configurations. In Figure 13, using the simulations used for constructing Figure 12, we show that one can find relate with a good degree of approximation the globally averaged emission temperature $T_E=(LW_{toa}/\sigma)^{1/4}$, to the average rate of material entropy production (Figure 13a) and to the efficiency of the climate system (Figure 13b). Interestingly, the empirical relations are only marginally changed when halving the rotation rate of the planet (black crosses) with respect to the present-day value (purple circles), thus suggesting a good degree of robustness. If one could provide convincing arguments and methods for constructing such relations, it would be possible to express nonequilibrium thermodynamical properties of the system in terms of parameters which are more directly accessible through measurements [*Lucarini et al.*, 2013].

4.3.3. Applications to Planetary Sciences

The discovery of hundreds of planets outside the solar system (exoplanets) [*Seager and Deming*, 2010] is extending the scope of planetary sciences toward the study of the so-called *exoclimates* [*Heng*, 2012a]. A large number of the exoplanets discovered so far are tidally locked to their parental star, experiencing extreme stellar forcing on the dayside where temperature up to 2000 K can be reached. Starlight energy, deposited within the atmosphere at the planet's dayside, is then transported by atmospheric circulation to the nightside. Such a system, similarly to the Earth's climate, works like a heat engine (sections 4.1.2 and 4.2).

The strength of the day-to-night enthalpy flux controls the ratio of outgoing long-wave energy fluxes from the nightside and dayside $\xi = LW_{night}/LW_{day}$, called efficiency of heat redistribution in the astrophysical

literature. Observations through infrared light curves show that the hotter the planet, the more inefficient the atmospheres are at redistributing stellar energy leading to larger day-night temperature differences. Numerical simulations [*Perna et al.*, 2012] show that ξ varies between 0.2 (low heat redistribution) and 1 (full heat redistribution) and depends critically on the atmospheric optical properties and the intensity of the stellar irradiance. Relating this definition of efficiency with the many different definitions used to characterize global circulations [*Johnson*, 2000; *Schubert and Mitchell*, 2013; *Perna et al.*, 2012; *Ambaum*, 2010] and understanding their differences would be useful to provide a link between energy conversion and energy transport in planetary atmospheres.

A thorough understanding of dissipative processes is fundamental for dealing with planetary atmospheres [*Goodman*, 2009; *Pascale et al.*, 2013]. Dissipative processes are poorly known on solar system planets and on exoplanets. Let us make some examples. In hot Jupiters temperatures may be very high (≥ 1500 K), allowing for thermal ionization (governed by the *Saha equation*) and thus fast-moving (in hot Jupiters winds ~ 1 km s^{-1}) electric charges. This induces an electric current toward the interior of the planet, where energy is then converted into heat by ohmic dissipation. Another dissipative mechanism believed to be a common feature in planetary atmospheres is shock wave breaking [*Batygin and Stevenson*, 2010; *Heng*, 2012b]. Note that the indirect method (equation (68)) could, in principle, be applied in order to infer information about the dissipative processes in the interior of exoplanets [*Schubert and Mitchell*, 2013], where radiative fluxes are the only piece of information we can access.

5. Climate Response and Prediction

In the previous section, we have investigated the climate as a nonequilibrium physical system and have emphasized the intimate relation between forcing, dissipation, energy conversion, and irreversibility. The same approach can be brought to a more theoretical level by taking the point of view of nonequilibrium statistical mechanics.

Nonequilibrium statistical mechanics provides the natural setting for investigating the mathematical properties of forced and dissipative chaotic systems, which live in a nonequilibrium steady state (NESS). In this state, typically, the phase space contracts, entropy is generated, and the predictability horizon is finite. Deviations from this behavior are possible, but extremely unlikely. Conceptually, nonequilibrium steady states are generated when a system is put in contact with reservoirs at different temperatures or chemical potentials, and one disregards the transient behaviors responsible for the relaxation processes [*Gallavotti*, 2006]. This fits well the description of the nonequilibrium properties of the climate system given in section 4.

The science behind nonequilibrium statistical mechanical systems is still in its infancy, so that, as opposed to the equilibrium case, we are not able to predict the properties of a system given the parameters describing its internal dynamics and the boundary conditions, except in special cases where the dynamics is trivial.

It is then important to choose a suitable mathematical setting for being able to state some useful general results and compare numerical experiments with theory. The mathematical paradigm we will consider is the one of so-called *Axiom A systems* [*Eckmann and Ruelle*, 1985; *Ruelle*, 1989], which, according to the *Chaotic Hypothesis* [*Gallavotti*, 1996], can be considered as good *effective* models of chaotic systems with many degrees of freedom.

In general, we can say that an (time-continuous) Axiom A system [*Eckmann and Ruelle*, 1985; *Ruelle*, 1989] obeys an evolution equation of the form $\dot{x} = F(x), x \in R^n$ and possesses an invariant measure $\rho(dx)$ supported on its attractor, which is, roughly speaking, the set of points where the system is asymptotically attracted to.

If forcing and dissipation are present, the attractor is *strange*, i.e., it does not look locally at all like a smooth manifold, so that we cannot write $\rho(dx) = \rho(x)dx$, where $\rho(x)$ is the density. Instead, in the very intuitive language of Lorenz, it looks like the Cartesian product of a smooth manifold and a fractal set. The smooth manifold corresponds to the unstable directions of the flow, which make the system chaotic, while the Cantor set corresponds to the contracting directions, which result from dissipation. The invariant measure $\rho(dx)$ gives the weight to be used in phase space to compute the expectation of any observable A, which agrees, thanks to ergodicity, to the long-time average, so that

$$\langle A \rangle = \rho(A) = \int \rho(dx)A(x) = \lim_{T \to \infty} \frac{1}{T} \int_0^T dt A(x(t))$$

with probability 1 with respect to the choice of the initial conditions.The invariant measure of an Axiom A system is of Sinai-Ruelle-Bowen (SRB) type [*Eckmann and Ruelle*, 1985; *Ruelle*, 1989; *Young*, 2002]. This has many consequences, including the fact that the measure is stable against weak stochastic forcing (see also the discussion in *Lucarini* [2012]).

Ruelle [1997, 1998a, 1998b, 2009] recently proved that in the case of an Axiom A system, its SRB measure, despite the geometrical complexity of the attractor supporting it, has also an extremely fascinating degree of regularity. In fact, there is a smooth dependence of the SRB measure to small perturbations of the flow, and it is possible to derive corresponding explicit formulas. This approach is especially useful for studying the impact of changes in the internal parameters of a system or of small modulations to the external forcing, and various studies have highlighted the practical relevance of Ruelle theory for studying what we may call the sensitivity of the system to small perturbations. We will here recapitulate some features of the Ruelle response theory and argue that it is a potentially useful tool for studying various classes of GFD problems, and, most notably for addressing rigorously and in an unified perspective climate change prediction, climate response, and climate sensitivity.

5.1. Response Formulas and Fluctuation-Dissipation Theorem

Let us consider an Axiom A dynamical system whose evolution equation can be written as $\dot{x} = F(x)$ and let us assume that it possesses an invariant SRB measure $\rho^{(0)}(\mathrm{d}x)$. *Ruelle* [1997, 1998a, 1998b, 2009] has shown that if the system is weakly perturbed so that its evolution equation can be written as

$$\dot{x} = F(x) + \Psi(x)T(t), \tag{71}$$

where $\Psi(x)$ is a weak time-independent forcing and $T(t)$ is its time modulation, it is possible to write the modification to the expectation value of a general smooth observable A as a perturbative series:

$$\rho(A)_t = \sum_{n=0}^{\infty} \rho^{(n)}(A)_t, \tag{72}$$

where $\rho^{(0)}(A)_t = \rho^{(0)}(A)$ is the expectation value of A according to the unpertubed invariant measure ρ^0 related to the dynamics $\dot{x} = F(x)$, while $\rho^{(n)}(A)_t$ with $n \geq 1$ represents the contribution due to nth-order processes [*Lucarini*, 2008].

Limiting our attention to the linear case we have

$$\rho^{(1)}(A)_t = \int_{-\infty}^{+\infty} \mathrm{d}\tau_1 G_A^{(1)}(\tau_1)T(t - \tau_1), \tag{73}$$

where the first-order Green function can be expressed as follows:

$$G_A^{(1)}(\tau_1) = \int \rho^0(\mathrm{d}x)\Theta(\tau_1)\Psi(x) \cdot \nabla A(x(\tau_1)), \tag{74}$$

where Θ is the usual Heaviside distribution ($\Theta(x) = 1$ if $x > 0, \Theta(x) = 0$ if $x < 0$), whose derivative is the Dirac's delta. Equations (73) and (74) are key ingredients for studying climate response. Before continuing in this direction, we want to use these equations to discuss the celebrated Fluctuation-Dissipation Theorem (FDT) [*Kubo*, 1957].

In systems possessing a smooth invariant measure (which, as discussed above, is *not* typically the case for Axiom A systems), like when equilibrium conditions apply or stochastic forcing is imposed, we can write $\rho^0(\mathrm{d}x) = \rho^0(x)\mathrm{d}x$, where $\rho^0(x)$ is the so-called *density*. In this case, we can rewrite equation (74) as follows:

$$\rho^{(1)}(A)_t = \int_{-\infty}^{+\infty} \mathrm{d}\tau_1\Theta(\tau_1) \times \int \mathrm{d}x\rho^0(x)B(x)A(x(\tau_1))T(t - \tau_1), \tag{75}$$

where $B(x) = -\nabla \cdot \left(\rho^0(x)\Psi(x)\right)/\rho^0(x)$. In other terms, one can predict the response at any time horizon t from the knowledge of the lagged correlation between the chosen observable A and the observable B, which depends on the invariant measure ρ^0 and on the perturbation vector field Ψ (see *Colangeli and Lucarini* [2014] for a detailed discussion on the physical meaning of B). Equation (75) provides a very general form of the FDT [*Ruelle*, 1998a; *Lacorata and Vulpiani*, 2007], which extends the results by [*Kubo*, 1957]. Recently, the FTD for system possessing a smooth invariant measure result has been extended to the nonlinear case [*Lucarini and Colangeli*, 2012].

The more common forms of the FDT can be obtained by taking one or more of the following assumptions: (1) the perturbation flow is the form $\Psi(x) = \epsilon \hat{x}_i$ and (2) the observable is of the form $A(x) = x_j$, where x_k is the kth component of the x vector and $\hat{x}_k$ is the corresponding unit vector. In this case, equation (75) takes the form:

$$\rho^{(1)}(x_j)_t = -\epsilon \int_{-\infty}^{+\infty} d\tau_1 \Theta(\tau_1) \times \int dx \rho^0(x) \partial_i \log[\rho^0(x)] x_j(\tau_1) T(t - \tau_1). \tag{76}$$

If one takes the additional simplifying assumption that unperturbed invariant measure has a Gaussian form, so that $\rho^0(x) = 1/\mathcal{Z} \exp(-\beta \sum_{j=1}^{N} x_j^2/2)$, where $\beta > 0$ and $\mathcal{Z}$ is the partition function we obtain

$$\rho^{(1)}(x_j)_t = \epsilon \beta \int_{-\infty}^{+\infty} d\tau_1 \Theta(\tau_1) \int dx \rho^0(x) x_i x_j(\tau_1) T(t - \tau_1) = \epsilon \beta \int_{-\infty}^{+\infty} d\tau_1 \Theta(\tau_1) C_{i,j}(\tau_1) T(t - \tau_1), \tag{77}$$

where $C_{i,j}$ is the lagged correlation between x_i and x_j in the unperturbed state.

Unfortunately, the link between linear response of the system to external perturbations and its internal fluctuations seems more elusive when the unperturbed state has a singular invariant measure. *Ruelle* [2009] shows that since the unperturbed invariant $\rho^{(0)}(dx)$ is singular, the response of the system contains two contributions, such that the first may be expressed in terms of a correlation function evaluated with respect to the unperturbed dynamics along the space tangent to the attractor (unstable manifold) and is formally identical to what given in equation (75). This part of the response decays rapidly due to decay of correlations due to chaos. On the other hand, the second term, which has no equilibrium counterpart, depends on the dynamics along the stable manifold, and hence, it may not be determined from the unperturbed dynamics and is also quite difficult to compute numerically. These properties suggest the basic fact, already suggested heuristically by *Lorenz* [1979], that in the case of nonequilibrium systems internal and forced fluctuations of the system are not equivalent, the former being restricted to the unstable manifold only.

Despite such a serious mathematical difficulty, the application of FDT, even in extremely simplified, quasi-Gaussian, approximation, has enjoyed a good success in climate [*Langen and Alexeev*, 2005; *Gritsun and Branstator*, 2007] even if it is clear that the ability of FDT in predicting the response to perturbation depends critically on the choice of the observable of interest, on the length of the integrations needed for constructing the approximation of the invariant measure, and, of course, on the validity of the linear approximation [*Cooper and Haynes*, 2011; *Cooper et al.*, 2013].

There are, in fact, various ways to circumvent the problem of the rigorous nonequivalence between forced and free fluctuations. Apart from the obvious smoothing effect due to unavoidable physical or numerical noise, when considering smooth, coarse-grained observables (like this of climatic interest), one expects to see little influence of the fine structure of the invariant measure of chaotic deterministic systems, as projections from high-dimensional spaces to lower dimensional ones are involved [*Marconi et al.*, 2008] and coarse-graining effects can be invoked [*Wouters and Lucarini*, 2013]. One expects that the FDT will perform better in predicting the response of the system if one considers as observable A quantities like the globally averaged surface temperature rather than, e.g., the surface temperature in an individual grid point. Further comments can be found at the end of section 6.

5.2. Computing the Response
5.2.1. Spectroscopic Method
If we select $T(t) = \epsilon \cos(\omega_0 t) = \epsilon/2(\exp(-i\omega_0 t) + \exp(i\omega_0 t))$ as modulating factor of the perturbation field $\Psi(x)$, from equation (73) we derive

$$\tilde{\rho}^{(1)}(A)_t = \epsilon/2 \int_{-\infty}^{+\infty} d\tau_1 G_A^{(1)}(\tau_1) \exp(-i\omega_0(t - \tau_1)) + \epsilon/2 \int_{-\infty}^{+\infty} d\tau_1 G_A^{(1)}(\tau_1) \exp(i\omega_0(t - \tau_1))$$

$$= \epsilon/2 \exp(-i\omega_0 t) \chi_A^{(1)}(\omega_0) + \text{c.c.}, \tag{78}$$

where $\chi_A^{(1)}(\omega_0)$ is the Fourier transform of $G_A^{(1)}(t)$, usually referred to as linear susceptibility, evaluated at frequency $\omega = \omega_0$, and c.c. indicates complex conjugate. Therefore, under the hypothesis of linearity, by performing an ensemble of experiments where the forcing is of the form $T(t) = \epsilon \cos(\omega_0 t)$, we can extract the linear susceptibility at frequency ω by selecting the ω_0 component of the Fourier transform of the signal $\tilde{\rho}^{(1)}(A)_t$ obtained by taking the ensemble average of the difference between the time series of A in the perturbed and unperturbed case. By changing systematically the frequency ω of the forcing, one can reconstruct the susceptibility $\chi_A^{(1)}(\omega)$ on a chosen interval of frequencies. It is useful to recapitulate some useful features of the susceptibility:
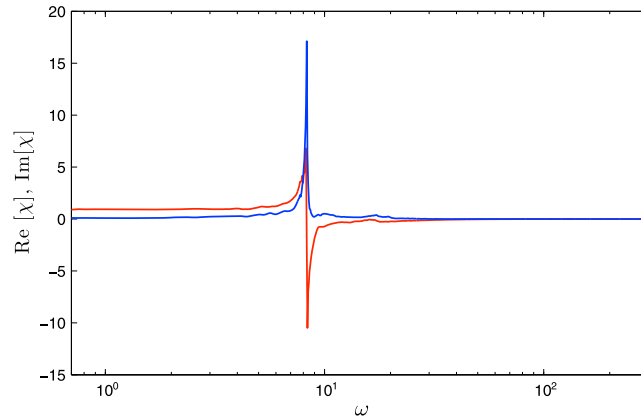
Figure 14. Measured real (blue line) and imaginary (red line) parts of the susceptibility z variable of the Lorenz 63 model (data from *Lucarini* [2009]).

1. Resonances in the susceptibility function correspond to spectral ranges where the system is extremely sensitive to forcings. In Figure 14 we show the real and imaginary parts of the susceptibility for z variable of the *Lorenz* [1963] model for the *classical* values of the parameters ($m = 1$, $\sigma = 10$, $r = 28$, $\beta = 8/3$) and a given choice of the forcing ($\Psi(x) = [0; x; 0]^{\mathsf{T}}$, $T(t) = 2\epsilon\cos(\omega t)$). We find that for $\omega \sim 8.3$, a very peaked spectral feature is apparent. Such a resonance is due to the Unstable Periodic Orbits (UPO) of the system with the corresponding period [*Eckhardt and Ott*, 1994]. UPOs populate densely the attractors of chaotic systems and constitute the so-called skeleton of the dynamics. In the case geophysical flows, UPOs have been associated to modes of low-frequency variability [*Gritsun*, 2008]. One can, more qualitatively, associate resonance to positive feedbacks acting on time scales corresponding to the resonant frequency.

2. While $|\chi_A^{(1)}(\omega)|$ measures the amplitude of the response of the system to perturbation at frequency ω, $\arctan(\Im\{\chi_A^{(1)}(\omega)\}/\Re\{\chi_A^{(1)}(\omega)\})$ gives the phase delay between the forcing and the response, because $\Re\{\chi_A^{(1)}(\omega)\}$ ($\Im\{\chi_A^{(1)}(\omega)\}$) gives the component of the response that is in phase (out of phase) with the forcing. Depending on the forcing, on the system, and on the observable, this angle can vary significantly even in a relatively small range of frequencies, as a result of resonances.

3. The two components $\Im\left\{\chi_A^{(1)}(\omega)\right\}$ and $\Re\left\{\chi_A^{(1)}(\omega)\right\}$ are connected by integral equations, the so-called Kramers-Kronig relations [*Lucarini et al.*, 2005; *Lucarini*, 2008, 2009; *Ruelle*, 2009]. Such relations have their foundation in the causality of the Green function (due to the presence of the Heaviside distribution in equation (74)) and establish a fundamental connection between the response at different time scales:

$$\Re\{\chi_A^{(1)}(\omega)\} = \frac{2}{\pi}P\int d\omega' \frac{\omega'\Im\{\chi_A^{(1)}(\omega')\}}{\omega'^2 - \omega^2};\tag{79}$$

$$\Im\{\chi_A^{(1)}(\omega)\} = -\frac{2\omega}{\pi}P\int d\omega' \frac{\omega'\Re\{\chi_A^{(1)}(\omega')\}}{\omega'^2 - \omega^2}.\tag{80}$$

where P indicates that the integral is taken in principal part [*Arfken et al.*, 2005]. In particular, one finds that

$$\Re\{\chi_A^{(1)}(0)\} = \frac{2}{\pi}\int d\omega' \frac{\Im\{\chi_A^{(1)}(\omega')\}}{\omega'},\tag{81}$$

which provides a link between the static response—the sensitivity—and the out-of-phase response at all frequencies. A large literature exists in optics, acoustics, condensed matter physics, particle physics, signal processing on the theory and on the many applications of Kramers-Kronig relations, and on the related *sum rules*, which provide integral constraints related to the asymptotic behavior of the susceptibility [*Lucarini et al.*, 2005].

In Figure 15 we present the real and imaginary parts of the susceptibility of the mean energy e of the celebrated *Lorenz* [1996] model:

$$\frac{dx_i}{dt} = x_{i-1}(x_{i+1} - x_{i-2}) - x_i + F\tag{82}$$

where $i = 1, 2, \ldots, N$, and the index i is cyclic so that $x_{i+N} = x_{i-N} = x_i$, and $e = 1/N\sum_{j=1}^{N} x_j^2/2$. The quadratic term in the equations simulates advection, the linear one represents thermal or mechanical damping and the constant one is an external forcing (see details on the experiments in *Lucarini and Sarno* [2011], performed using $N = 40$ and $F = 8$). The system is perturbed by the vector field $\Psi(x) = [1; \ldots; 1]^{\mathsf{T}}$ modulated
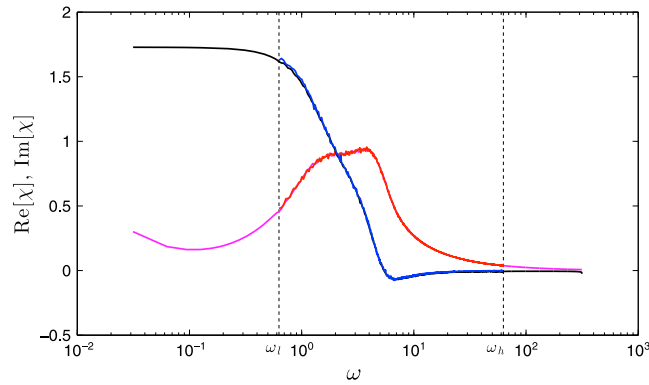
Figure 15. Measured real (blue line) and imaginary (red line) part of the susceptibility for the average energy of the Lorenz 96 model. The rigorous extrapolation of the susceptibility obtained via Kramers-Kronig analysis is reported (real part: black line; imaginary part: magenta line) (data from *Lucarini and Sarno* [2011]).

by $T(t) = 2\epsilon\cos(\omega t)$. The resulting real and imaginary parts of $\chi_e^{(1)}(\omega)$ are reported in Figure 15, together with the output of the data inversion performed via Kramers-Kronig relations. From the susceptibility, as discussed in *Lucarini and Sarno* [2011], it is possible to derive the corresponding Green function by applying the inverse Fourier transform. This has been the first application of the Kramers-Kronig theory in a geophysical context.

5.2.2. Broadband Forcing
If, instead, we select $T(t) = \delta(t)$, we derive from equation (74) that $\rho^{(1)}(A)_t = G_A^{(1)}(t)$, i.e., the Green function corresponds to the relaxation of an ensemble of trajectories of the system

after a finite displacement along $\Psi(x)$. Obviously, we have that $\tilde{\rho}^{(1)}(A)_\omega = \chi_A^{(1)}(\omega)$, where the "~" symbol, indicates, as customary, that a Fourier transform has been applied, so that the Fourier transform of the signal is the linear susceptibility. Therefore, using just one ensemble of experiments where the perturbation is described by an impulsive forcing, we can gather the same information on the response of the system which in the previous case required an accurate sampling of different frequencies.

Let us look at the problem from a slightly more general point of view. We apply the Fourier transform to both sides of equation (73) and obtain

$$\tilde{\rho}^{(1)}(A)_\omega = \chi_A^{(1)}(\omega)\tilde{T}(\omega); \qquad (83)$$

Choosing a sine or cosine function with argument $\omega_0 t$ for the function $T(t)$ amounts to selecting as $\tilde{T}(\omega)$ the sum of two δ's centered in $\omega = \pm\omega_0$. Therefore, the input (forcing) allows only a small portion of the information to derived on the system from the output (response). Let us assume that we choose the modulation $T(t)$ such that $\tilde{T}(\omega)$ is not vanishing for any ω, so that we have a broadband modulation, where, e.g., $|\tilde{T}(\omega)|$ for large values of ω decreases like a power law. If we perform an ensemble of simulations of the forced system, measure $\tilde{\rho}^{(1)}(A)_\omega$, we can invert equation (73) and readily derive

$$\chi_A^{(1)}(\omega) = \frac{\tilde{\rho}^{(1)}(A)_\omega}{\tilde{T}(\omega)}. \qquad (84)$$

Therefore, one single set of experiments is, in fact all we need to do to learn about the linear response properties of the system for the observable A. If we want to predict the response at finite and infinite time of the system to forcing with the same spatial pattern $\Psi(x)$ but with different time modulation $R(t)$, we can derive $G_A^{(1)}(t)$ from $\chi_A^{(1)}(\omega)$ obtained via equation (84) and then plug it into equation (73). Alternatively, one can write

$$\tilde{\rho}^{(1)}(A)_\omega^R = \tilde{\rho}^{(1)}(A)_\omega^T \frac{\tilde{R}(\omega)}{\tilde{T}(\omega)}, \qquad (85)$$

where the upper indices R and T have been inserted for clarity and then compute the inverse Fourier transform to derive the response at all times, or if we apply the inverse Fourier transform to equation (84), we can compute the response to the R perturbation as:

$$\rho^{(1)}(A)_t^R = \int_{-\infty}^{+\infty} d\tau_1 G_A^{(1)}(\tau_1) R(t - \tau_1). \qquad (86)$$

5.3. Prediction via Response Theory
The real test of the quality of an experimentally derived linear Green function $G_A^{(1)}$ is the assessment of its ability to support predictions about the system's response to any temporal pattern of forcing $R(t)$. The real benefit of the broadband approach described here relies on exploiting linearity, and so deriving $G_A^{(1)}$ from
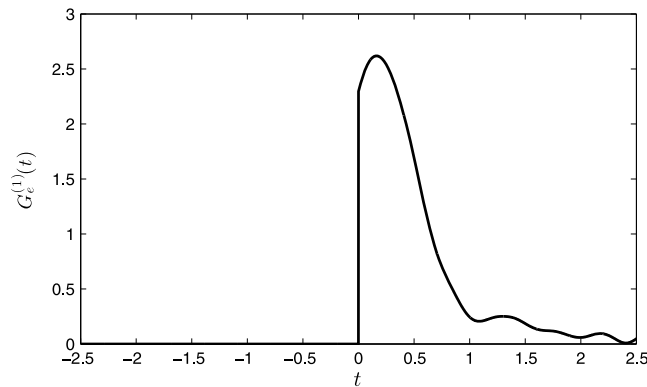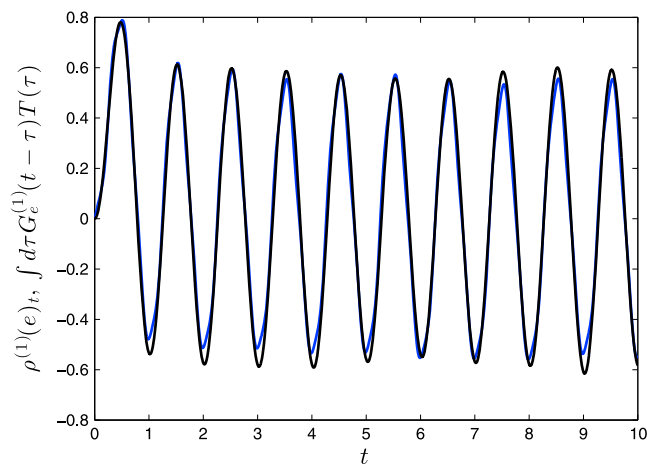
Figure 16. Linear Green function $G_e^{(1)}(t)$ for the average energy e of the *Lorenz* [1996] model obtained by considering a step-like perturbation and using equation (B7). Compare with Figure 4 in *Lucarini and Sarno* 2011.

just one ensemble of simulations, each performed with the same modulation $T(t)$. Computing the $G_A^{(1)}$ per se might be in fact of little relevance.

At this regard, we have performed additional experiments on the *Lorenz* [1996] model mirroring what presented in section 5.2.1. In this case, we have chosen as time modulation $T(t) = \epsilon\Theta(t)$, whose spectrum is indeed broadband $(\tilde{T}(\omega)/\epsilon = \pi\delta(\omega) + iP[1/\omega]$, where P indicates the principal part). In this case, we have

$$G_e^{(1)}(t) = \frac{\mathrm{d}}{\mathrm{d}t}\rho^{(1)}(e)_t. \qquad (87)$$

Using about 1/100 of the computing time needed in *Lucarini and Sarno* [2011], we have produced an estimate of the Green function of comparable quality (see Figure 16). Additionally, we decided to check the predictive power of the reconstructed Green function given in Figure 16 by testing its performance in predicting, through equation (73), the response of the system to a perturbation having temporal pattern given by $T(t) = \epsilon \sin(2\pi t)$ ($\epsilon = 0.25$). The results are presented in Figure 17. The agreement between the measured value of $\rho^{(1)}(e)_t$ and the value predicted using $\int \mathrm{d}\tau G_e^{(1)}(\tau)T(t - \tau)$ is remarkable. One must emphasize that the agreement is comparable if one selects $\epsilon = 1$, thus moving away from the linear regime.

5.4. Climate Response, Climate Change Prediction

Let us take inspiration from the previous example in order to get some results of stricter geophysical relevance: we want to perform predictions on the impact of increases in the CO_2 concentration on the globally averaged surface temperature as simulated by a climate model, the simplified yet Earth-like PLASIM [*Fraedrich et al.*, 2005]. In what follows we present some new results (see also discussion in *Ragone et al.* [2014]), with the goal of proving the feasibility of the proposed methodology. Let us summarize the main points:


Figure 17. Prediction of finite-time response of the average energy e of the *Lorenz* [1996] model to a forcing with modulation $T(t) = \epsilon \sin(2\pi t)$ ($\epsilon = 0.25$). Observed response $\rho^{(1)}(e)_t$ (blue line) versus prediction obtained using the linear Green function $G_e^{(1)}(t)$ shown in Figure 16.

1. We take $\dot{x} = F(x)$ as the system of equations describing the discretized version of a given model of the continuum partial differential equations describing the evolution of the climate in a baseline scenario with set boundary conditions and values for, e.g., the CO_2 concentration and the value of the solar constant. We assume, for simplicity, that system model does not feature daily or seasonal variations in the radiative input at the top of the atmosphere.

2. Let us choose for the observable A the globally averaged surface temperature of the planet T_S.

3. We study the perturbed system $\dot{x} = F(x) + f(t)\Psi(x)$. Let us choose as perturbation field $\Psi(x)$ the convergence of radiative fluxes due to change in the logarithm of the atmospheric CO_2 concentration.
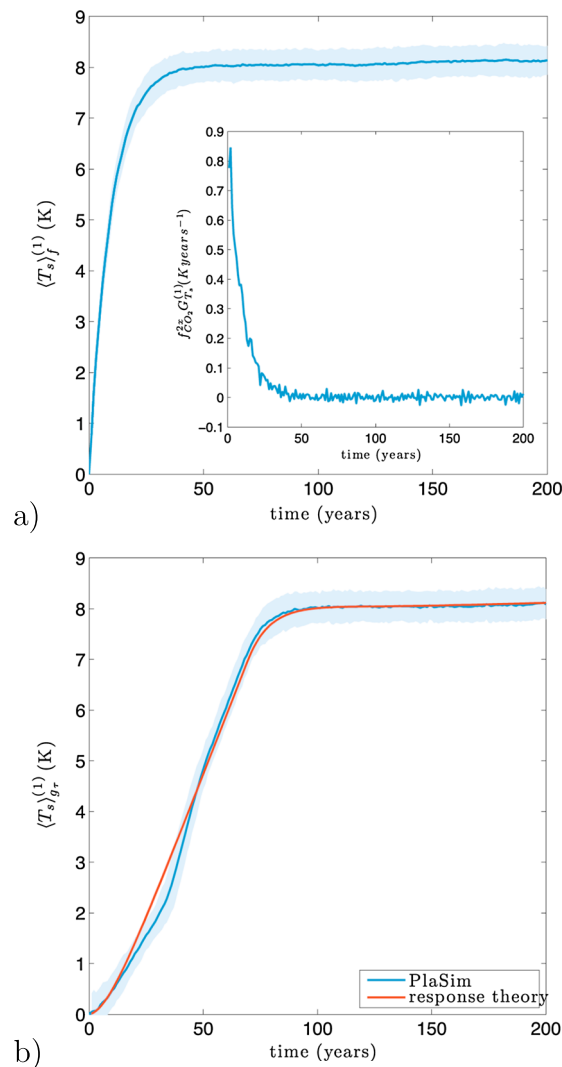
Figure 18. Studying climate change using response theory. (a) Change in T_S after an instantaneous doubling of the CO_2 concentration. The lightly colored band indicates the two-standard deviation range around the ensemble mean. Insert: Green function of the T_S. (b) Comparison between GCM simulations (blue) and response theory prediction (red) for 1% per year increase of the CO_2 concentration up doubling. Lightly colored band as in Figure 18a.

We want to be able to predict at finite and infinite time the response of the system to one of the standard CO_2 forcing scenario given by the Intergovernmental Panel on Climate Change (IPCC) by performing an independent set of perturbed model integrations.

4. The test perturbation is modulated by the function $f(t) = \epsilon\Theta(t)$, where ϵ is such that we double the amount of CO_2 concentration in the atmosphere. A progressively increasing concentration of CO_2 from a baseline value to a new stabilization concentration.

5. We perform 200 simulations, each lasting 200 years for both scenarios of CO_2 forcing. Our experiments are performed using PLASIM [*Fraedrich et al.*, 2005] with a T21 spatial resolution, 10 vertical layers in the atmosphere, and swamp ocean having depth of 50 m.

From the time series of the ensemble mean of the change of T_S—$\rho^{(1)}(T_S)_t$—resulting from the sudden increase in the CO_2, we derive the Green function $G_{T_S}^{(1)}(t)$ using equation (87) (see Figure 18a). Climate sensitivity is, in fact, defined by equation (81). Given the chosen pattern of forcing, we can rewrite is as follows:

$$\Delta_T = \mathfrak{R}\{\chi_{T_S}^{(1)}(0)\} = \frac{2}{\pi}\int d\omega' \mathfrak{R}\{\tilde{\rho}^{(1)}(T_S)_{\omega'}\}, \quad (88)$$

which relates climate response at all frequencies to its sensitivity.

In order to test the predictive power of the response theory, we then convolute the Green function with the temporal pattern of forcing of the second set of experiments.

We choose as test experiment the classical IPCC scenario of 1% per year exponential increase of CO_2 concentration up to doubling of the initial concentration (realized in $\tau \sim 70$ years and constant concentration afterward). We select as baseline CO_2 concentration 360 ppm. Since our relevant control parameter is the logarithm of the CO_2 concentration, the second pattern of forcing $g(t)$ is, in fact, a ramp increasing linearly with time from 0 to ϵ in $\tau \sim 70$ years, with constant value equal to ϵ for larger times. The results are presented in Figure 18b, where we compare the predicted pattern of increase (blue line), obtained using equation (86), with the measured one (black line). The agreement is remarkable, both on the short and on the long time scales, while a some discrepancy exists between 20 and 50 years lead time, where strong nonlinear effects due to ice-albedo feedback are dominant (not shown).

Apparently, despite all the nonlinear feedbacks of the climate model, the response to changes in the logarithm of CO_2 concentration can be accurately described by linear response theory at all time scales. Nonlinearity in the underlying equations and the presence of strong positive and negative feedbacks do not rule out the possibility of constructing accurate methods for predicting the response. In fact, the methods described here could be extended to the nonlinear case by looking at the response in the frequency domain [*Lucarini*, 2008, 2009], even if the data quality requirements are obviously stricter.

The result presented here suggests that many of the scenarios of greenhouse gases concentration included in the IPCC reports [*IPCC*, 2001, 2007, 2013] may in fact be partly redundant, as for certain variables might be accurately described by linear response theory starting from just one scenario. Equations (84) and (85) constitute the basis for predicting climate response at all scales.

Obviously, with a given set of forced experiments, it is possible to derive the sensitivity to the given forcing for as many climatic observables as desired. It is important to note that, for a given finite intensity ϵ of the forcing, the accuracy of the linear theory in describing the full response depends also on the observable of interest. Moreover, the signal-to-noise ratio and, consequently, the time scales over which predictive skill is good may change a lot from variable to variable. The results presented in this section extend to a more general setting and with stronger foundation the excellent intuition by *Hasselmann et al.* [1993] on the use of the linear response for addressing the problem of the so-called *cold start* of coupled atmosphere-ocean models.

Here we have shown results from just one observable primary climatic interest. The analysis of other observables will shed light on the mechanisms determining the climate response to the forcing due to changes n the atmospheric composition. As an example, the analysis of the response of large-scale meridional gradients of temperature at surface and in the middle troposphere will provide information on changes in the midlatitude circulation. The existence of approximate functional relationship between the susceptibilities of different observables [*Lucarini*, 2009] would provide the key for defining rigorously the so-called emergent constraints [*Bracegirdle and Stephenson*, 2012].

In practical terms, the applicability of response theory corresponds to having smooth dependence of climate properties with respect to some given parameters. Indeed, this is not the case in the vicinity of tipping points (see Figure 12). Response theory, may, nonetheless, suggests rigorous ways for defining and detecting tipping points, because one expects that these are associated to a divergence of the linear response.

Finally, in order to talk about predictability, we need to specify what are the time scales over which we expect to have satisfactory predictive skills. In fact, linear response theory allows for deriving some scaling laws for addressing this matter. The main obstacle for achieving a good degree of predictability is the uncertainty on the estimate of response signal given in equation (83) from the outcomes of the numerical experiments because of the finiteness of the ensemble and of the duration of each numerical simulation. See a detailed discussion of this issue in *Ragone et al.* [2014].

6. Multiscale Systems and Parametrizations

The climate system features nontrivial behavior on a large range of temporal and spatial scales [*Peixoto and Oort*, 1992; *Vallis*, 2006; *Lucarini*, 2013; *Fraedrich and Böttger*, 1978]. When representing such a complex system in a numerical simulation, the ratio of smallest to largest time scale determines the number of required time steps and the number of interactions between scales that have to be calculated at each step can increase exponentially with the range of spatial variables. It is therefore clear that, no matter which are the available computing resources, we are able to simulate explicitly only the variables relevant for the given ranges of spatial and temporal scales. Different choices of such ranges correspond to different approximate theories of geophysical fluid dynamics aimed at describing specific phenomenologies, a prominent case being that of quasi-geostrophic theory [*Klein*, 2010].

A manifestation of the inability to treat ultraslow variability can be found in the usual practice in climate modeling of choosing fixed or externally driven boundary conditions, such as done when assuming a fixed mass or extent for the land-based glaciers, or imposing a specific path of CO_2 concentration for the atmosphere. Instead, the impossibility of treating accurately fast processes requires the construction of so-called parametrizations able to account, at least approximately, for the effect of the small scales on the large scales, as a function of the properties of the large-scale variables. This is the case of several important physical processes, such as, e.g., deep and shallow atmospheric convection, gravity wave drag, clouds, and mixing in the ocean.
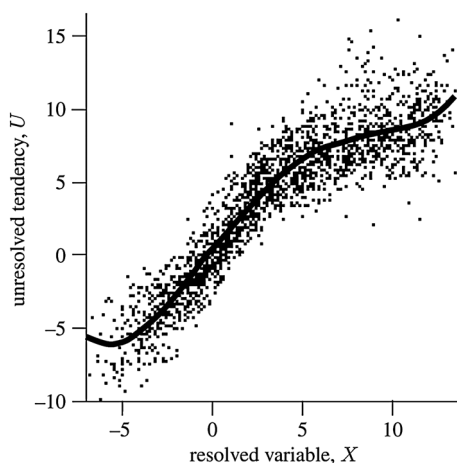
Figure 19. Diagram describing how to parametrize the effect of the fast variables on the tendency of the slow variables X. The solid line U—see y axis—corresponds to M_X in equation (90), while the variability associated to the cloud of points needs to be represented via a stochastic term like η in equation (90). Reprinted with permission from *Wilks* [2005]. Copyright ©2005 Royal Meteorological Society.

Parametrizing small-scale processes is important because such unresolved processes impact the dynamics of larger scales in terms of error growth, predictability, and climatic biases. Presently, most of the parametrizations used in climate models are deterministic; i.e., for a given state of the resolved variables, the effect of the unresolved scales on the resolved scales is uniquely determined. We often refer to these as *bulk parametrizations*. More recently, it has been emphasized that such a point of view should be modified for taking into account the fact that many different states of the unresolved variables are compatible with a given state of the resolved variables. This leads to considering the possibility of using stochastic parametrizations [*Palmer and Williams*, 2009; *Franzke et al.*, 2014] which show promising abilities in reducing biases and reproducing more effectively the uncertainties associated to performing mode reduction.

When a large time scale separation exists between the resolved and unresolved variables, the problem of parametrization can be cast as follows. We consider a system of the form $\dot{Z} = F(Z)$, $Z \in R^N$, and we divide the state vector $Z = (X, Y)$, where X are the slow components we are interested into and Y are the fast components we want to parametrize. We rewrite the evolution equation as follows:

$$\frac{\mathrm{d}X}{\mathrm{d}t} = G_X(X, Y) = F_X(X) + \Phi_X(X, Y)$$
$$\frac{\mathrm{d}Y}{\mathrm{d}t} = G_Y(X, Y) = F_Y(Y) + \Phi_Y(X, Y), \tag{89}$$

where we have split the dynamics of each set of variables into an autonomous part and into the coupling terms. The basic goal is to be able to write as an equation of the form

$$\frac{\mathrm{d}X}{\mathrm{d}t} = F_X(X) + M_X(X) + \eta(X), \tag{90}$$

where M_X and η correspond to the deterministic and stochastic components of the parametrization, respectively. A now classic example of empirical construction and of testing of stochastic parametrizations is given by *Wilks* [2005] (see Figure 19).

It must be emphasized that many of the approaches used so far have been based on the existence of a time scale separation between microscopic and macroscopic processes, following, conceptually, the pioneering point of view proposed by *Hasselmann* [1976]. If one does assume such a vast time scale separation between the slow variables X and the fast variables Y, averaging and homogenization methods [*Arnold*, 2001; *Kifer*, 2004; *Pavliotis and Stuart*, 2008] allow for deriving an effective autonomous dynamics for the X variables, able to encompass the impact of the dynamics of the Y variables. The motivation most often stated for the applicability of this theory to climate science is the setting considered by Hasselmann, where fast *weather* systems influence slow *climate* dynamics.

Unfortunately, in many practical cases of interest in geophysical fluid dynamics, such a scale separation does not exist—see, e.g., the classical study by *Mitchell* [1976]—so that there is no spectral gap able to support univocally the identification of the X and Y variable. In fact, when the resolution of a numerical model is changed, all the parametrizations have to be retuned, because the set of resolved variables has changed.

Here we will focus on analytical methods that allow one to derive reduced models from the dynamical equations of a full model. Projector operator techniques have been introduced in statistical mechanics with the goal of effectively removing the Y variables. In particular, considerable interest has been raised by the Mori-Zwanzig approach, through which a formal—albeit practically inaccessible—solution for the evolution

of the X variables is derived [*Zwanzig*, 1961; *Mori*, 1965; *Zwanzig*, 2001]. These equations in general contain both a correlated noise term and a memory term. Some attempts have been made to make approximation to the Mori-Zwanzig projected equations to obtain practically useful equations. In applications of stochastic mode reduction in climate science, the memory term is usually not taken into account. This term could, however, be very relevant in systems without a time scale separation, as, for example, in the parametrization of cloud formation in an atmospheric circulation model. The presence of memory in such systems has been discussed by *Bengtsson et al.* [2013], *Davies et al.* [2009], and *Piriou et al.* [2007]. Note that, when we consider coupled systems where asynchronous integration is used, memory effects are implicitly present in the dynamics.

Besides considering the limit of infinite time scale separation, another point of view can be taken, namely considering the limit of weak coupling between the dynamical processes occurring at different scales. In this limit, the dynamics retains the correlated noise and memory dependence that appeared in the Mori-Zwanzig reduced equations. The advantage of looking at this limit is, however, that the noise autocorrelation function and memory kernel can now be written as simple correlation and response functions of the unresolved dynamics.

6.1. Averaging and Homogenization

When applying averaging and homogenization techniques, one considers dynamical systems where a small parameter ϵ controls the time scale separation between a slow and fast evolution in the system. The prototypical set of equations for such a problem is

$$\frac{dX}{dt} = G_X(X, Y)$$
$$\frac{dY}{dt} = G_Y(X, Y) = \frac{1}{\epsilon}\tilde{G}_Y(X, Y).$$

The parameter ϵ controls the time scale separation between the variables X and Y, which becomes infinite as $\epsilon \to 0$.

As the time scale separation becomes large, on the typical time scale for the variable Y, the value of X will remain almost constant. The fast variable Y will obey an evolution defined by (X, Y) for the current fixed value of X. On the much longer time scale connected to the slow system, the evolution of X integrates out the rapid fluctuation of Y. As in the law of large numbers, the overall effect of all these integrated fluctuations can be substituted by one single value. It can be shown that for finite time T, the following applies

1. the trajectory $X(t)$ converges to a solution of:

$$\frac{d\bar{X}}{dt} = \bar{G}_{\bar{X}}(\bar{X}),$$

where $\bar{G}_{\bar{X}}(\bar{X}) = \rho_{\bar{X}}(G_X(\bar{X}, Y))$ is the averaged value of the tendency; and
2. the average is taken over the invariant measure $\rho_{\bar{X}}$ of the Y variable of the dynamical system

$$\frac{dY}{dt} = G_Y(\bar{X}, Y)$$

resulting when $\bar{X}$ is considered as a fixed forcing parameter.

Let us consider a simple example system.

$$\frac{dX}{dt} = (1 - Y^2)X$$
$$\frac{dY}{dt} = -\frac{1}{\epsilon}Y + \sqrt{\frac{2}{\epsilon}}\frac{dW}{dt}.$$

The Y system is here independent of X. The invariant measure of the fast Y system is a Gaussian distribution with zero mean and unit variance. Taking the average of $G_X(X, Y) = (1 - Y^2)X$ under the invariant measure of Y, we see that the averaged equation in this case is the uninteresting equation $\dot{X} = 0$.

This simple example immediately motivates the use of homogenization methods. Here one scales the equation to a longer time scale $\theta = \epsilon t$, the so-called diffusive time scale and then performs an asymptotic

expansion. Similarly to how correctly rescaling the sums of the law of large number leads to the more interesting central limit theorem, which describes the fluctuations around the average value, in the setting of time scale-separated systems we get stochastic behavior on the diffusive time scale. For the example considered above, we get a *weak convergence* to a reduced stochastic differential equation for the *X* variable instead of the trivial dynamical system obtained before [*Pavliotis and Stuart*, 2008].

The theory for averaging and homogenization in time scale-separated stochastic differential equations is well understood, with results for both one-way and two-way couplings between the levels [*Bakhtin and Kifer*, 2004]. As usual, the theory is more complicated for deterministic systems. Examples of dynamical systems can be constructed where for a large set of initial conditions of *Y*, the solution for *X* does not converge to the averaged solution [*Kifer*, 2008]. Furthermore, if the *Y* system has long time correlations, such as in a system with regime behavior, the homogenized system may converge badly and an extension based on a truncation of the transfer operator has been proposed [*Schütte et al.*, 2004].

Abramov [2012] has recently presented a study of uncertainty and predictability of the slow dynamics for a system of geophysical relevance. A study of averaging and homogenization for idealized climate models, with a range of examples, can be found in *Monahan and Culina* [2011]. Another rather successful attempt in this direction is given in *Majda et al.* [2001]. In *Strounine et al.* [2010] stochastic mode reduction is applied to a three-level quasi-geostrophic model, whereas in *Arnold et al.* [2003] the authors perform mode reduction on a simple coupled atmosphere-ocean model. Another application of homogenization to a toy model for the large-scale dynamics of the atmosphere can be found in *Frank and Gottwald* [2013]. Averaging for the case where one deals with partial differential equations, as is relevant for climate modeling, is discussed by *Dymnikov and Filatov* [1997].

A study of homogenization for geophysical flows was performed in *Bouchet et al.* [2013]. The slow system is considered to be the evolution of zonal jets of a barotropic flow, which is forced by noise. The fast degrees of freedom are those representing the fast nonzonal turbulence. Homogenization has also been applied in *Dolaptchiev et al.* [2013] to the Burgers' equation, where the slow variables are taken to be averages over large grid boxes and the fast variables are the subgrid variables.

When one wants to consider very large time scales (for example, times of the order of $\exp(1/\epsilon)$), one needs to look beyond the central limit type theorems of homogenization and consider so-called large deviation results. These describe, for example, the transitions between disconnected attractors of the averaged equations [*Kifer*, 2009] and are of great relevance for studying tipping points [*Lenton et al.*, 2008], going beyond simple one-dimensional approximate theories (see, e.g., discussion in *Lucarini et al.* [2012]).

6.2. Projection Operator Techniques

Projection operator techniques do not constitute a mode reduction per se but are a way to rewrite the dynamical equation of a multilevel equations to depend only on a subset of variables. A projection is carried out on the level of the observables to remove unwanted, irrelevant, and usually fast degrees of freedom. The price one has to pay for this apparent reduction is the appearance of additional terms that are as difficult to compute as the original system. It can, however, be a useful starting point for further approximations. These techniques are also known as the Mori-Zwanzig approach [*Zwanzig*, 1960, 1961; *Mori et al.*, 1974].

If a dynamical system is defined on a manifold $\mathcal{M}$, one defines a projection $\mathcal{P}$ from the space of observable functions on the full-phase space $\mathcal{M}$ to a space of observables which are considered to contain only the interesting dynamics. Many different choices are possible; if the manifold $\mathcal{M}$ consists, for example, of a product of submanifolds $\mathcal{K}$ of relevant and $\mathcal{L}$ of irrelevant variables, one can take a conditional expectation with respect to a measure on $\mathcal{M}$, given the value of the relevant variables $X \in \mathcal{K}$:

$$(\mathcal{P}A)(X) = \frac{\int_{\mathcal{N}} A(X, Y)\rho(X, Y)\mathrm{d}Y}{\int_{\mathcal{N}} \rho(X, Y)\mathrm{d}Y} \, .$$

Another possible choice is a projection onto a set of functions on $\mathcal{M}$, such as linear functions of the coordinates in a Euclidean phase space. In general, one can think at various ways of performing *coarse graining*.

Let us go back to our general formulation of a dynamical system of the form $\dot{Z} = F(Z)$, $Z \in R^N$. The evolution of an observable $A(Z)$ can be written as $\dot{A}(Z) = F(Z) \cdot \nabla_Z A(Z)$, which can be written as $\dot{A} = LA$, often referred
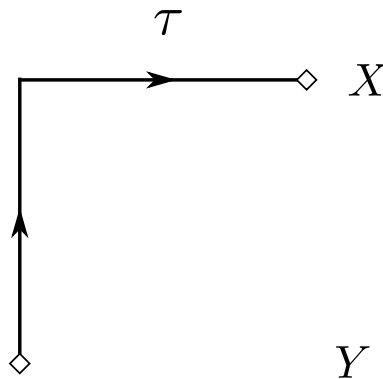
Figure 20. Diagram describing the mean field effect of the Y variables on the X variables. Term M in equation (94).

to as the Liouville equation. The evolution operator L is split into its projection $\mathcal{P}L$ onto the relevant space of observables and the complement $\mathcal{Q}L := (1 - \mathcal{P})L$. As described by *Zwanzig* [2001], a generalized Langevin equation can then be derived based on Dyson's formula for operator exponentials

$$e^{tL} = e^{tQL} + \int_0^t e^{(t-s)L}\mathcal{P}Le^{sQL}\mathrm{d}s. \tag{91}$$

We write the Liouville equation for an observable A as

$$\frac{\mathrm{d}A(t)}{\mathrm{d}t} = LA(t) = e^{tL}LA = e^{tL}\mathcal{P}LA + e^{tL}\mathcal{Q}LA.$$

The factor $\exp(tL)$ in the second term can be further expanded by making use of equation (91). This gives the following equation

$$\frac{\mathrm{d}A(t)}{\mathrm{d}t} = e^{tL}\mathcal{P}LA + (e^{tQL} + \int_0^t \mathrm{d}s\, e^{(t-s)L}\mathcal{P}Le^{sQL})\mathcal{Q}LA.$$

Zwanzig [2001] proposes the following interpretation of this equation. The first term on the right-hand side corresponds to the regular, deterministic dynamics of the system. The second term can be seen as describing a contribution from correlated noise, dependent on the initial conditions of the irrelevant degrees of freedom. The third term (under the integral) represents the memory of the system due to the presence of irrelevant variables that have interacted with the relevant ones in the past. In other terms, the price we pay by separating somewhat arbitrarily relevant from irrelevant degrees of freedom is that the irrelevant degrees of freedom act as a stochastic component and, somewhat counterintuitively, as proxies for the past state of the relevant degrees of freedom. Note that we have done nothing more than manipulating the original evolution equation $\dot{A} = LA$. Correspondingly, the Mori-Zwanzig equation in itself does not simplify the problem. In order to derive a set of equations that are useful for numerical simulations, assumptions need to be made about the dynamical system.

Several approximations to the Mori-Zwanzig equations have been proposed in the literature. There are the short- and long-memory approximations made in the method of optimal prediction [*Chorin and Hald*, 2013; *Hald and Kupferman*, 2001; *Chorin et al.*, 2006; *Chorin and Stinis*, 2006; *Chorin et al.*, 2000; *Park et al.*, 2007; *Chorin et al.*, 1998; *Bernstein*, 2007; *Chorin et al.*, 2002].

In the limit of an infinite time scale separation between the relevant and irrelevant variables, the stochastic component of the parametrization can be represented as a white noise term, while the memory (also known as *non-Markovian*) term vanishes, as the irrelevant variables decorrelate quickly. Therefore, in such a limit the Mori-Zwanzig decomposition is equivalent to the homogenization method of section 6.1. For a comparison of the short-memory approximation of Mori-Zwanzig to homogenization for climate-relevant models, see *Stinis* [2006]. We also refer the reader to recent results of *Chekroun et al.* [2013a, 2013b], where general mathematical results for the procedure of mode reduction, with thorough geometrical and dynamical interpretations, are given.

Applications of the Mori-Zwanzig approach to fluid dynamics can be found in *Stinis* [2007], *Chandy and Frankel* [2009], *Hald and Stinis* [2007], and *Hou* [2007]. A simple approximation to Mori-Zwanzig has been applied to jet formation on a beta plane in *Tobias and Marston* [2013].

6.3. Weakly Coupled Systems

We now consider dynamical systems consisting of two systems with a weak coupling. In this case an expansion of the dynamics can be

Figure 21. Diagram describing the impact of fluctuations of the Y variables on the X variables. Term σ in equation (94).
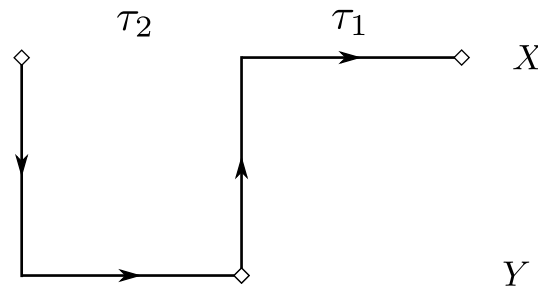
Figure 22. Diagram describing the non-Markovian effect of the X variables on themselves, mediated by the Y variables. Term h in equation (94).

made in orders of the coupling, giving insight into what properties of the coupled systems determines the memory kernel and correlated noise that appeared in the Mori-Zwanzig approach [*Wouters and Lucarini*, 2012, 2013], because no assumptions are taken regarding time scale separation.

A possible application of this theory in climate science can be found in the interaction between cloud formation and large-scale atmospheric flow, where there is no distinct time scale separation, but instead the coupling could be considered as weak. The weak coupling limit of a tropical ocean-atmosphere model has also been considered in the literature [*Neelin and Jin*, 1993].

Let us go back to equation (89). In this setting, the background vector field F consists of a Cartesian product $(F_X, F_Y)^\top$ of the vector fields F_X and F_Y defining the autonomous X and Y dynamics. The perturbing vector field δF is a coupling $(\Psi_X, \Psi_Y)^\top$ between the two systems. We rewrite the full dynamical system as

$$\frac{\mathrm{d}X}{\mathrm{d}t} = F_X(X) + \epsilon \Psi_X(X, Y)$$
$$\frac{\mathrm{d}Y}{\mathrm{d}t} = F_Y(Y) + \epsilon \Psi_Y(X, Y), \tag{92}$$

where ϵ is added in order to clarify what kind of perturbative expansion we consider. For simplicity of presentation, for now we consider the case where $\Psi_X(X, Y) = \Psi_X(Y)$ and $\Psi_Y(X, Y) = \Psi_Y(X)$. We will come back to the general case later.

Given that the coupling term $\epsilon\Psi$ can be seen as a small perturbation to the uncoupled system, one can make use of response theory to study the change of long time means under a change in the coupling parameter ϵ. We can therefore use the response formalism described in section 5. After lengthy calculations, one obtains the explicit expression for

$$\rho(A)_t = \rho^0(A)_t + \rho^{(1)}(A)_t + \rho^{(2)}(A)_t + O(\Psi^3). \tag{93}$$

As shown by *Wouters and Lucarini* [2012], if one collects these first- and second-order responses to the coupling Ψ, an identical change in expectation values from the unperturbed ρ_0 up to third order in Ψ can be obtained by adding a Y independent forcing to the tendency of the X variables as follows:

$$\frac{\mathrm{d}X(t)}{\mathrm{d}t} = F_X(X(t)) + M + \sigma(t) + \int_0^\infty \mathrm{d}\tau h(\tau, X(t - \tau)), \tag{94}$$

where $M = \rho_{0,Y}(\Psi_X)$ is an averaged version of the Y to X coupling, σ is a stochastic term, mimicking the two time correlation properties of the unresolved variables, and h is a memory kernel that introduces the non-Markovianity. A diagrammatic representation of processes responsible that these three additional terms are parametrizing is given in Figures 20–22. Figure 20 refers to the mean-field effect, which is captured by the first-order correction, and corresponds to the deterministic parametrization. Figure 21 describes the effect of the fluctuations of the unresolved variables, which results into an effective stochastic term in the parametrization. Finally, Figure 22 clarifies how memory effects enter into the picture of the parametrization: the resolved variables at a given time impact the resolved variables at a later time through a transfer of information mediated by the unresolved variables. The memory effect is present due to the finite time scale difference between resolved and unresolved variables, which also ensures that the stochastic contribution shown in Figure 21 cannot be represented by a white noise process. In *Wouters and Lucarini* [2013] this reduced equation was shown to be related to an expansion in the coupling strength of a Mori-Zwanzig equation.

If the coupling functions Ψ_X and Ψ_Y are allowed to be dependent on both X and Y, the above analysis can still be carried out. In practical terms, this accounts for the possibility that the coupling terms are function of

both the variables we want to parametrize and of those we want to keep explicitly represented in our model. For the case of separable couplings $\Psi_X(X, Y) = \Psi_{X,1}(X)\Psi_{X,2}(Y)$ and $\Psi_Y(X, Y) = \Psi_{Y,1}(X)\Psi_{Y,2}(Y)$, the average term becomes X dependent and the noise term becomes multiplicative instead of additive. An expression for more general couplings can be derived by decomposing the coupling functions into a basis of separable functions and then the same procedure can be applied. See *Wouters and Lucarini* [2012].

7. Summary and Conclusions

The goal of this review paper is the provision of an overview of some ideas emerging at the interface between climate science, physics, and mathematics, with the objective of contributing to bridging the gap between different scientific communities. The topics have been selected by the authors with the goal of covering (at least partially) relevant aspects of the deep symmetries of geophysical flows, of the processes by which they convert and transport energy, and generate entropy, and of constructing relevant statistical mechanical models able to address fundamental issues like the response of the climate system to forcings, the representation of the interaction across scales, the definition of relevant physical quantities able to describe succinctly the dynamics of the system. This review also informs the development and testing of climate models of various degrees of complexity, by analyzing their physical and mathematical well-posedness and for constructing parametrizations of unresolved processes, and by putting the basis for constructing diagnostic tools that able to capture the most relevant climate processes.

The Nambu formulation of geophysical fluid dynamics explored in section 2 emphasizes the existence, in the inviscid and unforced case, of nontrivial conserved quantities that are embedded in the equations of motion. Such quantities play a fundamental role, analogous to the role of energy, in the description of the state and of the dynamics of the system, and can be regarded as observables of great relevance also in the case where dissipation and forcing are present. Moreover, the Nambu formalism suggests us ways for devising very accurate numerical schemes, which do not have spurious diffusive behavior.

The symmetry properties of the flow in the inviscid limit allow the construction of the ensembles describing the equilibrium statistical mechanical properties of the geophysical flows (section 3), where the vorticity—in the two-dimensional case—plays the role of the most important physical quantity. Starting from the classical construction due to Onsager of the gas of interacting vortices, the theory leads us to construct a theory of barotropic and baroclinic QG turbulence.

Taking the point of view of nonequilibrium systems, we have that thanks to the presence of gradients of physical quantities like temperature and chemical concentrations—in first instance due to the inhomogeneity of the incoming solar radiation, of the optical properties of the geophysical fluids, and of the boundary conditions—the climate system can transform available potential energy into kinetic energy via internal instabilities, resulting in organized fluid motions. In section 4 the analysis of the energy and entropy budgets of the climate system is shown to provide a comprehensive picture of climate dynamics, new tools for testing and auditing climate models and measuring climate change, for investigating of the climate tipping points, and for studying the properties of general planetary atmospheres.

Section 5 introduces some basic concepts of nonequilibrium statistical mechanics, connecting the macroscopic properties described in the previous section to the features of the family of chaotic dynamical systems which constitute the backbone of the mathematical description of nonequilibrium systems. For such systems, the relationship between internal fluctuations and response to forcings is studied with the goal of developing methods for predicting climate change. After clarifying the conditions under which the FDT is valid, we present some new results such as a successful climate prediction for decadal and longer time scales. In this sense, we show that the problem of climate change is mathematically well posed.

Nonequilibrium statistical mechanics is also the subject of section 6, where we show how the Mori-Zwanzig formalism supports the provision of rigorous methods for constructing parametrizations of unresolved processes. It is possible to derive a surrogate dynamics for the coarse-grained variable of interest for climatic purposes, incorporating, as result of the coupling with the small-scale, fast variables, a deterministic, a stochastic, and a non-Markovian contribution, corresponding to memory effects, which add to the unperturbed dynamics. The same results can be obtained using the response theory described in section 5, thus showing that the construction of parametrizations for weather and for climate models should have common ground.

Among the many topics and aspects left out of this review, we need to mention recent developments aimed at connecting the complementary, rather than opposing *Lorenz* [1963] and *Hasselmann* [1976] perspectives on complex dynamics, which focus on deterministic chaos and stochastic perturbations to dynamical systems, respectively. We refer in particular to the idea of constructing time-dependent measures for nonautonomous dynamical systems [*Chekroun et al.*, 2011] through the introduction of the so-called *pullback attractor*, which is the geometrical object the trajectories initialized in a distant past tend to at time *t* with probability 1 as a result of the contracting dynamics. Such an object is not invariant with time, as a result of the time-dependent forcing, but, under suitable conditions on the properties of the dynamical system, the supported measure has at each instant properties similar to those of the (invariant) SRB measure one can construct for, e.g., autonomous Axiom A dynamical [*Ruelle*, 1989]. Such an approach allows for treating in a coherent way the presence of modulations in the dynamics of the system, without the need of applying response formulas or of assuming time scale separations, and in particular allows for analyzing the case where the forcing is stochastic, leading to the concept of random attractor [*Arnold*, 1988]. On a different line of research, it is instead possible to use Ruelle response theory for computing the impact of adding stochastic noise on chaotic dynamical systems [*Lucarini*, 2012]. One finds the rate of convergence of the stochastically perturbed measure to the unperturbed one and discovers the general result that adding noise enhances the power spectrum of any given observables at all frequencies. The difference between the power spectrum of the perturbed and unperturbed system can be used, mirroring an FDT, for computing the response of the system to deterministic perturbations.

The methods, the ideas, and the perspectives presented in this paper are partially overlapping, partially complementary, partly in contrast. In particular, it is not obvious, as of today, whether it is more efficient to approach the problem of constructing a theory of climate dynamics starting from the framework of Hamiltonian mechanics and quasi-equilibrium statistical mechanics or taking the point of view of dissipative chaotic dynamical systems and of nonequilibrium statistical mechanics, and even the authors of this review disagree. The former approach can rely on much more powerful mathematical tools, while the latter is more realistic and epistemologically more correct, because, obviously, the climate is, indeed, a nonequilibrium system. Nonetheless, the experience accumulated in many other scientific branches (chemistry, acoustics, material science, optics, etc.) has shown that by suitably applying perturbation theory to equilibrium systems one can provide an extremely accurate description of nonequilibrium properties. Such a lack of unified perspective, of well-established paradigms, should be seen as sign of the vitality of many research perspectives in climate dynamics.

Appendix A: Glossary

For the benefit of the reader, we report here the most relevant symbols used in this paper, indicating if the same symbol is used with different meaning.

$\mathcal{H}$	Hamiltonian functional
$\{\bullet, \bullet\}_P$	Standard Poisson brackets
$\mathbf{u}$	Velocity vector (two- or three-dimensional)
$\mathbf{u}_a$	Absolute velocity vector (including planetary rotation)
$\nabla \cdot$	Divergence operator (two- or three-dimensional)
$\nabla_h \cdot$	Horizontal divergence operator for three-dimensional vectors
∇	Gradient operator (two- or three-dimensional)
∇_h	Horizontal gradient operator for three-dimensional fields
ψ	Stream function
ω	Vorticity function (two-dimensional dynamics)
$\boldsymbol{\omega}$	Vorticity vector (three-dimensional dynamics)
$\boldsymbol{\omega_a}$	Absolute vorticity vector (including planetary vorticity)
S	Symplectic matrix [0, −1; 1, 0];
$\mathcal{J}$	Jacobian operator
$\mathcal{X}$	Generic functional
$\delta \mathcal{X} / \delta a$	Functional derivative of $\mathcal{X}$ with respect to the function a.
$\{\bullet, \bullet, \bullet\}$	Nambu brackets
μ	Horizontal divergence of the velocity field

h_T	Total thickness of the fluid (shallow water equations)
h	Helicity
h_a	Absolute helicity (including planetary rotation)
$f = f_0 + \bar{\beta}y$	Planetary vorticity in beta plane approximation (y indicates the south-north coordinate)
Φ	Geopotential
Q	Quasi-geostrophic potential vorticity
q	Potential vorticity for shallow water equations (section 2); specific humidity (section 4)
N	Brunt-Väisälä frequency
ρ	Density of the fluid (sections 2 and 4); invariant measure of the system (sections 3, 5, and 6).
$\mathbf{\Omega}$	Earth's angular velocity vector
Π	Ertel's potential vorticity
$\mathcal{E}$	Enstrophy functional
β	Inverse temperature
$\mathcal{E}_\rho$	Potential enstrophy functional
$\mathcal{S}$	Entropy functional
$\mathcal{M}$	Mass functional
$\mathcal{Z}$	Partition function
$R_D = 2\pi/k_D$	Rossby deformation radius
$\mathscr{S}$	Mixing entropy
e	Specific energy per unit mass
i	Specific internal energy per unit mass
H	Relative humidity
g	Gravity
T	Temperature
C_v, C_W	Specific heat at constant volume
$s\ (\sigma = \rho s)$	Specific entropy per unit mass (per unit volume)
$\Omega(E)$	Structure function
L	Latent heat of vaporization (section 4); Liouville operator (section 6)
$\mathbf{F_R}$	Vector of radiative flux
$\mathbf{F_S}$	Vector of turbulent sensible heat flux
$\mathbf{F_L}$	Vector of turbulent latent heat flux
τ	Surface stress tensor
E	Total energy
P	Total static potential energy
K	Total kinetic energy
W	Conversion rate between potential and kinetic energy
D	Rate of dissipation of the kinetic energy
$\dot{\Phi}^+$	Net positive heating rate taking place at average temperature T^+
$\dot{\Phi}^-$	Net negative heating rate taking place at average temperature T^-
η	Climate efficiency
$\dot{S}_{\text{mat}}$	Rate of material entropy production of the climate system
$\dot{S}_{\text{fric}}$	Rate of material entropy production due to friction
$\dot{S}_{\text{diff}}$	Rate of material entropy production due to diffusion
$\dot{S}_{\text{hyd}}$	Rate of material entropy production due to the hydrological cycle
$\dot{S}_{\text{mat}}^v$	Rate of material entropy production of the climate system due to vertical processes
$\dot{S}_{\text{mat}}^h$	Rate of material entropy production of the climate system due to horizontal processes
$\rho^{(1)}(A)$	First-order correction to the expectation value of the observable A
$G_A^{(1)}(t)$	First-order Green function for the observable A
$\chi_A^{(1)}(\omega)$	First-order susceptibility function for the observable A
Δ_T	Climate sensitivity
$\mathcal{P} = 1 - \mathcal{Q}$	Projection operator performing coarse graining on the dynamics and eliminates irrelevant degrees of freedom; $\mathcal{Q}$ is the complementary operator

References

Abramov, R. V. (2012), Suppression of chaos at slow variables by rapidly mixing fast dynamics through linear energy-preserving coupling, *Commun. Math. Sci.*, *10*(2), 595–624.

Abramov, R. V., and A. Majda (2008), New approximations and tests of linear fluctuation-response for chaotic nonlinear forced-dissipative dynamical systems, *J. Nonlinear Sci.*, *18*, 303–341, doi:10.1007/s00332-007-9011-9.

Adams, D. K., and N. O. Rennò (2005), Thermodynamic efficiencies of an idealized global climate model, *Clim. Dyn.*, *25*, 801–813.

Ambaum, M. H. P. (2010), *Thermal Physics of the Atmosphere*, 256 pp., Wiley, New York.

Arfken, G. B., H. J. Weber, and F. E. Harris (2005), *Mathematical Methods for Physicists: A Comprehensive Guide*, 6th ed., Academic Press, Berlin.

Arnold, L. (1988), *Random Dynamical Systems*, Springer, New York.

Arnold, L. (2001), Hasselmann's program revisited: The analysis of stochasticity in deterministic climate models, *Stochastic Clim. Models*, *49*, 141–158.

Arnold, L., P. Imkeller, and Y. Wu (2003), Reduction of deterministic coupled atmosphere-ocean models to stochastic ocean models: A numerical case study of the Lorenz-Maas system, *Dyn. Syst.*, *18*(4), 295–350, doi:10.1080/14689360310001607979.

Arnold, V. (1992), *Catastrophe Theory*, 3rd ed., Springer, Berlin.

Bakhtin, V., and Y. Kifer (2004), Diffusion approximation for slow motion in fully coupled averaging, *Probab. Theor. Relat. Fields*, *129*(2), 157–181, doi:10.1007/s00440-003-0326-7.

Bartello, P. (1995), Geostrophic adjustment and inverse cascades in rotating stratified turbulence, *J. Atmos. Sci.*, *52*, 4410–4428.

Basdevant, C., and R. Sadourny (1975), Ergodic properties of inviscid truncated models of two-dimensional incompressible flows, *J. Fluid Mech.*, *69*, 673–688, doi:10.1017/S0022112075001620.

Batygin, K., and D. J. Stevenson (2010), Inflating hot Jupiters with Ohmic dissipation, *Astrophys. J. Lett.*, *714*(2), L238–L24, doi:10.1088/2041-8205/714/2/L238.

Bayr, T., D. Dommenget, T. Martin, and S. Power (2014), The eastward shift of the Walker Circulation in response to global warming and its relationship to ENSO variability, *Clim. Dyn.*, doi:10.1007/s00382-014-2091-y.

Becker, E. (2003), Frictional heating in global climate models, *Mon. Weather Rev.*, *131*, 508–520.

Bengtsson, L., M. Steinheimer, P. Bechtold, and J.-F. Geleyn (2013), A stochastic parametrization for deep convection using cellular automata, *Q. J. R. Meteorol. Soc.*, *675*, 1533–1543, doi:10.1002/qj.2108.

Bernstein, D. (2007), Optimal prediction of Burgers's equation, *Multiscale Model. Simul.*, *6*(1), 27–52, doi:10.1137/060651720.

Bihlo, A. (2008), Rayleigh-Bénard convection as a Nambu-metriplectic problem, *J. Phys. A*, *41*, 292,001, doi:10.1088/1751-8113/41/29/292001.

Boffetta, G. (2007), Energy and enstrophy fluxes in the double cascade of two-dimensional turbulence, *J. Fluid Mech.*, *589*, 253–260.

Boschi, R., V. Lucarini, and S. Pascale (2013), Bistability of the climate around the habitable zone: A thermodynamic investigation, *Icarus*, *226*(2), 1724–1742, doi:10.1016/j.icarus.2013.03.017.

Bouchet, F., and E. Simonnet (2009), Random changes of flow topology in two-dimensional and geophysical turbulence, *Phys. Rev. Lett.*, *102*, 94,504, doi:10.1103/PhysRevLett.102.094504.

Bouchet, F., and A. Venaille (2012), Statistical mechanics of two-dimensional and geophysical flows, *Phys. Rep.*, *515*, 227–295, doi:10.1016/j.physrep.2012.02.001.

Bouchet, F., C. Nardini, and T. Tangarife (2013), Kinetic theory of jet dynamics in the stochastic barotropic and 2D Navier-Stokes equations, *J. Stat. Phys.*, *153*, 572–625, doi:10.1007/s10955-013-0828-3.

Bracegirdle, T. J., and D. B. Stephenson (2012), On the robustness of emergent constraints used in multimodel climate change projections of Arctic warming, *J. Clim.*, *26*(2), 669–678, doi:10.1175/JCLI-D-12-00537.1.

Budyko, M. (1969), The effect of solar radiation variations on the climate of the Earth, *Tellus*, *21*, 611–619.

Chandy, A. J., and S. H. Frankel (2009), The t-model as a large eddy simulation model for the Navier-Stokes equations, *Multiscale Model. Simul.*, *8*(2), 445–462, doi:10.1137/090760787.

Charney, J. G. (1947), The dynamics of long waves in a baroclinic westerly current, *J. Meteorol.*, *4*(5), 136–162, doi:10.1175/1520-0469(1947)004<0136:TDOLWI>2.0.CO;2.

Chavanis, P.-H. (2009), Dynamical and thermodynamical stability of two-dimensional flows: Variational principles and relaxation equations, *Eur. Phys. J. B*, *70*, 73–105, doi:10.1140/epjb/e2009-00196-1.

Chavanis, P.-H., and J. Sommeria (1996), Classification of self-organized vortices in two-dimensional turbulence: The case of a bounded domain, *J. Fluid Mech.*, *314*, 267–297, doi:10.1017/S0022112096000316.

Chavanis, P.-H., and J. Sommeria (1997), Thermodynamical approach for small-scale parametrization in 2D turbulence, *Phys. Rev. Lett.*, *78*, 3302–3305, doi:10.1103/PhysRevLett.78.3302.

Chekroun, M. D., E. Simonnet, and M. Ghil (2011), Stochastic climate dynamics: Random attractors and time-dependent invariant measures, *Physica D*, *240*(21), 1685–1700, doi:10.1016/j.physd.2011.06.005.

Chekroun, M. D., H. Liu, and S. Wang (2013a), On stochastic parameterizing manifolds: Pullback characterization and non-Markovian reduced equations, *ArXiv of PDEs*, 143 pp., arXiv:1310.3896.

Chekroun, M. D., H. Liu, and S. Wang (2013b), Non-Markovian reduced systems for stochastic partial differential equations: The additive noise case, *ArXiv of PDEs*, arXiv:1310.3896.

Chorin, A., and P. Stinis (2006), Problem reduction, renormalization, and memory, *Commun. Appl. Math. Comput. Sci.*, *1*(1), 1–27, doi:10.2140/camcos.2006.1.1.

Chorin, A. J., and O. H. Hald (2013), *Stochastic Tools in Mathematics and Science, Texts in Applied Mathematics*, vol. 58, 3rd ed., Springer, New York.

Chorin, A. J., A. P. Kast, and R. Kupferman (1998), Optimal prediction of underresolved dynamics, *Proc. Natl. Acad. Sci. U.S.A.*, *95*(8), 4094–4098.

Chorin, A. J., O. H. Hald, and R. Kupferman (2000), Optimal prediction and the Mori-Zwanzig representation of irreversible processes, *Proc. Natl. Acad. Sci. U.S.A.*, *97*(7), 2968–2973, doi:10.1073/pnas.97.7.2968.

Chorin, A. J., O. H. Hald, and R. Kupferman (2002), Optimal prediction with memory, *Physica D*, *166*(3–4), 239–257, doi:10.1016/S0167-2789(02)00446-3.

Chorin, A. J., O. H. Hald, and R. Kupferman (2006), Prediction from partial data, renormalization, and averaging, *J. Sci. Comput.*, *28*(2–3), 245–261, doi:10.1007/s10915-006-9089-5.

Cichowlas, C., P. Bonaïti, F. Debbasch, and M. E. Brachet (2005), Effective dissipation and turbulence in spectrally truncated Euler flows, *Phys. Rev. Lett.*, *95*(26), 264,502, doi:10.1103/PhysRevLett.95.264502.

Colangeli, M., and V. Lucarini (2014), Elements of a unified framework for response formulae, *J. Stat. Mech.*, *2014*(1), P01002, doi:10.1088/1742-5468/2014/01/P01002.

Cooper, F. C., and P. H. Haynes (2011), Climate sensitivity via a nonparametric fluctuation-dissipation theorem, *J. Atmos. Sci.*, *68*(5), 937–953.

Cooper, F. C., J. G. Esler, and P. H. Haynes (2013), Estimation of the local response to a forcing in a high dimensional system using the fluctuation-dissipation theorem, *Nonl. Process. Geophys.*, *20*(2), 239–248, doi:10.5194/npg-20-239-2013.

Cullen, M. J. P. (2006), *A Mathematical Theory of Large-Scale Atmosphere/Ocean Flow*, Imperial College Press, London, U. K.

Cummins, P. F., and G. Holloway (1994), On eddy-topographic stress representation, *J. Phys. Oceanogr.*, *24*(3), 700–706.

Dauxois, T., S. Ruffo, E. Arimondo, and M. Wilkens (eds.) (2002), *Dynamics and Thermodynamics of Systems With Long Range Interactions, Lecture Notes in Physics*, vol. 602, Springer, New York.

Davies, L., R. S. Plant, and S. H. Derbyshire (2009), A simple model of convection with memory, *J. Geophys. Res.*, *114*, D17202, doi:10.1029/2008JD011653.

de Groot, S., and P. Mazur (1984), *Non-Equilibrium Thermodynamics*, 510 pp., Dover, New York.

Dewar, R., C. Lineweaver, R. Niven, and K. Regenauer-Lieb (2013), Beyond the second law: An overview, in *Beyond the Second Law: Entropy Production and Non-Equilibrium Systems*, pp. 3–27, Springer, Berlin Heidelberg, Germany.

DiBattista, M., and A. J. Majda (2001), Equilibrium statistical predictions for baroclinic vortices: The role of angular momentum, *Theor. Comput. Fluid Dyn.*, *14*(5), 293–322.

Dijkstra, H. (2013), *Nonlinear Climate Dynamics*, Cambridge Univ. Press, Cambridge, N. Y.

DiNezio, P., G. Vecchi, and A. Clement (2013), Detectability of changes in the Walker circulation in response to global warming, *J. Clim.*, *26*, 4038–4048, doi:10.1175/JCLI-D-12-00531.1.

Dolaptchiev, S. I., U. Achatz, and I. Timofeyev (2013), Stochastic closure for local averages in the finite-difference discretization of the forced Burgers equation, *Theor. Comput. Fluid Dyn.*, *27*(3–4), 297–317, doi:10.1007/s00162-012-0270-1.

Donges, J. F., Y. Zou, N. Marwan, and J. Kurths (2009), Complex networks in climate dynamics, *Eur. Phys. J. Special Top.*, *174*(1), 157–179, doi:10.1140/epjst/e2009-01098-2.

Donohoe, A., and D. Battisti (2012), What determines meridional heat transport in climate models?, *J. Clim.*, *25*, 3832–3859.

Dubinkina, S., and J. Frank (2007), Statistical mechanics of Arakawa's discretizations, *J. Comput. Phys.*, *227*(2), 1286–1305, doi:10.1016/j.jcp.2007.09.002.

Dutton, J. A. (1973), The global thermodynamics of atmospheric motions, *Tellus*, *25*, 89–110.

Dvorak, R. (2008), *Extrasolar Planets*, Wiley-VCH, Berlin.

Dymnikov, V. P., and A. N. Filatov (1997), *Mathematics of Climate Modeling*, Birkhauser, Boston, Mass.

Eady, E. T. (1949), Long waves and cyclone waves, *Tellus*, *1*(3), 33–52, doi:10.1111/j.2153-3490.1949.tb01265.x.

Eckhardt, B., and G. Ott (1994), Periodic orbit analysis of the Lorenz attractor, *Z. für Phys. B*, *93*(2), 259–266, doi:10.1007/BF01316970.

Eckmann, J. P., and D. Ruelle (1985), Ergodic theory of chaos and strange attractors, *Rev. Mod. Phys.*, *57*, 617–656, doi:10.1103/RevMod-Phys.57.617.

Egger, J. (1999), Numerical generation of entropies, *Mon. Weather Rev.*, *127*, 2211–2216.

Emanuel, K. (1991), The theory of hurricanes, *Ann. Rev. Fluid. Mech.*, *23*, 179–196.

Emanuel, K., and M. Bister (1996), Moist convective velocity and buoyancy scales, *J. Atmos. Sci.*, *53*, 3276–3285.

Enderton, D., and J. Marshall (2009), Controls on the total dynamical heat transport of the atmosphere and oceans, *J. Atmos. Sci.*, *66*, 1593–1611.

Errico, R. M. (1984), The statistical equilibrium solution of a primitive-equation model, *Tellus A*, *36*(1), 42–51.

Eyink, G. L., T. W. N. Haine, and D. J. Lea (2004), Ruelle's linear response formula, ensemble adjoint schemes and Lévy flights, *Nonlinearity*, *17*(5), 1867, doi:10.1088/0951-7715/17/5/016.

Fasullo, J., and K. Trenberth (2008), The annual cycle of the energy budget. Part II: Meridional structures and poleward transports, *J. Clim.*, *21*, 2313–2325.

Fofonoff, N. P. (1954), Steady flow in a frictionless homogeneous ocean, *J. Mar. Res.*, *13*, 254–262.

Fox, D. G., and S. A. Orszag (1973), Inviscid dynamics of two-dimensional turbulence, *Phys. Fluids*, *16*, 169–171.

Fraedrich, K., and H. Böttger (1978), A wavenumber-frequency analysis of the 500 mb geopotential at 50°N, *J. Atmos. Sci.*, *35*(4), 745–750, doi:10.1175/1520-0469(1978)035<0745:AWFAOT>2.0.CO;2.

Fraedrich, K., and F. Lunkeit (2008), Diagnosing the entropy budget of a climate model, *Tellus A*, *60*(5), 299–304.

Fraedrich, K., H. Jansen, E. Kirk, U. Luksch, and F. Lunkeit (2005), The planet simulator: Towards a user friendly model, *Meteorol. Z.*, *14*(3), 299–304, doi:10.1127/0941-2948/2005/0043.

Frank, J. E., and G. A. Gottwald (2013), Stochastic homogenization for an energy conserving multi-scale toy model of the atmosphere, *Physica D*, *254*, 46–56, doi:10.1016/j.physd.2013.03.010.

Franzke, C. L. E., T. J. O'Kane, J. Berner, P. D. Williams, and V. Lucarini (2014), Stochastic climate theory and modeling, *WIREs Clim. Change.*, doi:10.1002/wcc.318.

Frederiksen, J. S., and T. J. O'Kane (2008), Entropy, closures and subgrid modeling, *Entropy*, *10*, 635–683.

Frederiksen, J. S., and B. L. Sawford (1980), Statistical dynamics of two-dimensional inviscid flow on a sphere, *J. Atmos. Sci.*, *37*, 717–732, doi:10.1175/1520-0469(1980)037<0717:SDOTDI>2.0.CO;2.

Gallavotti, G. (1996), Chaotic hypothesis: Onsager reciprocity and fluctuation-dissipation theorem, *J. Stat. Phys.*, *84*(5–6), 899–925.

Gallavotti, G. (2006), Stationary nonequilibrium statistical mechanics, *Encyclopedia Math. Phys.*, *3*, 530–539.

Gassmann, A. (2013), A global hexagonal C-grid nonhydrostatic dynamical core (ICON-IAP) designed for energetic consistency, *Q. J. R. Meteorol. Soc.*, *139*, 152–175, doi:10.1002/qj.1960.

Gassmann, A., and H.-J. Herzog (2008), Towards a consistent numerical compressible non-hydrostatic model using generalized Hamiltonian tools, *Q. J. R. Meteorol. Soc.*, *134*, 1597–1613, doi:10.1002/qj.297.

Ghil, M. (1976), Climate stability for a Sellers-type model, *J. Atmos. Sci.*, *33*, 3–20.

Ghil, M., et al. (2011), Extreme events: Dynamics, statistics and prediction, *Nonlinear Processes Geophys.*, *18*(3), 295–350, doi:10.5194/npg-18-295-2011.

Gianfelice, M., F. Maimone, V. Pelino, and S. Vaient (2012), On the recurrence and robust properties of Lorenz'63 model, *Commun. Math. Phys.*, *313*, 745–779.

Goodman, J. (2009), Thermodynamics of atmospheric circulations on hot Jupiters, *Astrophys. J.*, *693*, 1645–1649, doi:10.1088/0004-637X/693/2/1645.

Goody, R. (2000), Sources and sinks of climate entropy, *Q. J. R. Meteorol. Soc.*, *126*, 1953–1970.

Goody, R. (2007), Maximum entropy production in climate theory, *J. Atmos. Sci.*, *64*, 2735–2739.

Gritsun, A., and G. Branstator (2007), Climate response using a three-dimensional operator based on the fluctuation-dissipation theorem, *J. Atmos. Sci.*, *64*(7), 2558–2575.

Gritsun, A. S. (2008), Unstable periodic trajectories of a barotropic model of the atmosphere, *Russ. J. Numer. Anal. Math. Model.*, *23*, 345–367.

Hald, O. H., and R. Kupferman (2001), Convergence of optimal prediction for nonlinear Hamiltonian systems, *SIAM J. Numer. Anal.*, *39*(3), 983–1000, doi:10.1137/S0036142900374482.

Hald, O. H., and P. Stinis (2007), Optimal prediction and the rate of decay for solutions of the Euler equations in two and three dimensions, *Proc. Natl. Acad. Sci. U.S.A.*, *104*(16), 6527–6532, doi:10.1073/pnas.0700084104.

Hasselmann, K. (1976), Stochastic climate models. Part I. Theory, *Tellus*, *28*(6), 473–485.

Hasselmann, K., R. Sausen, E. Maier-Reimer, and R. Voss (1993), On the cold start problem in transient simulations with coupled atmosphere-ocean models, *Clim. Dyn.*, *9*(2), 53–61, doi:10.1007/BF00210008.

Hasson, S., V. Lucarini, and S. Pascale (2013), Hydrological cycle over South and Southeast Asian river basins as simulated by PCMDI/CMIP3 experiments, *Earth Syst. Dyn.*, *4*(2), 199–217, doi:10.5194/esd-4-199-2013.

Heng, K. (2012a), The study of climates of alien worlds, *Am. Sci.*, *100*(4), 334–341.

Heng, K. (2012b), On the existence of shocks in irradiated exoplanetary atmospheres, *Astrophys. J. Lett.*, *761*, L1, doi:10.1088/2041-8205/761/1/L1.

Herbert, C. (2013), Additional invariants and statistical equilibria for the 2D Euler equations on a spherical domain, *J. Stat. Phys.*, *152*, 1084–1114.

Herbert, C. (2014), Nonlinear energy transfers and phase diagrams for geostrophically balanced rotating-stratified flows, *Phys. Rev. E*, *89*, 033008, doi:10.1103/PhysRevE.89.033008.

Herbert, C., B. Dubrulle, P.-H. Chavanis, and D. Paillard (2012), Statistical mechanics of quasi-geostrophic flows on a rotating sphere, *J. Stat. Mech.*, *2012*, P05023, doi:10.1088/1742-5468/2012/05/P05023.

Herbert, C., A. Pouquet, and R. Marino (2014), Restricted Equilibrium and the energy cascade in rotating and stratified flows, *J. Fluid Mech.*, *758*, 374–406.

Hernandez-Deckers, D., and J.-S. von Storch (2012), Impact of the warming pattern on global energetics, *J. Clim.*, *25*, 5223–5240.

Hoffman, P., and D. Schrag (2002), The snowball Earth hypothesis: Testing the limits of global change, *Terra Nova*, *14*, 129–155, doi:10.1046/j.1365-3121.2002.00408.x.

Hogg, N. G., and H. M. Stommel (1985), Hetonic explosions: The breakup and spread of warm pools as explained by baroclinic point vortices, *J. Atmos. Sci.*, *42*, 1465–1476.

Holloway, G. (1986), Eddies, waves, circulation, and mixing: Statistical geofluid mechanics, *Ann. Rev. Fluid Mech.*, *18*, 91–147.

Holloway, G. (1992), Representing topographic stress for large-scale ocean models, *J. Phys. Oceanogr.*, *22*, 1033–1046.

Holloway, G. (2004), From classical to statistical ocean dynamics, *Surv. Geophys.*, *25*, 203–219, doi:10.1007/s10712-004-1272-3.

Holton, J. (2004), *An Introduction to Dynamic Meteorology*, 531 pp., Accademic Press, New York.

Hou, T. Y. (2007), Organized structures, memory, and the decay of turbulence, *Proc. Natl. Acad. Sci.*, *104*(16), 6498–6499, doi:10.1073/pnas.0700639104.

Intergovernmental Panel on Climate Change (IPCC) (2001), *IPCC Third Assessment Report: Working Group I Report "The Physical Science Basis"*, Cambridge Univ. Press, Cambridge, U. K.

Intergovernmental Panel on Climate Change (IPCC) (2007), *IPCC Fourth Assessment Report: Working Group I Report "The Physical Science Basis"*, Cambridge University Press, Cambridge, U. K.

Intergovernmental Panel on Climate Change (IPCC) (2013), *IPCC Fifth Assessment Report: Working Group I Report "The Physical Science Basis"*, Cambridge Univ. Press, New York.

Johnson, D. (1989), The forcing and maintenance of global monsoonal circulations: An isentropic analysis, *Adv. Geophys.*, *31*, 43–316, doi:10.1016/S0065-2687(08)60053-9.

Johnson, D. (1997), General coldness of climate models and the second law: Implications for modeling the Earth system, *J. Clim.*, *10*, 2826–2846.

Johnson, D. R. (2000), Entropy, the Lorenz energy cycle, and climate, in *General Circulation Model Development: Past, Present and Future*, edited by D. A. Randall, pp. 659–720, Acad. Press, New York.

Kalnay, E. (2003), *Atmospheric Modeling, Data Assimilation and Predictability*, Cambridge Univ. Press, Cambridge, U. K.

Kazantsev, E., J. Sommeria, and J. Verron (1998), Subgrid-scale eddy parameterization by statistical mechanics in a barotropic ocean model, *J. Phys. Oceanogr.*, *28*, 1017–1042, doi:10.1175/1520-0485(1998)028<1017:SSEPBS>2.0.CO;2.

Kifer, Y. (2004), Some recent advances in averaging, in *Modern Dynamical Systems and Applications: Dedicated to Anatole Katok on his 60th Birthday*, pp. 385–403, Cambridge Univ. Press, Cambridge, U. K.

Kifer, Y. (2008), Convergence, nonconvergence and adiabatic transitions in fully coupled averaging, *Nonlinearity*, *21*(3), T27, doi:10.1088/0951-7715/21/3/T01.

Kifer, Y. (2009), Large deviations and adiabatic transitions for dynamical systems and Markov processes in fully coupled averaging, *Mem. Am. Math. Soc.*, *201*(944), doi:10.1090/memo/0944.

Kleidon, A. (2009), Non-equilibrium thermodynamics and maximum entropy production, *Naturwissenschaften*, *96*, 653–677.

Klein, R. (2010), Scale-dependent models for atmospheric flows, *Ann. Rev. Fluid Mech.*, *42*(1), 249–274, doi:10.1146/annurev-fluid-121108-145537.

Kraichnan, R. (1967), Inertial ranges in two-dimensional turbulence, *Phys. Fluids*, *10*, 1417–1423, doi:10.1063/1.1762301.

Kraichnan, R., and D. Montgomery (1980), Two-dimensional turbulence, *Rep. Prog. Phys.*, *43*, 547, doi:10.1088/0034-4885/43/5/001.

Kubo, R. (1957), Statistical-mechanical theory of irreversible processes. I. General theory and simple applications to magnetic and conduction problems, *J. Phys. Soc. Jpn.*, *12*(6), 570–586, doi:10.1143/JPSJ.12.570.

Kuroda, Y. (1991), On the Casimir invariant of Hamiltonian fluid mechanics, *J. Phys. Soc. Jpn.*, *60*, 727–730.

Lacorata, G., and A. Vulpiani (2007), Fluctuation-response relation and modeling in systems with fast and slow dynamics, *Nonlinear Processes Geophys.*, *14*, 681–694.

Landau, L. D., and E. M. Lifshits (1996), *Mechanics*, Butterworth-Heinemann, Oxford, U. K.

Langen, P. L., and V. A. Alexeev (2005), Estimating $2 \times CO_2$ warming in an aquaplanet GCM using the fluctuation-dissipation theorem, *Geophys. Res. Lett.*, *32*, L23708, doi:10.1029/2005GL024136.

Ledwell, J. R., E. T. Montgomery, K. L. Polzin, L. C. St. Laurent, R. W. Schmitt, and J. M. Toole (2000), Evidence for enhanced mixing over rough topography in the abyssal ocean, *Nature*, *403*(6766), 179–182.

Lee, T. D. (1952), On some statistical properties of hydrodynamical and magneto-hydrodynamical fields, *Q. Appl. Math.*, *10*, 69–74.

Legg, S., and J. Marshall (1993), A Heron model of the spreading phase of open-ocean deep convection, *J. Phys. Oceanogr.*, *23*, 1040–1056.

Lenton, T. M., H. Held, E. Kriegler, J. W. Hall, W. Lucht, S. Rahmstorf, and H. J. Schellnhuber (2008), Tipping elements in the Earth's climate system, *Proc. Natl. Acad. Sci. U.S.A.*, *105*(6), 1786–1793, doi:10.1073/pnas.0705414105.

Li, L., A. Ingersoll, X. Jiang, D. Feldmann, and Y. Yung (2008), Lorenz energy cycle of the global atmosphere based on reanalysis datasets, *Geophys. Res. Lett.*, *34*, L16813, doi:10.1029/2007GL029985.

Liepert, B., and F. Lo (2013), CMIP5 update of 'Inter-model variability and biases of the global water cycle in CMIP3 coupled climate models', *Environ. Res. Lett.*, *8*, 029401.

Liepert, B., and M. Previdi (2012), Inter-model variability and biases of the global water cycle in CMIP3 coupled climate models, *Environ. Res. Lett.*, *7*, 014006, doi:10.1088/1748-9326/7/1/014006.

Lorenz, E. (1955), Available potential energy and the maintenance of the general circulation, *Tellus*, *7*, 157–167.

Lorenz, E. (1967), *The Nature and Theory of the General Circulation of the Atmosphere*, World Meteorological Organization, Publ. No. 218TP115, Geneva, Switzerland.

Lorenz, E. (1979), Forced and free variations of weather and climate, *J. Atmos. Sci.*, *36*, 1367–1376.

Lorenz, E. N. (1963), Deterministic nonperiodic flow, *J. Atmos. Sci.*, *20*, 130–141.

Lorenz, E. N. (1996), Predictability: A problem partly solved, in *GARP Publication Series*, vol. 16, pp. 132–136, WMO, Geneva, Switz.

Lovejoy, S., and D. Schertzer (2013), *The Weather and Climate: Emergent Laws and Multifractal Cascades*, Cambridge Univ. Press, Cambridge, U. K.

Lucarini, V. (2008), Response theory for equilibrium and non-equilibrium statistical mechanics: Causality and generalized Kramers-Kronig relations, *J. Stat. Phys.*, *131*, 543–558, doi:10.1007/s10955-008-9498-y.

Lucarini, V. (2009), Evidence of dispersion relations for the nonlinear response of the Lorenz 63 system, *J. Stat. Phys.*, *134*, 381–400, doi:10.1007/s10955-008-9675-z.

Lucarini, V. (2012), Stochastic perturbations to dynamical systems: A response theory approach, *J. Stat. Phys.*, *146*(4), 774–786, doi:10.1007/s10955-012-0422-0.

Lucarini, V. (2013), Modeling complexity: The case of climate science, in *Models, Simulations, and the Reduction of Complexity*, edited by U. Gähde, S. Hartmann, and J. Wolf, pp. 229–254, De Gruyter, Berlin.

Lucarini, V., and M. Colangeli (2012), Beyond the linear fluctuation-dissipation theorem: The role of causality, *J. Stat. Mech.*, *2012*(5), P05013, doi:10.1088/1742-5468/2012/05/P05013.

Lucarini, V., and K. Fraedrich (2009), Symmetry breaking, mixing, instability, and low-frequency variability in a minimal Lorenz-like system, *Phys. Rev. E*, *80*, 026,313, doi:10.1103/PhysRevE.80.026313.

Lucarini, V., and S. Pascale (2014), Entropy production and coarse graining of the climate fields in a general circulation model, *Clim. Dyn.*, *43*(3–4), 981–1000, doi:10.1007/s00382-014-2052-5.

Lucarini, V., and F. Ragone (2011), Energetics of climate models: Net energy balance and meridional enthalpy transport, *Rev. Geophys.*, *49*, RG1001, doi:10.1029/2009RG000323.

Lucarini, V., and S. Sarno (2011), A statistical mechanical approach for the computation of the climatic response to general forcings, *Nonlinear Processes Geophys.*, *18*, 7–28, doi:10.5194/npg-18-7-2011.

Lucarini, V., J. J. Saarinen, K.-E. Peiponen, and E. M. Vartiainen (2005), *Kramers-Kronig Relations in Optical Materials Research*, Springer, New York.

Lucarini, V., R. Danihlik, I. Kriegerova, and A. Speranza (2008), Hydrological cycle in the danube basin in present-day and XXII century simulations by IPCCAR4 global climate models, *J. Geophys. Res.*, *113*, D09107, doi:10.1029/2007JD009167.

Lucarini, V., K. Fraedrich, and F. Lunkeit (2010a), Thermodynamics of climate change: Generalized sensitivities, *Atmos. Chem. Phys*, *10*, 9729–9737.

Lucarini, V., K. Fraedrich, and F. Lunkeit (2010b), Thermodynamic analysis of snowball Earth hysteresis experiment: Efficiency, entropy production, and irreversibility, *Q. J. R. Meteorol. Soc.*, *136*, 2–11.

Lucarini, V., K. Fraedrich, and F. Ragone (2011), New results on the thermodynamic properties of the climate system, *J. Atmos. Sci.*, *68*, 2438–2458.

Lucarini, V., D. Faranda, and M. Willeit (2012), Bistable systems with stochastic noise: Virtues and limits of effective one-dimensional Langevin equations, *Nonlinear Processes Geophys.*, *19*(1), 9–22, doi:10.5194/npg-19-9-2012.

Lucarini, V., S. Pascale, R. Boschi, E. Kirk, and N. Iro (2013), Habitability and multistablility in Earth-like planets, *Astr. Nach.*, *334*(6), 576–588.

Majda, A., I. Timofeyev, and E. Vanden Eijnden (2001), A mathematical framework for stochastic climate models, *Commun. Pure Appl. Math.*, *54*(8), 891–974.

Marconi, U. M. B., A. Puglisi, L. Rondoni, and A. Vulpiani (2008), Fluctuation-dissipation: Response theory in statistical physics, *Phys. Rep.*, *461*, 111–195.

Margules, M. (1905), Über die energie der stürme, *Jahrb. Zentralantst. Meteorol.*, *40*, 1–26.

Marques, C., A. Rocha, and J. Corte-Real (2011), Global diagnostic energetics of five state-of-the-art climate models, *Clim. Dyn.*, *36*, 1767–1794.

Mayer, M., and L. Haimberger (2012), Poleward atmospheric energy transports and their variability as evaluated from ECMWF reanalysis data, *J. Clim.*, *25*, 734–752.

Merryfield, W. J. (1998), Effects of stratification on quasi-geostrophic inviscid equilibria, *J. Fluid Mech.*, *354*, 345–356.

Miller, J. (1990), Statistical mechanics of Euler equations in two dimensions, *Phys. Rev. Lett.*, *65*, 2137–2140, doi:10.1103/PhysRevLett.65.2137.

Mitchell, M. (1976), An overview of climatic variability and its causal mechanisms, *Quat. Res.*, *6*(4), 481–493, doi:10.1016/0033-5894(76)90021-1.

Miyazaki, T., T. Sato, H. Kimura, and N. Takahashi (2011), Influence of external flow field on the equilibrium state of quasi-geostrophic point vortices, *Geophys. Astrophys. Fluid Dyn.*, *105*(4–5), 392–408, doi:10.1080/03091929.2010.502118.

Monahan, A. H., and J. Culina (2011), Stochastic averaging of idealized climate models, *J. Clim.*, *24*(12), 3068–3088, doi:10.1175/2011JCLI3641.1.

Montgomery, D., and G. Joyce (1974), Statistical mechanics of "negative temperature" states, *Phys. Fluids*, *17*, 1139–1145, doi:10.1063/1.1694856.

Mori, H. (1965), Transport, collective motion, and Brownian motion, *Prog. Theor. Phys.*, *33*(3), 423–455.

Mori, H., H. Fujisaka, and H. Shigematsu (1974), A new expansion of the master equation, *Prog. Theor. Phys.*, *51*(1), 109–122, doi:10.1143/PTP.51.109.

Nambu, Y. (1973), Generalized Hamiltonian dynamics, *Phys. Rev. D*, *7*, 2403–2412.

Naso, A., P.-H. Chavanis, and B. Dubrulle (2011), Statistical mechanics of Fofonoff flows in an oceanic basin, *Eur. Phys. J. B*, *80*, 493–517, doi:10.1140/epjb/e2011-10440-8.

Neelin, J. D., and F.-F. Jin (1993), Modes of interannual tropical ocean-atmosphere interaction—A unified view. Part II: Analytical results in the weak-coupling limit, *J. Atmos. Sci.*, *50*(21), 3504–3522, doi:10.1175/1520-0469(1993)050<3504:MOITOI>2.0.CO;2.

Névir, P. (1998), Die Nambu-Felddarstellungen der Hydro-Thermodynamik und ihre Bedeutung für die dynamische Meteorologie, Habilitationsschrift, Freie Universitat, Berlin.

Névir, P., and R. Blender (1993), A Nambu representation of incompressible hydrodynamics using helicity and enstrophy, *J. Phys. A*, *26*, L1189–1193.

Névir, P., and M. Sommer (2009), Energy-vorticity theory of ideal fluid mechanics, *J. Atmos. Sci.*, *66*(7), 2073–2084, doi:10.1175/2008JAS2897.1.

Nikurashin, M., G. K. Vallis, and A. Adcroft (2013), Routes to energy dissipation for geostrophic flows in the Southern Ocean, *Nat. Geosci.*, *6*(1), 48–51, doi:10.1038/ngeo1657.

Onsager, L. (1949), Statistical hydrodynamics, *Il Nuovo Cimento*, *6*, 279–287, doi:10.1007/BF02780991.

Oort, A., L. Anderson, and J. Peixoto (1994), Estimates of the energy cycle of the oceans, *J. Geophys. Res.*, *99*, 7665–7688.

Ozawa, H., A. Ohmura, R. Lorenz, and T. Pujol (2003), The second law of thermodynamics and the global climate system: A review of the maximum entropy production principle, *Rev. Geophys*, *41*(4), 1018, doi:10.1029/2002RG000113.

Palmer, T. N., and P. Williams (2009), *Stochastic Physics and Climate Modelling*, Cambridge Univ. Press, Cambridge, U. K.

Paltridge, G. (1975), Global dynamics and climate—A system of minimum entropy exchange, *Q. J. R. Meteorol. Soc.*, *101*, 475–484.

Paltridge, G. (1978), The steady state format of global climate, *Q. J. R. Meteorol. Soc.*, *104*, 927–945.

Paret, J., and P. Tabeling (1997), Experimental observation of the two-dimensional inverse energy cascade, *Phys. Rev. Lett.*, *79*, 4162–4165.

Park, J. H., N. S. Namachchivaya, and N. Neogi (2007), Stochastic averaging and optimal prediction, *J. Vib. Acoust.*, *129*(6), 803–807, doi:10.1115/1.2748777.

Pascale, S., J. M. Gregory, M. Ambaum, and R. Tailleux (2011), Climate entropy budget of the HadCM3 atmosphere-ocean general circulation model and of FAMOUS, its low-resolution version, *Clim. Dyn.*, *36*, 1189–1206.

Pascale, S., F. Ragone, V. Lucarini, Y. Wang, and R. Boschi (2013), Nonequilibrium thermodynamics of an optically thin, dry atmosphere, *Planet. Space Sci.*, *84*, 48–65.

Pauluis, O. (2010), Water vapor and mechanical work: A comparison of carnot and steam cycles, *J. Atmos. Sci.*, *68*(1), 91–102, doi:10.1175/2010JAS3530.1.

Pauluis, O., and I. Dias (2012), Satellite estimated of precipitation-induced dissipation in the atmosphere, *Science*, *335*, 953–956.

Pauluis, O., and I. M. Held (2002a), Entropy budget of an atmosphere in radiative-convective equilibrium. Part I: Maximum work and frictional dissipation, *J. Atmos. Sci.*, *59*, 125–139.

Pauluis, O., and I. M. Held (2002b), Entropy budget of an atmosphere in radiative-convective equilibrium. Part II: Latent heat transport and moist processes, *J. Atmos. Sci.*, *59*, 140–149.

Pavliotis, G., and A. Stuart (2008), *Multiscale Methods, Texts in Applied Mathematics: TAM*, Springer, New York.

Pedlosky, J. (1987), *Geophysical Fluid Dynamics, Springer Study Edition*, Springer, New York.

Peixoto, J. P., and A. H. Oort (1992), *Physics of Climate*, Am. Inst. of Phys., New York.

Pelino, V., and F. Maimone (2007), Energetics, skeletal dynamics, and long-term predictions on Kolmogorov-Lorenz systems, *Phys. Rev. E*, *76*, 046214, doi:10.1103/PhysRevE.76.046214.

Perna, R., K. Heng, and F. Pont (2012), The effects of irradiation on hot jovian atmospheres: Heat redistribution and energy dissipation, *Astrophys. J.*, *751*, 59–76.

Piriou, J.-M., J.-L. Redelsperger, J.-F. Geleyn, J.-P. Lafore, and F. Guichard (2007), An approach for convective parameterization with memory: Separating microphysics and transport in grid-scale equations, *J. Atmos. Sci.*, *64*(11), 4127–4139, doi:10.1175/2007JAS2144.1.

Pouquet, A., and R. Marino (2013), Geophysical turbulence and the duality of the energy flow across scales, *Phys. Rev. Lett.*, *111*, 234,501, doi:10.1103/PhysRevLett.111.234501.

Prigogine, I. (1961), *Thermodynamics of Irreversible Processes*, Interscience, New York.

Probst, P., R. Rizzi, E. Tosi, V. Lucarini, and T. Maestri (2012), Total cloud cover from satellite observations and climate models, *Atmos. Res.*, *107*, 161–170, doi:10.1016/j.atmosres.2012.01.005.

Qi, W., and J. B. Marston (2014), Hyperviscosity and statistical equilibria of Euler turbulence on the torus and the sphere, *J. Stat. Mech.*, *2014*, P07020, doi:10.1088/1742-5468/2014/07/P07020.

Ragone, F., V. Lucarini, and F. Lunkeit (2014), A new framework for climate sensitivity and prediction, arXiv:1403.4908v2.

Rant, Z. (1956), Energie, ein neues wort für technische arbeitf̈higkeit, *Forsch. Ing.*, *22*, 36–37.

Rennò, N. O., and A. P. Ingersoll (1996), Natural convection as a heat engine: A theory for CAPE, *J. Atmos. Sci.*, *53*, 572–585.

Rhines, P. B. (1975), Waves and turbulence on a beta-plane, *J. Fluid Mech.*, *69*, 417–443.

Rhines, P. B. (1976), *The Dynamics of Unsteady Currents*.

Rhines, P. B. (1979), Geostrophic turbulence, *Ann. Rev. Fluid Mech.*, *11*, 401–441.

Robert, R., and J. Sommeria (1991), Statistical equilibrium states for two-dimensional flows, *J. Fluid Mech.*, *229*, 291–310, doi:10.1017/S0022112091003038.

Rose, B., and D. Ferreira (2013), Ocean heat transport and water vapor greenhouse in a warm equable climate: A new look at the low gradient paradox, *J. Clim.*, *26*, 2127–2136.

Ruelle, D. (1989), *Chaotic Evolution and Strange Attractors*, Cambridge Univ. Press, Cambridge, N. Y.

Ruelle, D. (1997), Differentiation of SRB states, *Commun. Math. Phys.*, *187*(1), 227–241.

Ruelle, D. (1998a), General linear response formula in statistical mechanics, and the fluctuation-dissipation theorem far from equilibrium, *Phys. Lett. A*, *245*, 220–224.

Ruelle, D. (1998b), Nonequilibrium statistical mechanics near equilibrium: Computing higher-order terms, *Nonlinearity*, *11*(1), 5–18.

Ruelle, D. (2009), A review of linear response theory for general differentiable dynamical systems, *Nonlinearity*, *22*(4), 855–870.

Salazar, R., and M. V. Kurgansky (2010), Nambu brackets in fluid mechanics and magnetohydrodynamics, *J. Phys. A*, *43*, 305,501, doi:10.1088/1751-8113/43/30/305501.

Salmon, R. (1978), Two-layer quasi-geostrophic turbulence in a simple special case, *Geophys. Astrophys. Fluid Dyn.*, *10*, 25–52, doi:10.1080/03091927808242628.

Salmon, R. (1988), Hamiltonian fluid mechanics, *Annu. Rev. Fluid Mech.*, *20*(1), 225–256.

Salmon, R. (1998), *Lectures on Geophysical Fluid Dynamics*, Oxford Univ. Press, Oxford, New York.

Salmon, R. (2005), A general method for conserving quantities related to potential vorticity in numerical models, *Nonlinearity*, *18*(5), R1–R16, doi:10.1088/0951-7715/18/5/R01.

Salmon, R. (2007), A general method for conserving energy and potential enstrophy in shallow water models, *J. Atmos. Sci.*, *64*, 515–531.

Salmon, R., G. Holloway, and M. C. Hendershott (1976), The equilibrium statistical mechanics of simple quasi-geostrophic models, *J. Fluid Mech.*, *75*, 691–703, doi:10.1017/S0022112076000463.

Saltzman, B. (2001), *Dynamical Paleoclimatology*, Acad. Press, New York.

Schneider, T. (2006), The general circulation of the atmosphere, *Annu. Rev. Earth Planet. Sci.*, *34*(1), 655–688, doi:10.1146/annurev.earth.34.031405.125144.

Schubert, G., and J. Mitchell (2013), Planetary atmospheres as heat engines, in *Comparative Climatology of Terrestrial Planets*, edited by S. J. Mackwell et al., Univ. of Ariz. Press and Lunar and Planet. Inst., 181–191.

Schütte, C., J. Walter, C. Hartmann, and W. Huisinga (2004), An averaging principle for fast degrees of freedom exhibiting long-term correlations, *Multiscale Model. Simul.*, *2*(3), 501–526, doi:10.1137/030600308.

Seager, S., and D. Deming (2010), Exoplanet atmospheres, *Ann. Rev. Astron. Astrophys.*, *48*, 631–672.

Sellers, W. (1969), A global climatic model based on the energy balance of the Earth-atmosphere system, *J. Appl. Meteorol.*, *8*, 392–400.

Shepherd, T. (1990), Symmetries, conservation laws, and hamiltonian structure in geophysical fluid dynamics, *Adv. Geophys.*, *32*, 287–338.

Sommer, M., and P. Névir (2009), A conservative scheme for the shallow-water system on a staggered geodesic grid based on a Nambu representation, *Q. J. R. Meteorol. Soc*, *135*(639), 485–494, doi:10.1002/qj.368.

Steinheimer, M., M. Hantel, and P. Bechtold (2008), Convection in Lorenz's global energy cycle with the ECMWF model, *Tellus A*, *60*, 1001–1022, doi:10.1111/j.1600-0870.2008.00348.x.

Stinis, P. (2006), A comparative study of two stochastic mode reduction methods, *Physica D*, *213*(2), 197–213, doi:10.1016/j.physd.2005.11.010.

Stinis, P. (2007), Higher order Mori-Zwanzig models for the Euler equations, *Multiscale Model. Simul.*, *6*(3), 741–760, doi:10.1137/06066504X.

Stone, P. H. (1978), Constraints on dynamical transports of energy on a spherical planet, *Dyn. Atmos. Oceans*, *2*, 123–139.

Storch, J.-S. V., C. Eden, I. Fast, H. Haak, D. Hernández-Deckers, E. Maier-Reimer, J. Marotzke, and D. Stammer (2012), An estimate of the Lorenz energy cycle for the world ocean based on the $1/10°$ STORM/NCEP simulation, *J. Phys. Oceanogr.*, *42*, 2185–2205.

Strounine, K., S. Kravtsov, D. Kondrashov, and M. Ghil (2010), Reduced models of atmospheric low-frequency variability: Parameter estimation and comparative performance, *Physica D*, *239*(3–4), 145–166, doi:10.1016/j.physd.2009.10.013.

Tailleux, R. (2013), Available potential energy and exergy in stratified fluids, *Ann. Rev. Fluid. Mech.*, *45*, 35–58.

Taylor, K. E., R. J. Stouffer, and G. A. Meehl (2012), An overview of CMIP5 and the experiment design, *Bull. Am. Meteorol. Soc.*, *93*, 485–498.

Tobias, S. M., and J. B. Marston (2013), *Phys. Rev. Lett.*, *110*(10), 104,502, doi:10.1103/PhysRevLett.110.104502.

Trenberth, K., and J. Fasullo (2012), Tracking Earth's energy: From El Niño to global warming, *Surv. Geophys.*, *33*(3–4), 413–426, doi:10.1007/s10712-011-9150-2.

Trenberth, K. E., and J. M. Caron (2001), Estimates of meridional atmosphere and ocean heat transports, *J. Clim.*, *14*, 3433–3443.

Trenberth, K. E., and J. T. Fasullo (2010), Simulation of present-day and twenty-first-century energy budgets of the Southern Oceans, *J. Clim.*, *23*, 440–454.

Turner, A., and H. Annamalai (2012), Climate change and the South Asian summer monsoon, *Nat. Clim. Change*, *2*, 587–595, doi:10.1038/nclimate1495.

Vallis, G. K. (2006), *Atmospheric and Oceanic Fluid Dynamics: Fundamentals and Large-Scale Circulation*, Cambridge Univ. Press, Cambridge, U. K.

Vallis, G. K., and M. E. Maltrud (1993), Generation of mean flows and jets on a beta-plane and over topography, *J. Phys. Oceanogr.*, *23*, 1346–1362.

Venaille, A. (2012), Bottom-trapped currents as statistical equilibrium states above topographic anomalies, *J. Fluid Mech.*, *699*, 500, doi:10.1017/jfm.2012.146.

Venaille, A., and F. Bouchet (2011), Solvable phase diagrams and ensemble inequivalence for two-dimensional and geophysical turbulent flows, *J. Stat. Phys.*, *143*, 346–380, doi:10.1007/s10955-011-0168-0.

Venaille, A., G. K. Vallis, and S. M. Griffies (2012), The catalytic role of beta effect in barotropization processes, *J. Fluid Mech.*, *709*, 490–515.

Wang, J., and G. K. Vallis (1994), Emergence of Fofonoff states in inviscid and viscous ocean circulation models, *J. Mar. Res.*, *52*, 83–127.

Warn, T. (1986), Statistical mechanical equilibria of the shallow water equations, *Tellus A*, *38*(1), 1–11.

Wild, M., D. Folini, C. Schär, N. Loeb, E. Dutton, and G. Kšnig-Langlo (2013), The global energy balance from a surface perspective, *Clim. Dyn.*, *40*(11-12), 3107–3134, doi:10.1007/s00382-012-1569-8.

Wilks, D. S. (2005), Effects of stochastic parametrizations in the Lorenz' 96 system, *Q. J. R. Meteorol. Soc.*, *131*(606), 389–407.

Woollings, T., and J. Thuburn (2006), Entropy sources in a dynamical core atmosphere model, *Q. J. R. Meteorol. Soc.*, *132*(614), 43–59, doi:10.1256/qj.04.189.

Wouters, J., and V. Lucarini (2012), Disentangling multi-level systems: Averaging, correlations and memory, *J. Stat. Mech.*, *2012*(3), P03003, doi:10.1088/1742-5468/2012/03/P03003.

Wouters, J., and V. Lucarini (2013), Multi-level dynamical systems: Connecting the Ruelle response theory and the Mori-Zwanzig approach, *J. Stat. Phys.*, *151*(5), 850–860, doi:10.1007/s10955-013-0726-8.

Wunsch, C. (2005), The total meridional heat flux and its oceanic and atmospheric partition, *J. Clim.*, *18*, 4374–4380.

Wunsch, C. (2012), *Discrete Inverse and State Estimation: With Geophysical Fluid Applications*, Cambridge Univ. Press, Cambridge, U. K.

Wunsch, C., and R. Ferrari (2004), Vertical mixing, energy, and the general circulation of the oceans, *Ann. Rev. Fluid Mech.*, *36*(1), 281–314, doi:10.1146/annurev.fluid.36.050802.122121.

Yatsuyanagi, Y., Y. Kiwamoto, H. Tomita, M. Sano, T. Yoshida, and T. Ebisuzaki (2005), Dynamics of two-sign point vortices in positive and negative temperature states, *Phys. Rev. Lett.*, *94*(5), 054,502, doi:10.1103/PhysRevLett.94.054502.

Young, L. (2002), What are SRB measures, and which dynamical systems have them?, *J. Stat. Phys.*, *108*, 733–754.

Zwanzig, R. (1960), Ensemble method in the theory of irreversibility, *J. Chem. Phys.*, *33*(5), 1338, doi:10.1063/1.1731409.

Zwanzig, R. (1961), Memory effects in irreversible thermodynamics, *Phys. Rev.*, *124*(4), 983–992.

Zwanzig, R. (2001), *Nonequilibrium Statistical Mechanics*, Oxford Univ. Press, Oxford, U. K.